

Monitoring land movement on urban roads using InSAR data

A.K. Bach

Technische Universiteit Delft

On the cover

The cover shows the *Surface and Object Motion Map or Bodemdalingkaart* of the Netherlands. The red areas indicate areas with large subsidence rates, the green areas have about neutral rates and the blues areas indicate areas which encounter uplift. The *bodemdelingkaart* is a collaboration of different universities (Delft University of Technology, University of Twente, University of Applied Sciences Utrecht), geodetic (SkyGeo, 06-GPS) and knowledge companies (KNMI) [12].

Monitoring land movement on urban roads using InSAR data

by

A.K. Bach

to obtain the degree of Master of Science
at the Delft University of Technology,
to be defended publicly on Wednesday June 30, 2021 at 1:00 PM.

Student number:	4208463	
Project duration:	June 15, 2019 – June 30, 2021	
Thesis committee:	Prof. dr. ir. J. Jommi,	TU Delft, supervisor
	dr. ir. D.J.M. Ngan-Tillard,	TU Delft
	F. Pisano,	TU Delft
	ir. E.A.V. van der Putte,	Sweco

An electronic version of this thesis is available at <http://repository.tudelft.nl/>.

Preface

Beste lezer,

Voor je ligt het laatste werk van mijn studententijd: mijn master thesis. Met veel trots presenteer ik dit rapport en kijk ik met veel genot terug op de afgelopen jaren.

Ik wil graag mijn professor, Cristina bedanken voor haar tijd en inzet in de begeleiding. Daarnaast wil ik Erik van der Putte van Sweco voor het aanbieden van deze opdracht en zijn expertise op dit gebied. Tot slot bedank ik mijn ouders, zusje en broertje voor de mentale support en mijn vriendinnen voor de geweldige studententijd.

Glück Auf!

Summary

Large areas in the Netherlands are subjected to ground subsidence. This subsidence can have a natural cause or an anthropocene cause. The subsiding ground is leading to a lot of problems on buildings and infrastructure. Therefore, it is desired to be able to predict the amount of ground subsidence expected in the subsiding areas, so preventive or solution-oriented actions can be taken.

This research is targeted to the area of the city Woerden, located in the western part of the Netherlands. The buildings in this city are founded on piles and therefore the focus has been put on roads. For the order of magnitude of the ground subsidence in this area, the satellite data has been obtained by Interferometric Synthetic Aperture Radar or InSAR. From the satellite data, a settlement rate and amplitude of seasonal oscillation can be deduced. The data has been analysed in order to uncover any coherence with the soil profile in the area. The main soil types of the soil layers are sand, peat and clay. The soil layers can be divided into the Echteld Formation and Nieuwkoop Formation and have been deposited during the Holocene.

Three different groups, group A to C, of locations are constructed. In group A the soil profiles do contain only sand and clay. The soil profiles of group B consists of sand, clay and some peat. Lastly, the soil profiles of group C contain sand, clay and a large amount of peat. The settlement rate was found to be the highest for the locations of group C, where the largest amount of peat is present within the soil profiles. The amplitude of the seasonal oscillation was found higher for group C than for group A. The amplitudes for group B can not clearly be categorised. There have been two variables analysed to find whether the satellite data is reflecting the soil profiles. These variables are the thickness of the soil layers, and the ratio of thickness and depth of the soil layers.

Looking at the settlement rate, a trendline for the data in group A could be constructed between the satellite data and both variables. Since the soil profiles of group B and group C also contain peat layers, the trendline for group A is used to predict the amount of settlement rate generated by the clay layers in group B and C. This part is subtracted from the total settlement rate and the remainder is assigned to be originating from the peat layers. Another trendline can be drawn for the residual settlement rate and the thickness, as well as the ratio thickness and depth of the peat layers. Both trendlines can be combined into one overall trendline. By back-calculating the settlement rate for the location by using the overall trendline, it can be calculated how well the trendline predicts the settlement rate. For the thickness of the soil layers, the trendline deviates 0.28 mm/year on average from the satellite data. For the ratio of thickness and depth of the soil layers, the constructed trendline deviates 0.30 mm/year on average from the satellite data, leading to a divergence of 7.1% and 7.5% respectively.

The same approach has been executed for the amplitude of the seasonal oscillation. These overall trendlines deviate 0.20 mm and 0.16 mm from the satellite data for the thickness and ratio of the thickness and depth of the soil layers respectively. The divergence is 13.8% for the trendline of the thickness of the soil layers and 9.5% for the trendline comprising the ratio thickness and depth of the soil layers.

In addition, it has been analysed whether the groundwater level has any influence on the settlement rate or amplitude of the seasonal oscillation. For the settlement rate, five different time periods have been analysed. It can be stated that fluctuations of the groundwater level do influence the settlement rate. The periods with a high groundwater level show a decrease in settlement rate. The effect of the groundwater level to the amplitude of the seasonal oscillation is not as clear. Although the seasonal trendlines show a seasonal effect, the peaks and troughs of the graphs are not occurring simultaneously.

The main conclusion is that for both the settlement rate and the amplitude of the seasonal oscillation a coherence exists for both variables. For the settlement rate, the optimal depth of influence is established to be 3 metres. The coherence between the settlement rate and the ratio of thickness and depth of the soil layers is slightly higher than the coherence of the thickness of the soil layers. For the amplitude of the seasonal

oscillation, the optimal depth of influence is found to be 1.5 metres. The coherence between the amplitude and the ratio of thickness and depth of the soil layers is lower than the coherence of the thickness of the soil layers. Additional research on the influence of the depth and fluctuation of the groundwater level is recommended since there are indications the groundwater level is playing a role. Also addition research should be performed in areas with corresponding ground profile to be able to establish a general conclusion to how well InSAR data portrays the soil profile.

List of Figures

2.1	Distribution in the Netherlands of the Echteld Formation and Nieuwkoop Formation	8
2.2	The development of different types of peat [18]	9
3.1	Contribution of compaction, isostasy and tectonics to ground subsidence in the Netherlands for the last 2.5 million years [24]	11
4.1	Geometry of a Synthetic Aperture Radar system [2]	16
4.2	Decomposition of the deformation vector represented in a top-view (left) and 3D view (right) [16]	17
4.3	Distributed Scatterer (left) and Persistent Scatterer (right) [7]	18
5.1	Location of the research area	19
5.2	The locations inside the research area	23
5.3	The locations and codes of the used monitoring wells	24
6.1	Link between the amplitude of seasonal oscillation and settlement rate	27
6.2	Individual measurement series (top) and trendlines (bottom) for location A3	28
6.3	Representative soil profiles of group A (left), group B (centre) en group C (right)	29
6.4	Graphs of settlement rate and thickness	30
6.5	Graphs showing the difference between the real and calculated values of the settlement rate	31
6.6	Graphs of settlement rate and ratio of thickness and depth	32
6.7	Graphs showing the difference between the real and calculated values of the settlement rate	32
6.8	Graphs of thickness of the clay layers and amplitude for profile length of 3m	33
6.9	Graphs of the thickness of the clay layer and amplitude for the top 1.5m of the profiles	34
6.10	Graphs of thickness of the peat layers in group B and group C and amplitude	35
6.11	Graphs showing the difference between the real and calculated values of the amplitude	35
6.12	Graphs of depth of the clay layers and amplitude of seasonal oscillation	36
6.13	Graphs of depth of the soil layers for group A and amplitude of seasonal oscillation (left) and group B and C and the residual amplitude of seasonal oscillation (right)	36
6.14	Graphs of the ratio between thickness and depth and amplitude for the top 1m of the profiles	37
6.15	Graphs showing the difference between the real and calculated values of the amplitude	37
6.16	Graphs of the seasonal trendlines for all locations of group A (top), group B (middle) and group C (bottom)	38
6.17	Averaged values of the water table per day measured by different monitoring wells located in the four different districts	39
6.18	Settlement rate calculated per period	40
6.19	Average value for the groundwater levels from starting date	40
6.20	Average value for the groundwater levels in time intervals	41
7.1	Difference value for the depth of investigation with corresponding values of R-squared for group A	44
A.1	Point positions of the locations attributed to group A	57
A.2	Point positions of the locations attributed to group B	57
A.3	Point positions of the locations attributed to group C	58
B.1	Individual measurement series (top) and trendlines (bottom) for location A1	59
B.2	Individual measurement series (top) and trendlines (bottom) for location A2	60
B.3	Individual measurement series (top) and trendlines (bottom) for location A3	60
B.4	Individual measurement series (top) and trendlines (bottom) for location A4	61
B.5	Individual measurement series (top) and trendlines (bottom) for location A5	61

B.6	Individual measurement series (top) and trendlines (bottom) for location A6	62
B.7	Individual measurement series (top) and trendlines (bottom) for location A7	62
C.1	Individual measurement series (top) and trendlines (bottom) for location B1	63
C.2	Individual measurement series (top) and trendlines (bottom) for location B2	64
C.3	Individual measurement series (top) and trendlines (bottom) for location B3	64
C.4	Individual measurement series (top) and trendlines (bottom) for location B4	65
C.5	Individual measurement series (top) and trendlines (bottom) for location B5	65
C.6	Individual measurement series (top) and trendlines (bottom) for location B6	66
C.7	Individual measurement series (top) and trendlines (bottom) for location B7	66
D.1	Individual measurement series (top) and trendlines (bottom) for location C1	67
D.2	Individual measurement series (top) and trendlines (bottom) for location C2	68
D.3	Individual measurement series (top) and trendlines (bottom) for location C3	68
D.4	Individual measurement series (top) and trendlines (bottom) for location C4	69
D.5	Individual measurement series (top) and trendlines (bottom) for location C5	69
D.6	Individual measurement series (top) and trendlines (bottom) for location C6	70
D.7	Individual measurement series (top) and trendlines (bottom) for location C7	70
E.1	Declaration of the different soil types shown in the soil profiles	71
E.2	Soil profiles belonging to the locations of group A	72
E.3	Soil profiles belonging to the locations of group B	73
E.4	Soil profiles belonging to the locations of group C	74

List of Tables

2.1	Lithological composition of the lithofacies ascribed to the Echteld Formation [49]	7
5.1	Settlement rates calculated by different methods	21
5.2	Number of points and maximum distance between the points for each location	22
5.3	Average groundwater level at different monitoring wells	24
6.1	Specifications of the different locations part of group A	28
6.2	Specifications of the different locations part of group B	29
6.3	Specifications of the different locations part of group C	30
6.4	Specification of the different periods	39

Contents

Preface	iii
Summary	vi
List of Figures	vii
List of Tables	ix
1 Introduction	1
2 Geological background	5
2.1 Echteld Formation	5
2.1.1 Depositional environment	5
2.1.2 Lithofacies	5
2.1.3 Lithological composition of the different lithofacies	6
2.1.4 Distribution and thickness of the formation	7
2.2 Nieuwkoop Formation	8
2.2.1 Depositional environment	8
2.2.2 Lithological composition	8
2.2.3 Distribution and thickness of the formation	9
3 Main contributing components to the subsidence in the Netherlands	11
3.1 Natural factors	11
3.1.1 Isostasy	12
3.1.2 Compaction	12
3.1.3 Tectonics.	12
3.2 Anthropocene factors	12
3.2.1 Compaction and consolidation	13
3.2.2 Resource extraction	13
3.2.3 Groundwater management	14
3.2.4 Soil ripening	14
4 InSAR	15
4.1 Radar	15
4.2 Synthetic Aperture Radar	15
4.3 Interferometric Synthetic Aperture Radar	16
4.3.1 Deformation phase	17
4.3.2 Phase unwrapping	18
4.3.3 Different scatterers.	18
4.3.4 Reliability and precision	18
5 Methodology	19
5.1 Research area	19
5.2 Calculation software	19
5.3 Satellite data	19
5.3.1 Measurements	20
5.3.2 Points	21
5.3.3 Locations	22
5.3.4 Coefficient of Determination.	23
5.4 Subsurface data	23
5.4.1 Groundwater data	24
5.4.2 Soil data	25

6	Results	27
6.1	Three different groups	27
6.1.1	Group A: 0 to -1 mm/year	28
6.1.2	Group B: -3 to -4 mm/year	29
6.1.3	Group C: -4 to -5 mm/year	29
6.2	Settlement rate	30
6.2.1	Thickness	30
6.2.2	Ratio thickness and depth	31
6.3	Amplitude of the seasonal oscillation	32
6.3.1	Thickness	33
6.3.2	Depth	35
6.3.3	Ratio thickness and depth	36
6.4	Influence of the water table	38
6.4.1	Amplitude of the seasonal oscillation	38
6.4.2	Settlement rate.	39
7	Discussion	43
7.1	Practical eligibility	46
8	Conclusions and recommendations	49
8.1	Recommendations	50
8.1.1	Improvements	50
8.1.2	Additional research	50
	Bibliography	53
A	Points per location	57
B	Data of the locations of group A	59
C	Data of the locations of group B	63
D	Data of the locations of group C	67
E	Soil profiles	71
E.1	Soil profiles - Group A.	72
E.2	Soil profiles - Group B.	73
E.3	Soil profiles - Group C.	74

Introduction

Large parts of the Netherlands are experiencing subsidence, leading to a variety of consequences. The subsidence can have natural causes. Firstly, the lithosphere below the Netherlands is still descending as a result of the melt of the large ice mass in Scandinavia, which was present during the last glacial period. Secondly, extension of the lithosphere takes place, decreasing the thickness of the crust. However, the major part of the subsidence can be ascribed to human activity. By lowering the groundwater level, the top layer of the subsurface is dehydrating and the organic matter of peat oxidises. Furthermore, extracting natural resources at large depth results in movement of the surface. Due to the removal of material, the pressure decreases and the subsurface equilibrium is disrupted, causing the overlying material to subside.

Subsidence of land is causing a lot of problems to buildings or infrastructure. Buildings can have shallow or deep foundation. A shallow foundation is situated near the surface, while a deep foundation transfers the load of the buildings to larger depth, for example by using piles. Buildings with a shallow foundation will subside along with the subsurface, causing damages such as cracks in the walls if the subsidence is not equally distributed over the building. Buildings constructed on a deep foundation will barely subside, however other problems arise. Firstly, the surroundings of the buildings do sustain settlement and for houses this means gardens do subside. Secondly, the subsiding surroundings cause the foundations to be placed higher, which is a problem for timber piles especially. If timber piles are situated above the groundwater level, the piles can decay (“paalrot”) and the loss of part of the piles cause subsidence of the structure above [23]. Thirdly, problems with infrastructure occur as a consequence of land subsidence. Subsidence of roads may lead to cracking of the pavement or an irregular road surface. Fourthly, cables, lines and pipes of public utility companies sustain subsidence which can cause them to break [23].

The subsidence is currently measured by three different methods: gravity measurements, Global Navigation Satellite Systems (GNSS) and Interferometry Synthetic Aperture Radar (InSAR). Gravity measurements make use of the gravity of the Earth to acquire absolute values of the displacement of the Earth's surface. Each object on Earth is subjected to a certain amount of gravity force. When the surface is subsiding, the gravity force on the along moving object is increasing. Currently, there are six stations in the Netherlands where gravity measurements are taken. To enhance the reliability of the measurements, the measurements have to be carried out for several years at suitable places [14].

For the GNSS method, the positions of certain fixed stations are measured in three dimensions (North, East and vertical). The foundations of these stations are normally fixed into deep layers and therefore the method cannot capture displacement of the shallow layers [13]. The position measurement takes place using time observation by means of satellites. The satellite transmits a signal, and the time of transmitting and the satellite position are stored. Whenever the reflected signal is returned, the time and new satellite position can be compared to the stored data and is used to calculate the distance to the satellite. At least the signals of four different satellites need to be received to obtain a three-dimensional position [1]. The most common GNSS is the Global Positioning System (GPS).

Synthetic Aperture Radar (InSAR) is a technique using satellites as well. The satellites transmit a signal, and amplitude and phase of the reflected signal is stored in an image. By acquiring different images at different times, the phase difference between the images can be used to calculate the displacement at millimetre scale. The advantage of InSAR is that the technique is not dependent on pre-determined physical markers. The locations of the measuring points are dependent on the strength of the reflected signal and the consistency of

the signal in time. Therefore, hard objects such as buildings and other infrastructure are suitable for InSAR measurements, but vegetation is not [44].

The displacement values are relative in time with respect to the first acquisition, which has a displacement value of zero. The measurements are also relative with respect to a reference point, which is generally placed at a location that is stable in terms of displacement. However, subsidence mechanisms occurring at large depth are assumed to affect all measuring points [13]. There is no clear distinction between deep and shallow subsidence, however, in general, deep subsidence can be interpreted as the subsidence caused by extraction of natural resources and natural factors, which will be explained later in section 3.1. In this report the shallow subsurface is referred to as the top three metres of the subsurface. The obtained displacement measurements which are analysed in this report, are relative to a reference point. Since the reference point is also subjected to deep subsidence and the displacement values represent the shallow subsidence.

All measuring points containing a time series of displacement values can be displayed on a deformation map [44] or surface, and object motion map [13]. On the front page of this report the 'Bodemdalingskaart' [12] is shown. The 'Bodemdalingskaart' was created through a collaboration of different organisations, such as the NCG (Netherlands Geodetic Commission), TU Delft and SkyGeo. SkyGeo is responsible for the data processing and visualisation of the InSAR data. The purpose of this map is to give an estimate of the movements on measuring point level.

Research question and methodology

InSAR is already used for different purposes, e.g. monitoring displacements for slope stability and subsidence measurements caused by mining activities or various engineering projects [42]. These applications are all events where displacements are generated by human activities. The aim of this research is to investigate whether InSAR data is useful at locations where the cause of land movement is less apparent. For that reason it will be analysed how the obtained displacement values have been affected by the presence of different soil types at the location of where displacement values are obtained. In addition, the impact of the groundwater level to the displacement values is analysed. The evaluated InSAR data has been obtained in the area of Woerden, which is a city in the western part of the Netherlands. The buildings in this city are constructed on a deep foundation and thus not subjected to shallow subsidence. Therefore, buildings cannot be used as a reflecting area of the InSAR data. To minimise the effect of the reflecting area, a stable surface is desired. Since roads are not affected by changes of vegetation, it has been chosen to only analyse displacement values obtained on roads. Therefore the main research question is:

To what extent can InSAR be used to monitor land movement mechanisms in the shallow subsurface on urban roads?

In order to answer the main research question, the following sub-questions have been formulated:

- *What coherence exists between the measured settlement rate and the soil types within the soil profile?*
- *What coherence exists between the amplitude of the seasonal oscillation obtained by the InSAR data and the soil types within the soil profile?*
- *To which extent can the observed InSAR data be explained by presence of the groundwater level in the soil profile?*

Firstly, suitable locations, located on asphalt roads, within the research areas, where InSAR data could be used are needed. To increase the reliability of the data, at least four different measuring points containing corresponding output are used. To minimise the contribution of several different subsidence mechanisms, only locations with no road construction or improvement will be used. Therefore, solely the effects of dehydration and groundwater level fluctuation will remain. For all suitable locations the soil profiles are collected. Finally, the data of soil profiles, the data of the groundwater levels and the data of the InSAR are combined.

Outline

First, the geological background of the research area is given in Chapter 2. The geological background and the corresponding soil types are important because they affect different subsidence mechanisms. The subsidence mechanisms occurring in the Netherlands are described in Chapter 3. In Chapter 4 a more detailed explanation of InSAR is given. Knowing different subsidence mechanisms and how InSAR works, the methodology of this research is described in Chapter 5. In Chapter 6 the results are presented and the results are discussed in Chapter 7. Lastly, the conclusion and recommendations are found in Chapter 8.

2

Geological background

In the top part of the investigated subsurface, four different soil types are encountered. The main soil types are sand, peat and clay. The soil types can be divided into two different formations. The sand and clay are part of the Echteld Formation, which consist of fluvial deposits. In addition, small layers of gravel can be found in this formation. The peat are described by the Nieuwkoop Formation. The formations can be encountered intertwined [9]. In this chapter the geological background of both formations is given. The geological background is divided into depositional environment, composition, thickness and distribution of the formations.

The Echteld Formation and the Nieuwkoop Formation both have been deposited during the Holocene. The Holocene is the current geological epoch which started approximately 11700 years ago with the ending of the last glacial period of the Pleistocene. Towards the end of the last glacial period, the temperature on Earth started to rise [8]. The temperature rise caused ice sheets to melt, which resulted in a rise of the sea water level as well. The increase in temperature stopped around 9500 years ago when the temperature reached the values as they are nowadays on Earth. However the melt of the remaining ice sheets continued and therefore the rise of the sea water level continued as well. The sea water level reached the current Dutch coastline about 8500 years ago [18].

2.1. Echteld Formation

The Echteld Formation is characterised by its heterogeneity in lithology. This is caused by the different depositional environments related to the river. The formation consists largely of deposits of meandering precursors of the current Rhine and Meuse [49].

2.1.1. Depositional environment

Meandering rivers are rivers which are sinuous in shape and only on the inside of the bends have depositional bars [36]. In general a meandering river moves sideways by erosion of the banks at the outer bends and sediment deposition on the banks at the inner bends. The water velocity is highest in the outer bends and lowest in the inner bends. The high velocity in the outer bends results in erosion of the banks. The lower water velocity in the inner bends allows sedimentation to take place. This sediment deposition is characterised by a fining upward sequence, meaning the grain size is increasing towards the base. The heavier particles, which are mostly the largest, are deposited first. With reducing water velocity, the lighter particles are deposited as well. Therefore, the lightest and in general smallest particles can be found on top. The sequence of large particles at the bottom and decreasing particle size towards to top is called a fining upward sequence [36]. For the Echteld Formation the depositional environment of a meandering river can be divided into seven lithofacies or sedimentary units. These lithofacies are channel deposits, abandoned river channel deposits, bank deposits, crevasse splay deposits, dyke burst deposits, flood basin deposits and delta deposits [9].

2.1.2. Lithofacies

Channels are depressions in the land surface that confine the water flow of the river [36]. Channel deposits predominantly consist of sand, varying in grain size from very fine to very coarse.

Two types of *abandoned channels* can be described. Firstly the river flow can change direction and form a new channel, leaving the old channel abandoned. This event is called avulsion and normally occurs instantly

and is usually triggered during large floods. It is also possible that the river flow takes a short-cut, disconnecting a small part of the channel, in most events one loop of the meandering river. The disconnected meander loop is also called an oxbow lake [36]. The water in the abandoned channels is standing and soil particles settle. The abandoned channels are silting up by supply of sediment by water during floods. Whenever the water depth becomes 2 metres or less, development of peat can arise [18]. In the abandoned channels the most common soil type is clay, which can be alternated with small layers of sand and peat [49].

The *banks* are the land areas alongside the channel. A levee is a bank of sediment on the edge of the river channel which is higher than the level of the banks and normally the river stays between the levees. However during periods of high water level the water can overturn the levees and sedimentation on the banks or floodplain take place. The lighter particles are in the water in the top part of the channel and during floods these particles are transported by the water onto the banks. Bank deposits mainly consists of clay, but also small layers of sand are found. Horizontal layering in the sediment can be observed [49].

A *crevasse splay* occurs when the water level in the river is high. The water will break through the levee and a small branched (crevasse splay)-channel is created into the bank. Sedimentation from the channel onto the bank appear. This sediment is coarser than the deposits of the banks. The result is a great lithological variation on short distances. When branching of the crevasse-channel itself occurs, a crevasse-complex can be constructed into the bank [18].

dyke burst deposits and crevasse splays have a similar origin, since both involve a levee breach. However, dyke burst deposits are deposited with much larger flow rates [8]. dyke burst deposits particularly occur where levees intersect old channels. The sandy surface below the levee induces seepage and an underwater vortex or kolk can be created. Behind the kolk the material is deposited in the shape of a fan [10].

The *flood basin* is the lowland area near a river and is found behind the banks. When flooding occurs, the water will overflow the banks and floods the flood basins. The subsurface of the flood basins is slightly concave and therefore water will rest in these areas. In the standing water the soil particles in the water will settle [18]. Clay is predominantly present in flood basins, but also some plant remains of reed and wood are observed [49].

Lastly *deltas* can be found at the end of the river, the so-called river mouth. The river mouth is located where the water of the river flows into a lake or the sea and the flow velocity is abruptly reduced by the standing water of the sea or lake. The suddenly reduced velocity results in deposition of the transported material, where the coarsest material is deposited first [36]. The delta deposits ascribed by the Eichteld formation predominantly consist of sand and often alternating layers of sand and clay are encountered [49].

Within the research area, most deposits have been deposited as (abandoned) channel or bank deposits. Most other lithofacies can also be encountered within the research area, however, delta deposits are certainly not found inside the area.

2.1.3. Lithological composition of the different lithofacies

Because of the large variety in the different lithofacies, the lithological composition of the lithofacies is summarised in Table 2.1. In general sand is deposited in or near the river channel. The clay particles are lighter and will be transported over larger distances, therefore clay is deposited outside the river channel where the flow velocity is less than in the channel.

The colour of all lithofacies can be said to be grey to brown. Above the phreatic surface the colour of the lithofacies is brown. Below the phreatic surface the colour of the lithofacies is gray, except organic clay which has a brown-gray colour. In general the channel, bank and crevasse splay deposits are calcareous below the phreatic surface.

Table 2.1: Lithological composition of the lithofacies ascribed to the Echteld Formation [49]

Unit	Occurrence of the soil type		Characteristics
	Predominantly	Occasionally	
Channel	Very fine to very coarse (63 – 2000 μm) sand, occasionally gravelly	Clay, sandy or strong silty	Lateral accretion surfaces Fining upward sequences Freshwater shells
Abandoned channel	Clay, weak to strong silty and occasionally organic	Very fine to moderately coarse (63 – 300 μm) sand Thin layers of peat	Freshwater shells
Bank	Clay, sandy and weak to strong silty	Very fine to fine (63 – 150 μm) sand	Remnants of freshwater shells
Crevasse splay	Clay, sandy and weak to strong silty Often thin layers of very fine to fine (63 – 300 μm) sand	Very fine to very coarse (63 – 2000 μm) sand	Freshwater shells Large lithological variation over short distances, in vertical and horizontal direction
Dyke burst	Clay, sandy and moderate to strong silty	Very fine to very coarse (63 – 2000 μm) sand	Very poor grain size sorting
Flood basin	Clay, weak to moderately silty and weak to strong organic		Plant residues of reed and wood
Delta	Very fine to fine (63 – 210 μm) sand	Clay, moderate to strong silty	Marine shells

2.1.4. Distribution and thickness of the formation

In Figure 2.1a the distribution of the Echteld Formation in the Netherlands is shown, along with today's larger Dutch rivers. It can be said that most of the deposits are located in the river basins of the Rhine and Meuse. The other parts of the formation are located near smaller rivers, which are originally branched channels of the Rhine.

The thickness of the Echteld Formation varies from 1 meter in the eastern part up to 20 metres in the western part of the Netherlands [9]. The thickness of the channel deposits is varying from 5 to 15 metres [49].

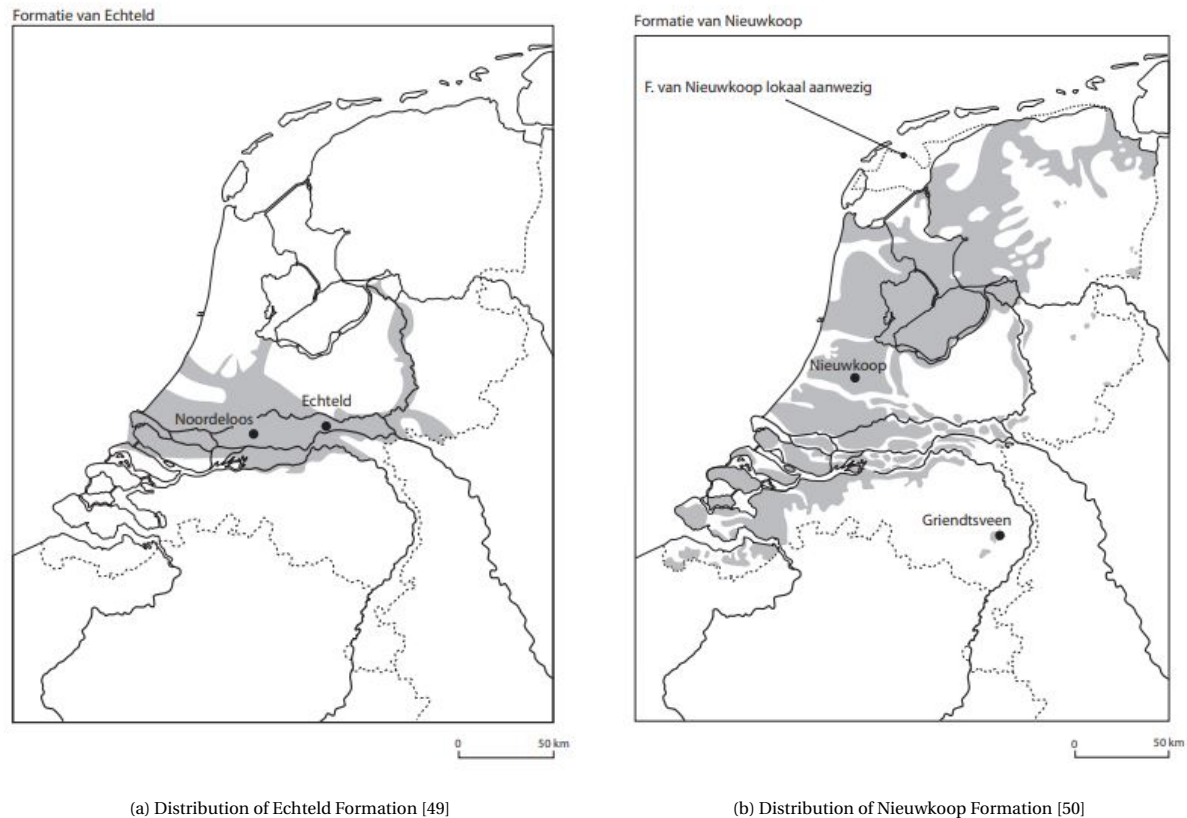


Figure 2.1: Distribution in the Netherlands of the Echteld Formation and Nieuwkoop Formation

2.2. Nieuwkoop Formation

The Nieuwkoop Formation can be subdivided into four different members, namely Griendtsveen, Holland Peat, Basal Peat and Flevomeer [9]. Only the Basal Peat member and Holland Peat member are located in the research area.

2.2.1. Depositional environment

The rise in sea water level also caused the groundwater level to rise, which created large swamps in the coastal areas. In these swamps the Basal Peat member was formed. Due to further increase of the sea water level, large parts of the coastal areas were flooded and mudflats were created which resulted in covering the Basal Peat by marine deposits, consisting of primarily clay [18].

The rise of the sea water level also induced the development of beach ridges parallel to the coast by supply of sand originating from the seabed of the North Sea. The beach ridges increased and connected and therefore the marine influence behind the beach ridge decreased, which resulted in the formation of lagoons behind the beach ridges. When the salinity of the water in the lagoons behind the beach ridge was reduced by supply of fresh water from rivers and rainfall, the Holland Peat member was formed [18].

2.2.2. Lithological composition

The predominant soil type of this formation is brown to black peat. Some of the peat can be characterised as clayey, the peat has a grey-brown to brown colour. Occasionally gyttja is present, which has a yellow to green-brown colour [50]. Gyttja is a fine-grained organic mud which can be formed when the water depth is at least 2 metres [9].

Classification of the peat is based on the nutrients in the environment in which the peat-forming plants occur. The environment can be eutrophic (high nutrient content) or oligotrophic (low nutrient content). In the different environments, different types of peat can develop depending on the present vegetation and

the water depth. The sequence for an eutrophic and oligotrophic environments are indicated in Figure 2.2. For an eutrophic environment the sequence is as follows: gyttja, reed peat (*rietveen*), sedge peat (*zeggeveen*), forest peat (*bosveen*) and swamp forest peat (*not indicated in Figure 2.2*). Gyttja develops when the water depth is more than 2 metres. When the water decreases below 2 metres, reed peat can develop. Sedge peat develops when the water depth is less than 0.5 meter. The difference between forest peat and swamp forest peat is the ratio of the present trees. When there are mainly birches (oligotrophic environment) or alders (eutrophic environment), it is called forest swamp. When the amounts of trees are equal, it is called swamp forest peat. In the oligotrophic environment, sphagnum peat (*mosveen*), heath peat (*not indicated in Figure 2.2*) and dy can develop. Dy is the oligotrophic brown-black variant of gyttja. In the Holland Peat member reed peat, sedge peat, forest peat, swamp forest peat, heath peat and sphagnum peat can be encountered. The Basal Peat member mainly consists of reed peat or forest peat, although gyttja and sedge peat can be present as well [9].

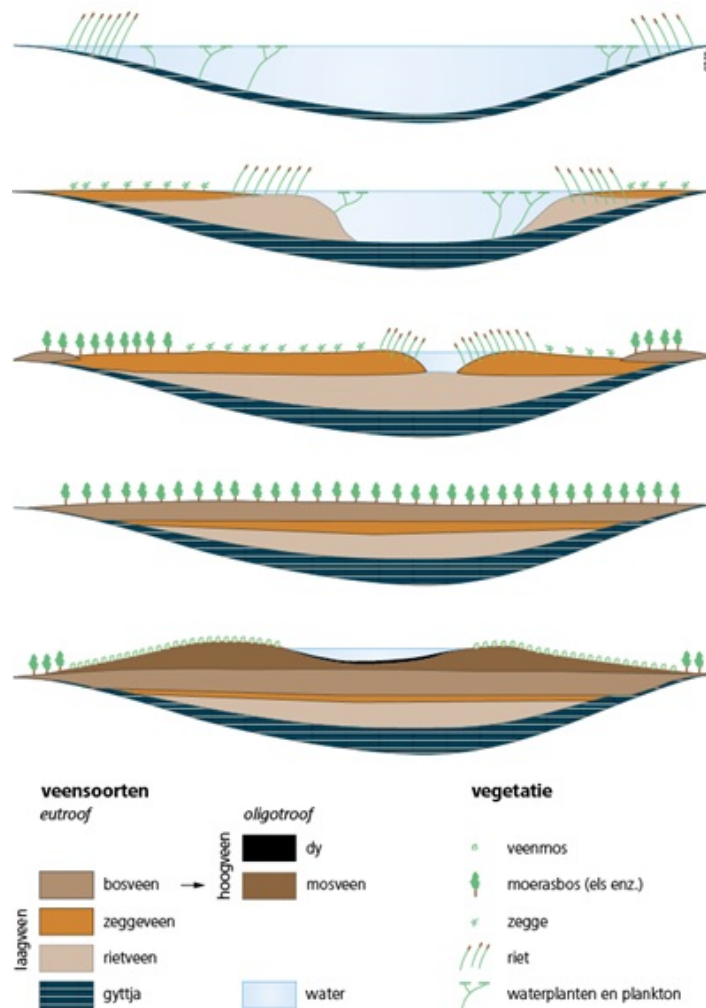


Figure 2.2: The development of different types of peat [18]

2.2.3. Distribution and thickness of the formation

The distribution of the Nieuwkoop Formation throughout the Netherlands is represented in Figure 2.1b. The formation is located near the deposits of the Echteld Formation and in the coastal regions, both northern and western coastal areas of the country. The thickness of the Nieuwkoop Formation is on average between 0.5 and 4 metres, however values of 8 metres or less than 0.1 meter can be encountered as well [50]. In general the thickness of the Basal Peat member is between 0.1 and 0.6 meter and the thickness of the Holland Peat member approximately 5 metres [48].

Main contributing components to the subsidence in the Netherlands

Subsidence is defined as "The sudden sinking or gradual downward settling of the Earth's surface with little or no horizontal motion" [27]. Subsidence is taking place largely throughout the Netherlands induced by various causes. These causes can be divided into natural and anthropocene factors. The natural factors are mechanisms which can not be controlled by human. The anthropocene factors are induced or reinforced by human activity. The most common causes for subsidence in the Netherlands are explained in this chapter.

3.1. Natural factors

The natural or geological factors of ground subsidence can be divided into isostasy, compaction and tectonic causes and these factors will be further explained in this section. Figure 3.1 indicates the values of these factors applicable in the Netherlands for the last 2.5 million years. The values for compaction are varying between -0.05 and 0.00 mm per year, for isostasy between -0.15 to 0.00 mm per year and for the tectonic causes between -0.07 to 0.03 mm per year. The positive values indicate tectonic causes also provoke uplift.

2.5 Ma - Present (Quaternary)

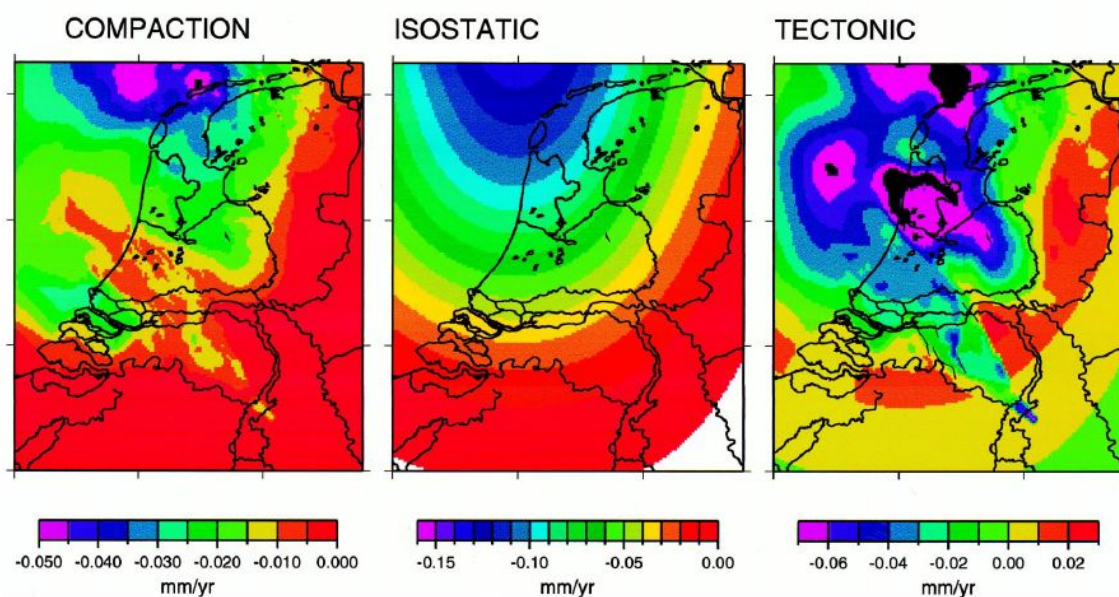


Figure 3.1: Contribution of compaction, isostasy and tectonics to ground subsidence in the Netherlands for the last 2.5 million years [24]

3.1.1. Isostasy

The two outer layers of the Earth are the lithosphere and the asthenosphere and their division is based on mechanical properties [21]. The lithosphere is the Earth's crust and part of the upper mantle and behaves as a rigid solid. The asthenosphere is the ductile and highly viscous part of the upper mantle and is found below the lithosphere [45]. Because of the ductility of the asthenosphere, buoyancy is created meaning the lithosphere floats on the asthenosphere [41].

In terms of subsidence, isostasy is the movement related to adjustment in buoyancy of the lithosphere due to mass changes induced by sediments, ice and water [24]. Two components of isostasy are glacio-isostasy and hydro-isostasy. Glacio-isostasy is the change in surface loads caused by the presence of ice sheets [6]. During the last glacial period northern Europe was covered by large ice sheets up to 2,5 km thick, which caused additional surface loads to the lithosphere and led to subsidence of hundreds of metres [18]. The elasticity of the lithosphere caused other nearby parts of the lithosphere, including the Netherlands, to raise. At the end of the last glacial period the temperature started rising and the ice sheets were melting. The melting of the ice sheets resulted in a decrease of the surface load, leading to post-glacial rebound. Post-glacial rebound is the process of returning to an isostatic equilibrium [22]. Currently parts of the Netherlands are still subsiding as a result of the post-glacial rebound.

Hydro-isostasy is the change in surface loads on the lithosphere caused by the presence of water. During glacial periods, the water is stored in ice sheets on land and therefore the loads on the oceanic crust are reduced resulting in uplift of the oceanic crust [6]. Melting of the ice sheets resulted in an increase of the sea-level and therefore flooding of The North Sea basin. The flooding increased the water loads leading to subsidence of the bottom of the basin and therefore enhancing the subsidence due to glacio-isostasy [9].

3.1.2. Compaction

Compaction is the subsidence caused by compression of layers of sediment or rock in vertical direction by loading of overlying sediment [24]. The solid-particles are not compressible itself but the soil skeleton is, therefore compaction occurs by reduction of the pore space. The additional load of the overlying sediment results in excess pore water or gas pressure. The excess pressure generates dissipation of the present water or gas and the rate of this dissipation is controlled by the permeability of the layer [29].

Cenozoic deposits in the Netherlands can be divided into Tertiary, Pleistocene and Holocene deposits. The Tertiary deposits mainly consists of large amounts of clay, deposited in a shallow marine environment. The Pleistocene and Holocene deposits are primarily of fluvial origin and the sediment mainly consists of sand for the Pleistocene deposits and clay and peat for the Holocene deposits [30]. Studies on the coastal areas of the Netherlands show that the Tertiary clay deposits largely contribute to the subsidence due to their substantial thickness and low permeability [28]. The contribution to the subsidence by the Holocene deposits is assumed to be small due to their relatively small thickness of the layers.

3.1.3. Tectonics

The lithosphere is not one piece of material, but it is broken into several tectonic plates and the Netherlands is located on the Eurasian Plate. The plates move relative to each other causing tension within the plates. The tensions are creating folds or faults within the rock layers and result in uplift or subsidence of the ground level [26]. As a result of normal faults, a horst and graben structure can arise, where the horst is a raised fault block bounded by the faults and a graben is a depressed fault block [21].

Figure 3.1 indicates some of the tectonic structures within the Netherlands. The green area in the southeast of the Netherlands is part of the Roer Valley Graben along with the Peel High, the red area on the northeast part of the graben [24]. The blue area in the western part is the West Netherlands Basin [39]. Also two pink areas can be seen, indicating large values of subsidence. These areas are the Zuiderzee Basin [24] for the southern pink area and the Vlieland Basin for the northern pink area [39].

3.2. Anthropocene factors

The anthropocene factors contributing to ground subsidence are a result of human activity. The most common causes by human activity are constructing of structures, resource extraction and groundwater level management and these causes will be briefly explained in this section.

3.2.1. Compaction and consolidation

Consolidation and compaction are processes which occur when the subsurface is loaded by the weight of buildings or infrastructure. The difference between compaction and consolidation lies in the presence of water within the pores. Consolidation is the process of volume change of a soil due to drainage of water out of the pores and compaction is the volume change of a soil due to drainage of air from the pores.

The applied load causes an increase in pore water pressure which leads to drainage of the excess water. The drainage of the water is dependent on the permeability of the soil. Sand does have a high permeability and drainage will occur rapidly. Drainage for soils with lower permeability, such as clay, will take much longer and therefore the final settlement will take place over a longer period of time. Besides the permeability of the layer, the rate of consolidation is affected by the thickness and compressibility of the layer. The highest values of subsidence due to consolidation can be found in weak clay or peat layers distributed during the Holocene. These layers are located in the northern and western parts of the Netherlands [15].

3.2.2. Resource extraction

Extraction of resources in the Netherlands can be divided into extraction of oil, gas, salt, coal or water. In this section, the consequences of extracting the different resources is briefly explained. The method of extracting and depth of extracting is not the same for the resources and therefore a different response of the subsurface is occurring. However, all responses will lead to subsidence.

3.2.2.1. Oil and gas

Extraction of oil or gas leads to a decrease of pore pressure in the reservoir rock. This reduction of pore pressure results in an increase of the total stress of the reservoir rock and as a consequence the rock layer will be compacting. The amount of subsidence as a result of the compaction is dependent on the depth of the extraction, the dimensions and size of the field and the mechanical properties of the reservoir rock [4]. The maximum subsidence in one of the largest gas field in the Netherlands, the Groningen gas field, is measured at 33 centimetres in the period of 1964 to 2013 [33]. The Netherlands counts 253 producing gas fields in total of which only 106 gas fields are located onshore. Also two out of twelve producing oil fields can be found onshore [46].

3.2.2.2. Salt and coal

Oil and gas extraction is not the only form of mining taken place in the Netherlands; salt is also being mined. Typically salt mining occurs as solution mining, a process where fresh water is pumped into the ground dissolving the salt and thereafter the brine is pumped out. The cavities created by the removal of the salt remain filled with brine. However, the brine in the cavities has a lower density than the initial salt. The potential subsidence in the regions occur due to compaction of the cavities by the changes of density and is dependent on the amount of extracted salt and the properties of the surrounding layers [26].

However, another used method is the squeeze-method. The squeeze-method is based on the mechanical properties of the salt, which becomes ductile at certain depth. The pressure within the salt cavern is lowered and the weight of the overlying sediment presses the salt towards the wells, where it will be pumped out. For this method no caverns are left but the subsidence occurs because the salt is removed and the overlying sediment is filling the loss of volume [34]. This method has been used at a location in Veendam and the subsidence at this location is expected to be 69 centimetres in 2025 [35].

In the past, mining of coal occurred in the southern part of the Netherlands, but the mines have been closed since 1974. During the underground mining operations, the area suffered subsidence up to several metres. Also the groundwater level was lowered by hundreds of metres in order to allow mining which also resulted in subsidence. The consequences nowadays are uplift of the area due to ongoing rise of the groundwater level [4]. Also the remaining adits and caverns can become unstable and could therefore collapse, which leads to subsidence on local scale [15].

3.2.2.3. Groundwater

Extraction of groundwater normally takes place in the subsurface with much lower depth than extraction of oil and gas. The layers of which groundwater are extracted is more sensitive for consolidation and compaction than layers located at higher depth. By extracting the groundwater, the water pressure in the layers is decreased and therefore consolidation occurs. Typical values for the annual rate of subsidence are in the order of a centimetre per year [26].

3.2.3. Groundwater management

In the Netherlands there are water boards, which are regional government organisations with the responsibility of maintenance of water barriers, waterways and water levels and wastewater purification [19]. Maintenance and managing of the groundwater level is important to prevent water shortage in periods of drought and flooding in periods of high rainfall. However, maintaining the groundwater level at a certain level has some disadvantages as well.

To maintain the groundwater levels, drainage of the water occurs when the water level is too high. Due to the drainage, the top layer of soil is dry causing consolidation and ripening of peat and clay sediments. The volume change of the soil due to consolidation occurs because of the decrease of water pressure [26]. The next section is about soil ripening to clarify the process.

3.2.4. Soil ripening

Soil ripening can occur in natural conditions. However, artificial drainage is a sudden process compared to the velocity of drainage in natural conditions and soil ripening proceeds more quickly under artificial drainage. This is why the process of soil ripening is mentioned as anthropocene effect of groundwater level management. Ripening of peat and clay sediments starts at the moment of drainage: oxygen enters the soil and chemical processes are started. Ripening can be divided into three sub-processes, namely physical, chemical and biological ripening. The different processes occur more or less simultaneously. Physical ripening includes all processes related to the dehydration of the colloidal part of the soil. Chemical ripening involves all chemical and physico-chemical changes of sediments, e.g. oxidation of different components in originally reduced environments. Biological ripening is the result of the activity of all sorts of fauna and flora present within the soil, such as withdrawing moisture from the soil by transpiration of the plant roots [37].

The two main consequences of soil ripening are the loss of organic material and of the water absorption qualities of the soil. As a result of chemical ripening, part of the organic material is oxidised and disappears. This process occurs in all types of sediment containing organic material but has the most effect on peat soil, since it means that part of the soil skeleton itself disappears resulting in reduction of the volume of the soil [37].

Part of physical ripening is the change of the microstructure of clay minerals and very small particles of organic material. Normally, water is stored in the cavities of the crystal lattice of the particles or form a small coating of water around the soil particles. Due to the physical ripening, water is withdrawn from the cavities and the volume of the sediment is reduced. The changes in structure also cause the soil not being capable of absorbing the same amount of water again in the cavities and therefore the process of withdrawal of water out of the cavities is an irreversible process [37].

4

InSAR

Remote sensing or satellites are increasingly important in the techniques of observing the Earth. InSAR or Interferometric Synthetic Aperture Radar is a remote sensing technique that can be used to derive movements of the Earth's surface on millimetre scale. This technique has been part of this study and therefore will be further explained in this chapter.

4.1. Radar

Radio Detection And Ranging (radar) is “a method, system or technique, including equipment components, for using beamed, reflected, and timed electromagnetic radiation to detect, locate or track objects, to measure altitude and to acquire a terrain image” [5]. The radar system consists of a transmitter and a receiver. The transmitter transmits electromagnetic pulses within the radio wave and microwave wavelengths. When an object is hit, the pulses will be reflected and the receiver will pick up these reflected signals [5]. The distance to the detected object can be determined by the two way travel time of the pulse. Furthermore, physical quantities such as size or surface roughness of the object can be derived [25]. The advantage of the use of radio waves and microwaves by radar is that these waves can pass through clouds, rain and dry snow and therefore radar is hardly obstructed by unfavourable weather conditions [5].

4.2. Synthetic Aperture Radar

Synthetic Aperture Radar (SAR) is part of the imaging radars [25]. The side-looking radar system is attached to an aircraft or satellite and its antenna transmits short pulses as the aircraft or satellite moves. The reflected pulses are received by the same antenna and used to produce an image. The limitation of the resolution in flight direction by the physical length of the antenna is reduced by the motion of the system, synthetically enlarging the length of the antenna. This enlargement of the antenna leads to an increase of the resolution in flight direction of about three orders of magnitude [25].

A representation of the geometry of a typical SAR system can be found in Figure 4.1. The azimuth is the flight direction of the aircraft or satellite and the range is the direction perpendicular to the flight direction. The slant range is the distance between the antenna and the hit object and is represent by R . The incidence angle or look angle is the angle between the surface normal and the radar beam and is often represented by θ . The radar footprint or the resolution cell is determined by the resolution in range and azimuth. The resolution cell is responsible for the radar reflection data of all scatterers mapped to a single pixel [25].

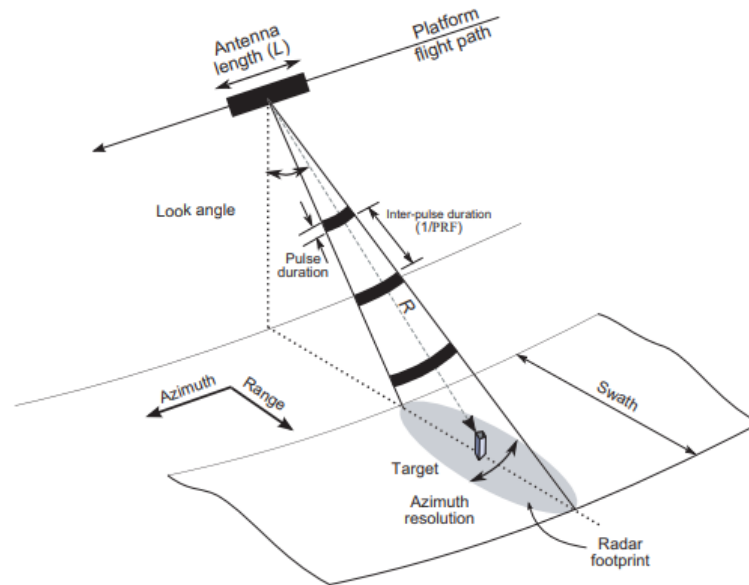


Figure 4.1: Geometry of a Synthetic Aperture Radar system [2]

The pixels are often represented as a grid, although it does not have a physical size since they are infinitesimally small points [25]. The data of one pixel includes the coherent sum of all reflected signals within that pixel, including a phase and an amplitude, stored as a complex number, Equation 4.1 [17].

$$P = A^i \psi \quad (4.1)$$

In this equation, i is the imaginary number and the amplitude and phase of the reflected signal are represented by A and ψ [17]. The amplitude gives the intensity I of the reflection as $A = \sqrt{I}$ [47].

The phase is determined by the time delay between transmitting and receiving the signal. The signal is a sinusoidal function and therefore time delay is equivalent to the phase change, ϕ , between the signals [3]. The formula for this phase change is found in Equation 4.2.

$$\theta = \frac{2\pi}{\lambda} 2R = \frac{4\pi}{\lambda} R \quad (4.2)$$

The sinusoidal function has a period of 2π , λ is the wavelength of the signal and $2R$ is the two-way distance, where R is the slant range [3].

The complex phasor can be divided into an imaginary and real part, $Im\{P\} = A \sin(\psi)$ and $Re\{P\} = A \cos(\psi)$ [47]. The real and imaginary part of the phasor are related to the amplitude (Equation 4.3) and phase (Equation 4.4).

$$A = \sqrt{(Re(P))^2 + (Im(P))^2} \quad (4.3)$$

$$\psi = \arctan\left(\frac{Im(P)}{Re(P)}\right) \quad (4.4)$$

4.3. Interferometric Synthetic Aperture Radar

Interferometric Synthetic Aperture Radar (InSAR) is a technique where the phase difference between two SAR-images is used to create an interferogram. Interferometry is used for the measurement of small displacements of an object. The images need to be aligned and resampled to the same grid since two observations are never retrieved from the exact same point. The complex phasors can be multiplied, giving a complex interferogram, which contains the phase difference and amplitude multiplication of the two data sets [25]. The formula to calculate the complex interferogram is given by Equation 4.5 [47].

$$P^{ms} = P_m \cdot P_s^* = A_m \cdot A_s \cdot \exp(i \cdot (\psi^m - \psi^s)) \quad (4.5)$$

In the formula $(.)^*$ denotes the complex conjugate part and m and s stands for the master and slave image. $(\psi^m - \psi^s)$ is the interferometric phase φ^{ms} for a single pixel, which is the difference in phase values of different images [17]. The formula for the calculation of the interferometric phase is shown by Equation 4.6 [47].

$$\varphi^{ms} = \psi^m - \psi^s = -2\pi a + \varphi_{flat} + \varphi_{topo} + \varphi_{defo} + \varphi_{atmo} + \varphi_{orb} + \varphi_{scat} + \varphi_{noise} \quad (4.6)$$

The phase ambiguity or a , is the number of full cycles. φ_{flat} is the 'flat Earth' phase and describes the contributions due to a reference ellipsoid, where topography is absent. φ_{topo} describes the influence of the present topography to the flat ellipsoidal surface. Both φ_{flat} and φ_{topo} are related to a different position of the antenna at acquiring the different images. φ_{defo} is the contribution as a result of the displacement of the surface, which causes a change in the signal travel path length. φ_{atmo} is the phase caused by the atmospheric delay, as a result of different atmospheric conditions during the two acquisitions. φ_{orb} is the phase difference due to error in the orbit parameters. φ_{scat} describes the difference between the scatter characteristics of the observed area within a resolution cell during the two acquisitions. In φ_{noise} all other sources of noise are collected, such as thermal and processing noise. [47]

4.3.1. Deformation phase

The displacement of the surface is of particular interest in this study and therefore the deformation phase will be briefly explained into more detail. The displacement causes a change in the travel path length and the phase can be calculated as represented in Equation 4.7 [47]. In this equation D_{LOS} is the measured difference in path length in the line of sight (LOS) or slant-range direction.

$$\varphi_{defo} = \frac{-4\pi}{\lambda} D_{LOS} \quad (4.7)$$

The line of sight measurement can measure both horizontal and vertical deformation. The measurement is the projection of the actual three-dimensional displacement vector, \vec{d} . This vector consists of a North (d_n), East (d_e) and up (d_u) direction. For a satellite with an orbit heading α , defined with respect to the North, the relation is shown by Equation 4.8 [47].

$$\begin{aligned} D_{LOS} &= d_u \cos(\theta) - \sin(\theta)[d_n \cos(\alpha - 3\pi/2) + d_e \sin(\alpha - 3\pi/2)] \\ &= d_u \cos(\theta) - \sin(\theta)[-d_n \sin(\alpha) + d_e \cos(\alpha)] \end{aligned} \quad (4.8)$$

The equation is applicable for a right-looking satellite and is slightly different for a left-looking satellite. In the formula θ is again the incidence angle and $(\alpha - 3\pi/2)$ is the angle with the azimuth look direction which is perpendicular to the satellite orbit. In Figure 4.2, the deformation vector components are represented visually.

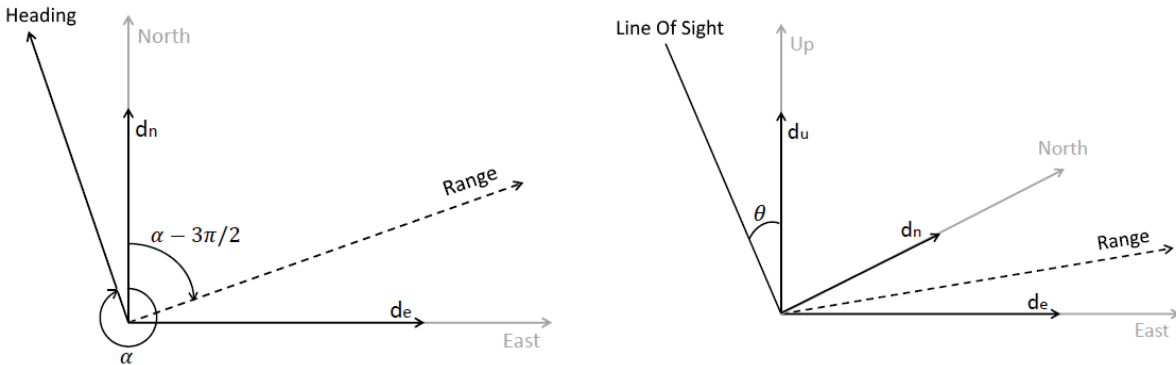


Figure 4.2: Decomposition of the deformation vector represented in a top-view (left) and 3D view (right) [16]

4.3.2. Phase unwrapping

The obtained interferogram only contains the relative phases in the interval $[-\pi, \pi)$ [25]. Phase unwrapping is the process of converting the relative phases to absolute phases by adding number of cycles (2π) to the relative phase [5]. The absolute phases are necessary because they can be translated to deformation values [47].

Phase unwrapping can be done by different methods and is often executed in two steps. The first step is always the most crucial since it strongly depends on the smoothness of the signal. For instance, using Persistent Scatterer Interferometry, a certain pixel is first unwrapped in time followed by spatial unwrapping. For this method a certain smoothness of the signal is required. Other methods can first unwrap spatially followed by an integration in time. [47]

4.3.3. Different scatterers

As described in Section 4.2, a pixel includes the coherent sum of all reflected signals or scatterers. The most common type of scatterers are the Persistent Scatterers and Distributed Scatterers, shown by Figure 4.3. The Persistent Scatterers are pixels that are dominated by one large reflector. The reflecting objects have high reflecting properties and reflect the majority of the signal. The strongest reflections come from buildings and other structures [44].

Distributed Scatterers is a pixel containing many weaker reflections, at a relatively similar strength. The derived displacement originates from a larger homogeneous area represented by multiple small reflections rather than one large reflection from a single object. When the transmitted signal hits a smooth object, most part of the signal bounces off and only a very small part is reflected to the satellite. Because roads can be considered as smooth objects, the Distributed Scatterers are applicable for roads [44].

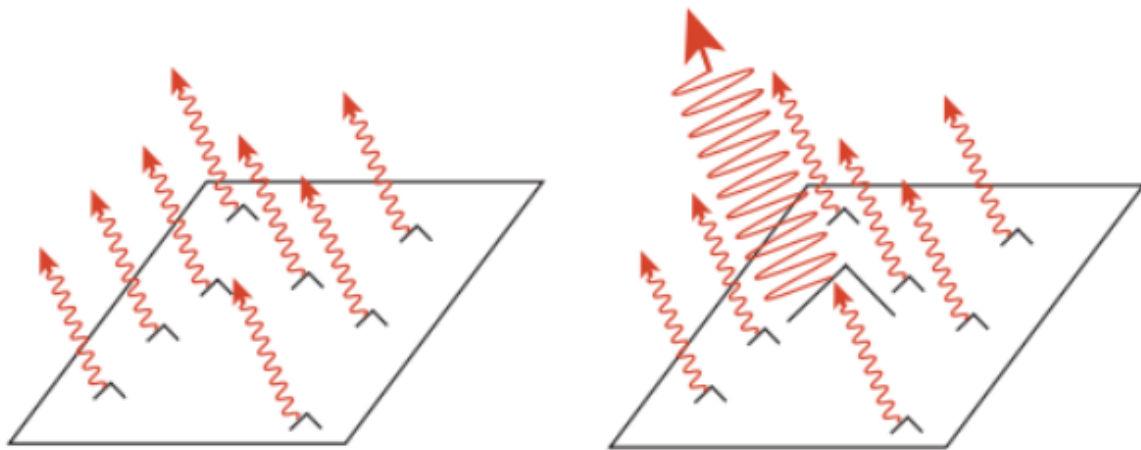


Figure 4.3: Distributed Scatterer (left) and Persistent Scatterer (right) [7]

4.3.4. Reliability and precision

The reliability of the measurements mostly depends on how well the phase unwrapping is performed. Crucial factors influencing the phase unwrapping are the noise level of the observations, the spatial and temporal smoothness of the actual deformation signal and the atmospheric influence [47].

The precision of the individual measurements and its point location depends on the satellite resolution. The resolution of the used data set is a high resolution with a size of 3.0 by 2.1 m. The precision of the individual measurement is 2 to 3 millimetres. The precision of the point location is in the order of 1 to 2 metres. This could mean a certain point appears to be in the water, while it actually gives the deformation of a quay wall [44].

5

Methodology

In this chapter the methodology is described. The data is divided into two groups, namely satellite data and subsurface data. In the satellite data section, usage of the provided satellite data is described as well as the derivatives of the provided satellite data. The subsurface data section describes the acquirement of the soil profiles. In this section the information about the ground water levels is given as well.

5.1. Research area

The data has been acquired in the area visualised in Figure 5.1. The research area has been limited to the city of Woerden, which is a city in the western part of the Netherlands. In this study only asphalt roads with no road construction for at least 10 years are used. Roads are used because they are flat surfaces constructed with a shallow foundation, meaning they move along with the ground movement. Foundations of roads consists of different layers of material to spread the loads originating from the road. The foundation layers below the roads analysed in this research are currently unknown and therefore have not been included. It is assumed for the roads, the external processes, such as consolidation, have been finished after 10 years if no construction works have taken place in the meantime.

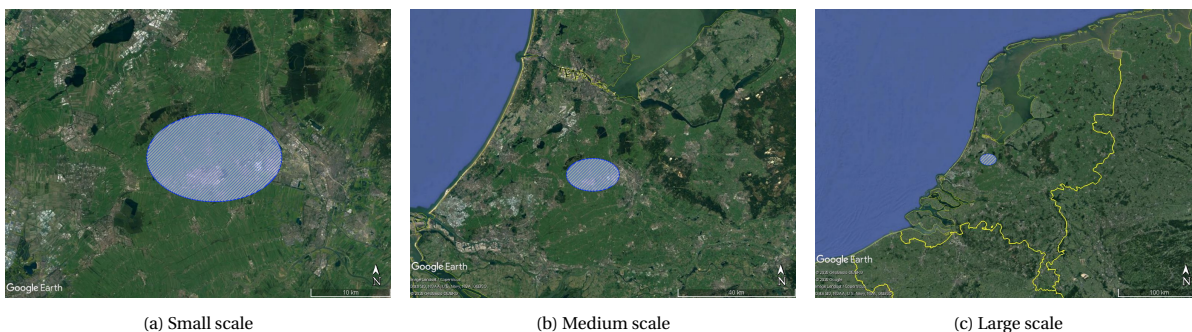


Figure 5.1: Location of the research area

5.2. Calculation software

The executed calculations for this research have been performed using MATLAB®. MATLAB has been developed by MathWorks and is programming language primarily designed for numeric computing. MATLAB can be used for statistics, calculation of functions, plotting of data, matrix manipulations, writing and implementing of algorithms and creation of graphical user interfaces [32].

5.3. Satellite data

In this research, the distinction is made between measurements, points and locations. Measurements are the individual displacement values computed on a certain date. The first displacement value is the start of the time series and this value is set to zero. All following displacement values are relative to the measurement. The series of multiple measurements form one point. For each point, a total of 99 measurements have been computed. The locations are the positions of corresponding points within the research area. There are 21

locations in the area consisting of multiple points, varying from four to eleven, and each of these points contains 99 measurements.

5.3.1. Measurements

Each series of measurements contains 99 individual measurements, which have been obtained between 22 November 2013 and 15 July 2017. The individual measurements are not useful for analysis, since the precision is not accurate enough as addressed in Section 4.3.4. However, the measurements can be used to obtain an overall and linear trendline. The overall trendline approximates the trend in the data of the measurement time series the best. The overall trendline shows fluctuation in the displacement values. The increase of the displacement values is partly reversed, followed by a new increase of displacement values. The linear trendline represents the resulting settlement rate since the increase of the displacement values is larger than the reversal.

Overall trendline

The overall trendline is the trendline which approaches the data best. The overall trendline consists of a linear component and a periodic component. The linear component includes the vertical movement of a measurement point in time and the periodic component comprises the seasonal effect. A certain measurement point can have a linear and periodic movement and all factors will have a certain value. However, one of the two components can also be absent. In that case, the factors of that component will be set to zero. The overall trendline can be derived using Equation 5.1.

$$y_i = x_1 + x_2 t_i + x_3 t_i^2 + x_4 \sin(2\pi t_i) + x_5 \cos(2\pi t_i) \quad (5.1)$$

In this formula y_i represents the displacement value derived at time t_i . The value for time t_i is given by the difference in time between the first measurement and measurement i , expressed in years minus 1.9317. The value 1.9317 represents the middle of the timeline and is derived by adding all differences in time between the first measurement and measurement i , divided by the total number of measurements, expressed in years. The value does not correspond to the difference in time between the first and last measurement divided by two, because the measurements are not constant in time. Normally the measurements are taken every 11 days, however some measurements are lacking which causes the middle of the timeline to shift.

The factors x_i determine the shape of the trendline. The shape factors for each measurement series are different and can be derived by solving a matrix equation with a $[A]\{x\} = \{y\}$ structure. Matrix A contains the time-dependent variables for each measurement. Each row of the matrix is constructed by the variables of the corresponding t_i , so there will be 99 rows and 5 columns in total. Since x_1 is not dependent on time, the first column exists of ones. Vector \bar{x} represents the shaping factors of the trendline and vector \bar{y} represents the displacement values at each t_i , given by the satellite data. The outline of the matrix equation is represented by Equation 5.2.

$$\begin{bmatrix} 1 & t_1 & t_1^2 & \sin(2\pi t_1) & \cos(2\pi t_1) \\ 1 & t_2 & t_2^2 & \sin(2\pi t_2) & \cos(2\pi t_2) \\ \vdots & \vdots & \vdots & \vdots & \vdots \\ 1 & t_{99} & t_{99}^2 & \sin(2\pi t_{99}) & \cos(2\pi t_{99}) \end{bmatrix} \cdot \begin{bmatrix} x_1 \\ x_2 \\ x_3 \\ x_4 \\ x_5 \end{bmatrix} = \begin{bmatrix} y_1 \\ y_2 \\ \vdots \\ y_{99} \end{bmatrix} \quad (5.2)$$

Linear trendline

The linear trendline disregards the seasonal effect of the measurements and is used to approach the vertical movement of the measurement points in time. The structure of the linear equation is $y_i = at_i + b$, where a and b are the slope and intercept with the y-axis respectively. For the construction of the linear trendline the function *polyfit*, a built-in function of MATLAB, has been used. The input for this function (referred to as p in this report) are the x-values and y-values of the function and the degree (n) of the desired polynomial fit, represented by Function 5.3. The result of p is a vector of length $n+1$ and contains the coefficients in descending powers, being a and b of the linear trendline.

$$p = \text{polyfit}(x, y, n) \quad (5.3)$$

Amplitude of seasonal oscillation

The amplitude of the seasonal oscillation indicates the magnitude of the seasonal effect. The amplitude is calculated using the factors x_4 and x_5 , which are the individual amplitudes of the sine and cosine components of Equation 5.1. The overall amplitude of the equation can be calculated by the equation shown in Equation 5.4.

$$\text{Amplitude of seasonal oscillation} = \sqrt{x_4^2 + x_5^2} \quad (5.4)$$

Settlement rate

The settlement rate can be calculated by using three different methods. The first method uses the data sheet provided by *SkyGeo*. For each point the linear displacement has been given. The given values have been averaged and are found in Table 5.1.

For the second and third method the function *polyfit* in MATLAB again has been used. For the second method the values of the overall trendline are used as input for the function. For the third method the measurement values for the different points are averaged first, given one set of the measurement values. This set of measurement values is used as the input for the *polyfit* function. This method does not exclude any outliers of the measurement values. This consequence can be seen in Table 5.1, since the settlement values for the third method are, in general, more diverging from the other values.

For the analysis of the results, the second method will be used since this method is less prone to outliers than the third method. Also the exact methodology for the establishment of the first method is not known. However, the third method will be used in Section 6.4.2 as the second method will not be practicable.

Table 5.1: Settlement rates calculated by different methods

Location	Method 1 [mm/year]	Method 2 [mm/year]	Method 3 [mm/year]
A1	-0.66	-0.73	-0.83
A2	-0.94	-0.99	-1.08
A3	-1.15	-1.20	-1.30
A4	-0.36	-0.45	-0.57
A5	-0.74	-0.71	-0.66
A6	-0.30	-0.34	-0.37
A7	-0.75	-0.85	-0.96
B1	-3.73	-3.67	-3.55
B2	-3.84	-3.84	-3.92
B3	-3.35	-3.48	-3.68
B4	-3.80	-3.64	-3.50
B5	-3.62	-3.57	-3.53
B6	-3.20	-3.28	-3.41
B7	-3.03	-2.98	-2.89
C1	-4.27	-4.29	-4.43
C2	-4.57	-4.51	-4.46
C3	-5.11	-5.07	-5.01
C4	-4.52	-4.40	-4.22
C5	-4.48	-4.39	-4.27
C6	-4.47	-4.48	-4.51
C7	-4.75	-4.79	-4.87

5.3.2. Points

The number of points represent the number of similar measurement series at one location. One single series of measurements would not be reliable because of the precision of the coordinates of the locations, see Section 4.3.4. By increasing the number of points, the covered area by the points is increased and it is less likely that all the points are not located on the road. It has been chosen to have at least four points per location. In Table 5.2, the number of the points for each location are given. The maximum distance between the points

has been given as well. The positions of the points per location are shown in Appendix A. The amplitudes and settlement rates used in the analysis of the results are an average of the points per location, but since the measurement series are comparable the average is a good representation.

Table 5.2: Number of points and maximum distance between the points for each location

Location number	Group A		Group B		Group C	
	Number of points	Maximum distance [m]	Number of points	Maximum distance [m]	Number of points	Maximum distance [m]
1	5	6	6	10	7	17
2	5	8	10	13	6	16
3	11	14	6	12	8	10
4	5	11	5	8	5	7
5	7	13	6	13	6	9
6	5	6	4	8	7	13
7	8	12	4	5	4	9

5.3.3. Locations

All three groups contain seven different locations, therefore there are 21 locations in total. The locations are located in four different districts in the city of Woerden. These districts are Schilderskwartier (developed in the 1960s), Bedrijventerrein Barwoutswaarder (developed in the 1980s), Bedrijventerrein Polanen (developed in the 1990s) and Middelland-Zuid (developed in the 1990s). The districts and the locations within these districts are represented in Figure 5.2. It should be remarked the different districts have been developed within different time periods and therefore the subsurface will be in different stages of subsidence due to different loading duration.

Schilderskwartier is one of the oldest districts of Woerden and is the only residential district of the involved districts. It can be noted that only one location is found in this district. Three main causes can be related to this small number of useful locations. Firstly, the major part of the roads have brick pavements rather than asphalt covering. Secondly, the few asphalt roads within the district are old and therefore have been under construction, which makes them not suitable for this research. Lastly, roads in residential areas are quite narrow and trees or buildings are close to the roads cause blockage of the satellite's sight.

The other three districts are industrial areas. These three districts are Bedrijventerrein Barwoutswaarder, Middelland-Zuid and Bedrijventerrein Polanen. One of the benefits of the industrial areas is the areas are much more open, since there are fewer trees or buildings directly located near the road, leading to less blocking of the satellite's sight. Another benefit is that the roads are mostly empty at the time of the satellite passing, where in the residential areas vehicles are placed on the roads and therefore influence the satellite data.

Middelland-Zuid and especially Bedrijventerrein Polanen bear a lot of locations. This is due to the fact the roads in these districts are relatively new, meaning the roads are hardly damaged and therefore do not need construction works, but they meet the 10 years requirement.

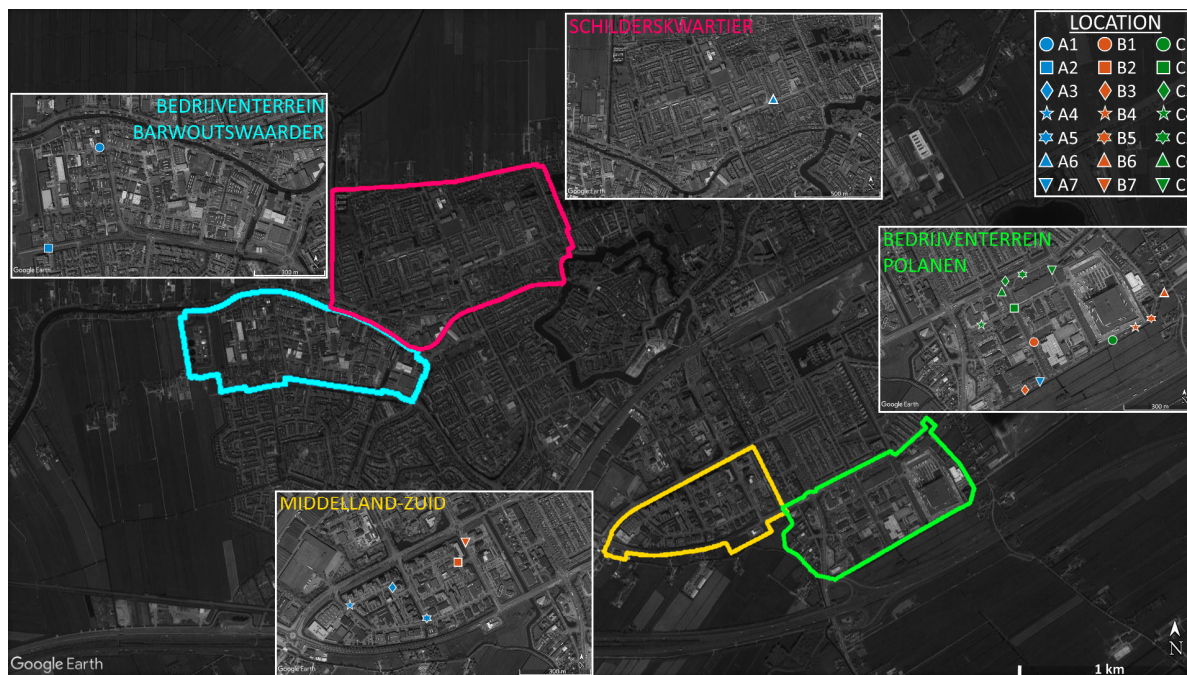


Figure 5.2: The locations inside the research area

5.3.4. Coefficient of Determination

The coefficient of determination, or R-squared (R^2), is a statistical measure that determines the ability of a model to predict or explain an outcome in a linear regression structure. The coefficient of determination indicates the proportion of the variance in the dependent variable that is predicted or explained by linear regression and the independent variable [20]. In case of simple linear regression, the R-squared value is the square of the correlation coefficient, which is a measure of correlation between two variables. The value of R-squared ranges from 0 to 1, where 1 means the linear regression line perfectly fits the data.

$$\begin{aligned}
 R^2 &= 1 - \frac{SSR}{SST} \\
 &= 1 - \frac{\sum_i (y_i - \hat{y}_i)^2}{\sum_i (y_i - \bar{y})^2}
 \end{aligned}
 \tag{5.5}$$

The value of R-squared can be determined by the function shown by Function 5.5. In this formula, SSR is the Sum of the Squared Regression, SST , the Sum of the Squared Total, y_i , the actual observation, \hat{y}_i , the predicted observation and \bar{y} is the mean of the actual observations [40].

The R-squared value can be determined by MATLAB as an intrinsic function, which is part of the Basic Fitting Tool [31]. The linear regression model is represented by the linear trendline and the R-squared value represents how well the trendline fits the data.

5.4. Subsurface data

When knowing the locations of useful satellite data, the soil profiles of these locations can be established. The technique of obtaining these soil profiles is explained in this section. Also some research has been done to the groundwater levels. The groundwater levels are significant because the presence of water impacts the soil behaviour of clay, such as reduction the shear strength and stiffness.

The depth of the boreholes and the groundwater levels are given relative to the Normaal Amsterdams Peil (NAP). The NAP is a reference level used for all levels of height and depth. The value of 0 m NAP is equal to the average sea level of the North Sea. The advantage of using a datum reference is that all levels are relative to the same point, making it easier to compare the levels.

5.4.1. Groundwater data

The city of Woerden lies within the working area of the water board *De Stichtse Rijnlanden*. The water board has divided the working area into smaller sections, and for each section a decision has been made on the water level to be maintained within that section [38]. This decision will be renewed every ten years.

The water board and the municipalities within their working area have founded a water innovation network named *Winnet*. One of the responsibilities of *Winnet* is to maintain the monitoring wells and data processing and analysis of the data produced by the monitoring wells. The monitoring wells measure the groundwater level each hour and the measured levels of each monitoring well can be found on the website of *Winnet*.

In Figure 5.3 the location of the used monitoring wells can be found. It can be seen that for each district, the data of two monitoring wells has been utilised. In Table 5.3 the average ground water level of these monitoring wells is given, as well as the ground level at the monitoring well and depth of the average ground water level. The average groundwater levels of the monitoring wells are used to make a deliberate assumption of the groundwater levels at the different locations. It should be remarked that the exact groundwater level can only be known by monitoring the groundwater level in time.

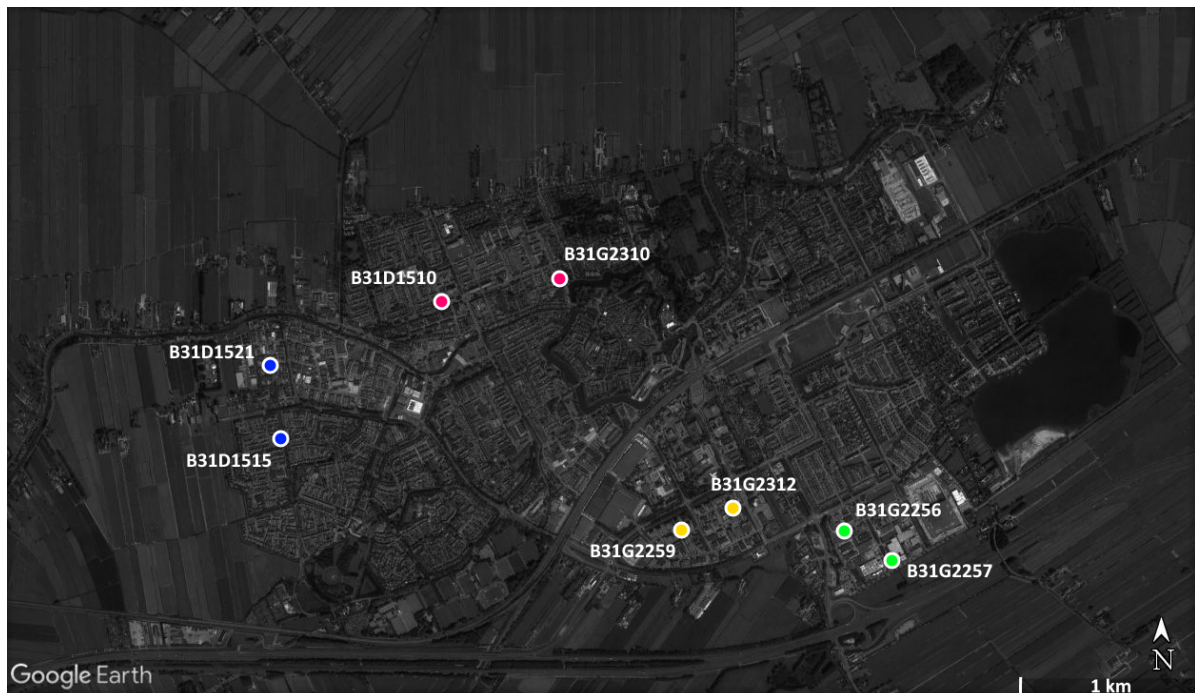


Figure 5.3: The locations and codes of the used monitoring wells

Table 5.3: Average groundwater level at different monitoring wells

Monitoring well	Average groundwater level [m NAP]	Ground level [m NAP]	Depth of average ground water level [m]
B31D1510	-1.68	+0.40	2.08
B31G2310	-1.58	+0.37	1.95
B31D1515	-1.56	-0.72	0.84
B31D1521	-1.81	-0.16	1.65
B31G2259	-1.41	-0.64	0.77
B31G2312	-1.86	-0.87	0.99
B31G2256	-1.47	-1.02	0.45
B31G2257	-1.80	-1.26	0.54

5.4.2. Soil data

The soil profile is largely varying at small distances because of the fluvial origin of the soil deposition. Due to the variation, it is important to get the soil profiles as close as possible to the locations of the satellite data. It is not possible to get the soil profiles directly beneath the satellite data, since the data is located on asphalt roads. Therefore, the soil profiles are taken in lawns adjoining the roads.

For the locations A3 and C4 the soil profiles are performed by the company *Eijkelkamp* which executed ground investigation when installing the monitoring wells. It has only been requested for these data locations since the locations were very close to these monitoring wells and therefore the soil profiles would be representative. All the other locations are not located near any monitoring wells and therefore the soil profiles had to be determined. The soil profiles are taken with a gouge auger. A gouge auger is a metal tube with one open side. A gouge auger is meant to push into soft soil and shows the soil profile with a length corresponding to the length of the tube. The used gouge auger had a tube with a length of one metre. An extension rod can be used to extend the distance between the gouge auger and handle, meaning larger depth can be reached. The taken soil profiles vary in length from 3 to 5 metres. The encountered soil inside the tube is divided into different soil sections and for each section the top and bottom is determined. The values of depth are rounded to tens of centimetres. The encountered soil inside the tube is determined by viewing and touching the soil.

A disadvantage of this method is that for each metre, the gouge auger has to be pulled out, meaning that for reaching four metres of depth the gouge auger has been pulled out three times. In case of very soft soil, the hole that has been created by pulling out the gouge auger can be partially back-filled by the soil. If the gouge auger is put in again there is a part of collapsed soil incorrectly assigned to a larger depth. This does eventually lead to a larger thickness of soil than there actually is present.

6

Results

The gathered locations have been divided into three groups, group A, B and C, and the division has been based on the settlement rate of the locations. Group A includes the locations with a settlement rate of 0 to -1 mm/year, group B the locations with a settlement rate of -3 to -4 mm/year and group C the locations with a settlement rate of -4 to -5 mm/year. In Figure 6.1 the relation between the amplitude of seasonal oscillation and settlement rate are indicated per group. The data and soil profiles of the different groups have been compared and it has been investigated if there is any connection between the soil profiles and the settlement rate obtained by the satellite measurements. The displacement values given by the satellite measurements can be approximated by a trendline. In this chapter the results are presented. First, the details of the locations of the three different groups are further discussed.

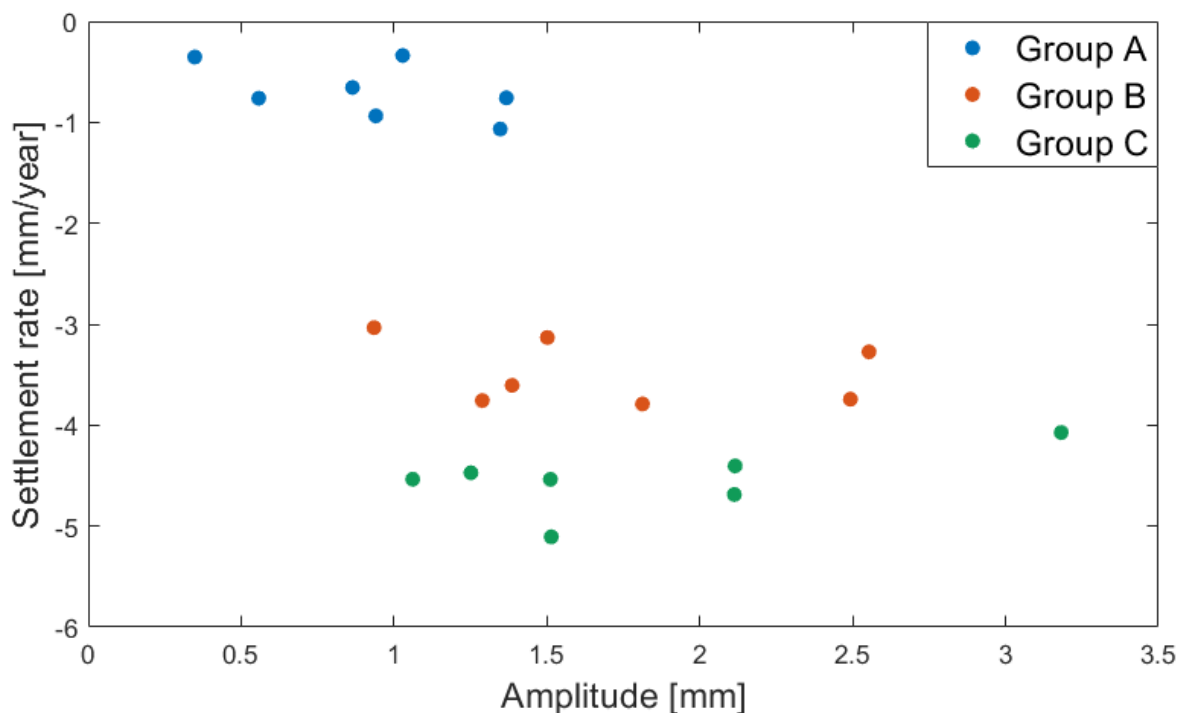


Figure 6.1: Link between the amplitude of seasonal oscillation and settlement rate

6.1. Three different groups

All the suitable locations have been divided into three different groups based on the settlement rates. Although some of the soil profiles are more than three metres, all the profiles have been given a maximum profile length of three metres. This has been done to optimise the comparison between the different locations, where some of the profile lengths are only three metres long. The displacement values measured by

the satellite for the individual locations are represented in Appendix B, Appendix C and Appendix D for the locations of group A, group B and group C respectively. In these appendices, the seasonal and linear trendlines and the amplitude can be found schematically. In Figure 6.2 the data of location A3 is displayed as an example. The following three sections present the data collected from the soil profiles as well as the values for the settlement rate and amplitude for the locations per group.

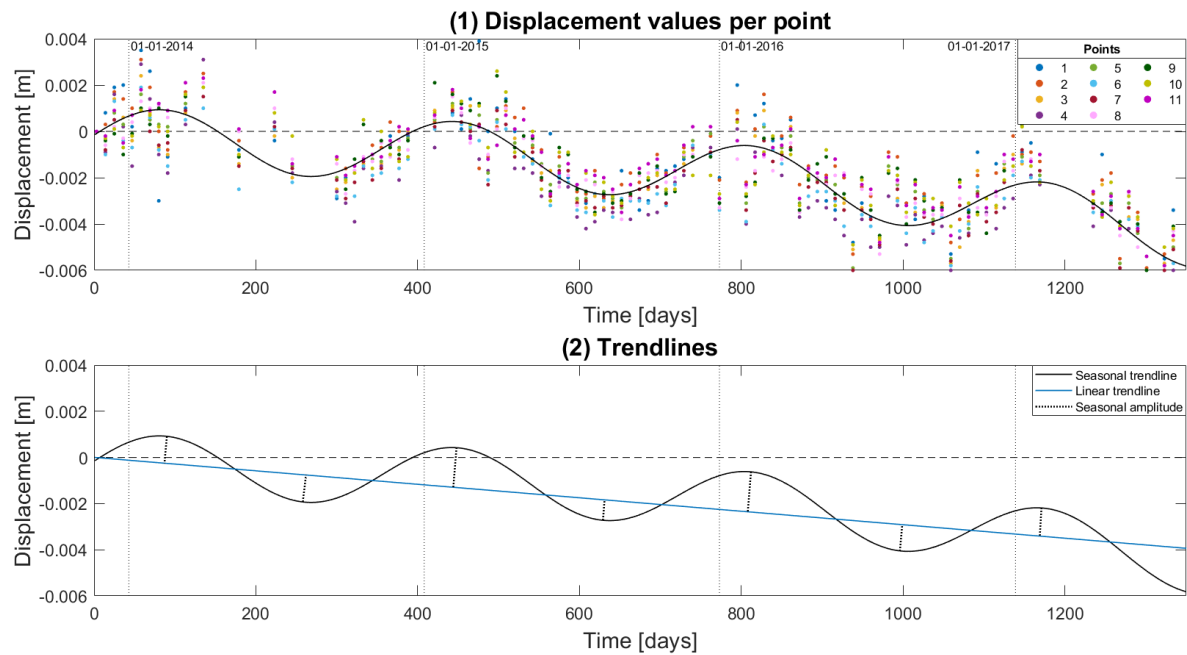


Figure 6.2: Individual measurement series (top) and trendlines (bottom) for location A3

6.1.1. Group A: 0 to -1 mm/year

Group A is the group with the lowest settlement rates. A representative soil profile for group A can be found in Figure 6.3 (left). All soil profiles of the different locations of this group can be found in Appendix E.1. An overview of the most substantial data is found in Table 6.1. Most of the soil profiles do not contain any peat layers, except for location A7. The peat layer is found within the top 3 metres and should be taken into account when evaluating the results.

It can be noticed that for location A3, the settlement rate is higher than 1 mm per year. However, since the soil profile does not show any remarkableness compared to the other soil profiles, it has been decided to keep the location.

Table 6.1: Specifications of the different locations part of group A

Location	Settlement rate [mm/year]	Amplitude [mm]	Ground level [m NAP]	Depth of the clay layer [m]	Total thickness clay layer [m]
A1	-0.73	0.864	-0.40	0.40	0.90
A2	-0.99	0.940	-0.60	0.40	2.60
A3	-1.20	1.347	-0.64	0.30	2.70
A4	-0.45	1.028	-0.50	0.40	1.40
A5	-0.71	0.558	-0.70	0.50	2.50
A6	-0.34	0.348	+0.40	0.60	0.50
A7	-0.85	1.367	-0.80	0.30	2.70

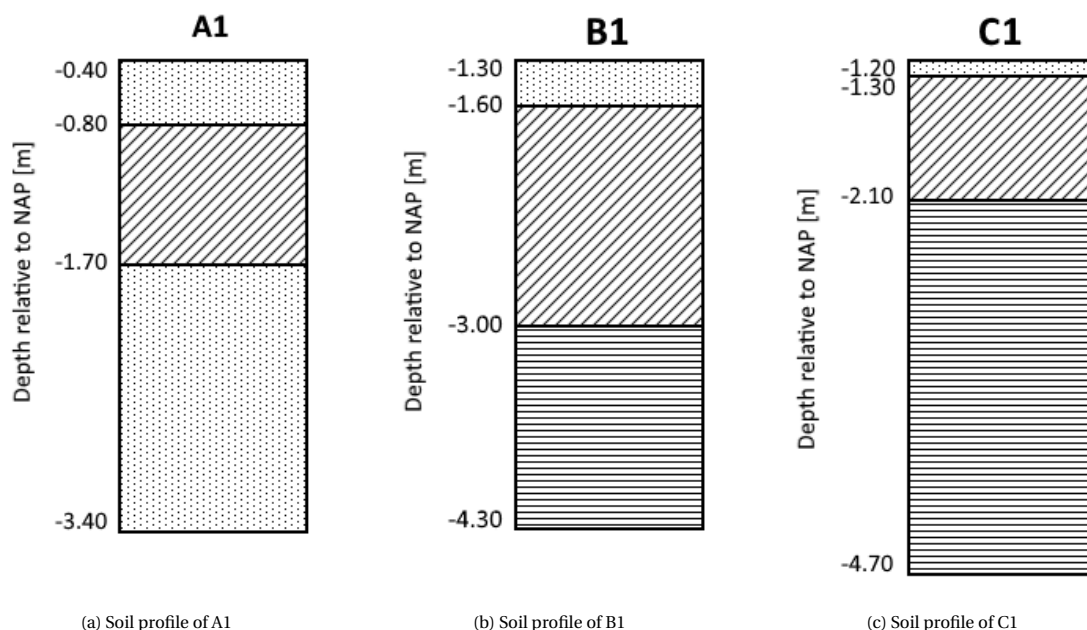


Figure 6.3: Representative soil profiles of group A (left), group B (centre) en group C (right)

6.1.2. Group B: -3 to -4 mm/year

The soil profiles of group B can be found in Appendix E.2. A representative soil profile for group B can be found in Figure 6.3 (centre). The soil profiles of group B show an alternation of clay and peat layers, introducing of difficulty in the evaluation of the results. In Table 6.2 the specifications of the soil profiles and data of the group B can be found. For the locations with soil profiles containing multiple clay layers, the total thickness indicated by the table is the total amount of the different layers summed. The depth remains the depth of the top clay layer.

For location B7 the settlement rate is slightly below the given interval. However, the value of the settlement rate by method 1, given in Table 5.1, is within the interval.

Table 6.2: Specifications of the different locations part of group B

Location	Settlement rate [mm/year]	Amplitude [mm]	Ground level [m NAP]	Depth of the clay layer [m]	Total thickness clay layer [m]	Depth of the peat layer [m]	Total thickness peat layer [m]
B1	-3.67	1.289	-1.30	0.30	1.40	1.70	1.30
B2	-3.84	2.493	-0.90	0.50	1.50	1.00	1.00
B3	-3.48	2.553	-0.9	0.20	1.80	1.40	1.00
B4	-3.64	1.813	-1.20	0.20	0.90	1.10	1.90
B5	-3.57	1.386	-1.20	0.40	0.60	1.00	2.00
B6	-3.28	1.502	-1.20	0.30	1.10	1.40	1.60
B7	-2.98	0.935	-1.00	0.50	2.00	1.40	0.50

6.1.3. Group C: -4 to -5 mm/year

Group C is the group with the highest settlement rates and the soil profiles contain the largest amount of peat as well. A representative soil profile for group C can be found in Figure 6.3 (right). The thickness of the peat layers is at least 2 metres, which can be seen in Table 6.3. The soil profiles of the locations of group C are shown in Appendix E.3.

It can be noticed that for location C3, the settlement rate is slightly above the given interval. However, since the soil profile does not show any remarkableness compared to the other soil profiles, it has been decided to keep the location.

Table 6.3: Specifications of the different locations part of group C

Location	Settlement rate [mm/year]	Amplitude [mm]	Ground level [m NAP]	Depth of the clay layer [m]	Total thickness clay layer [m]	Depth of the peat layer [m]	Total thickness peat layer [m]
C1	-4.29	3.182	-1.20	0.10	0.80	0.90	2.10
C2	-4.51	1.061	-1.40	0.50	0.40	0.90	2.10
C3	-5.07	1.514	-1.50	0.30	0.40	0.70	2.30
C4	-4.40	1.511	-1.02	0.40	0.60	1.00	2.00
C5	-4.39	1.251	-1.40	0.40	0.30	0.70	2.30
C6	-4.48	2.115	-1.60	0.20	0.60	0.80	2.20
C7	-4.79	2.113	-1.60	0.20	0.60	0.80	2.20

6.2. Settlement rate

The three groups were divided based on the settlement rate. The main difference within the soil profiles is the presence of peat, where the settlement rate is the lowest if no peat is present.

6.2.1. Thickness

Firstly, the thickness of the soil layers is examined. Because the soil profiles of group A do not contain peat, the settlement rate is induced by the clay layers. In Figure 6.4(a) the thickness of the clay layers and settlement rate is displayed, with a total length of the soil profiles of 3 metres. The four locations in the right corner (A2, A3, A5 and A7) seem to be restrained by the taken length of the soil profiles. The thickness of the clay layers at these locations is restricted by a limited depth of investigation, which is 3 metres. However, this does not mean no clay will be present below these depth. Nevertheless, a trendline has been established to estimate the settlement rate induced by the thickness of the clay layer. The trendline can be found in Equation 6.1, where T_c represents the thickness of the clay layer.

$$S_{clay} = -0.25 * T_c - 0.28 \quad (6.1)$$

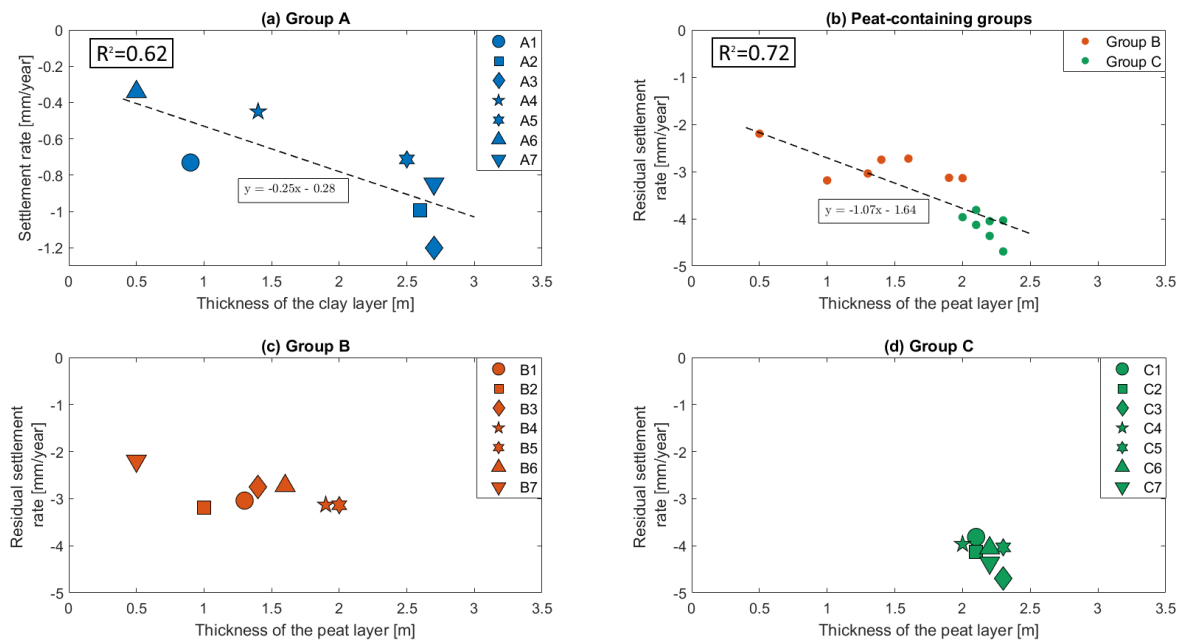


Figure 6.4: Graphs of settlement rate and thickness

For the peat containing groups the settlement rate is divided into two parts. The first part consists of the calculated settlement rate induced by the thickness of the present clay layers using the trendline. The second part is the settlement rate induced by the present peat layers, which is the remaining amount, so the total settlement rate minus the part induced by the clay layers. The remaining amount of settlement rate is further referred to as the residual settlement rate. Figure 6.4(b) shows the results of the residual settlement rate and the thickness of the peat layers for both group B and group C. The individual groups are addressed in Figure 6.4(c) for group B and Figure 6.4(d) for group C.

For the data of Figure 6.4(b) a trendline has been created as well, which is shown by Equation 6.2. In this formula, T_c represents the thickness of the peat layer.

$$S_{peat} = -1.07 * T_p - 1.64 \quad (6.2)$$

Combining Equation 6.1 and Equation 6.2 will give Equation 6.3. This equation is used to calculate the total settlement rate for the locations of group B and group C, which are the groups where the soil profiles contain both clay layers and peat layers.

$$\begin{aligned} S_{total} &= S_{clay} + S_{peat} \\ &= -0.25 * T_c - 1.07 * T_p - 1.92 \end{aligned} \quad (6.3)$$

The total settlement rate of each location has been calculated with Equation 6.3 and the differences between the obtained and calculated settlement rate have been evaluated in order to check the reliability of the function. The average absolute deviation is given in Figure 6.7(a). The average absolute deviation is 0.34 mm/year for group B and 0.22 mm/year for group C, leading to an average of 0.28 mm/year for all locations. The relative deviation is 9.5% and 4.7% for group B and group C respectively.

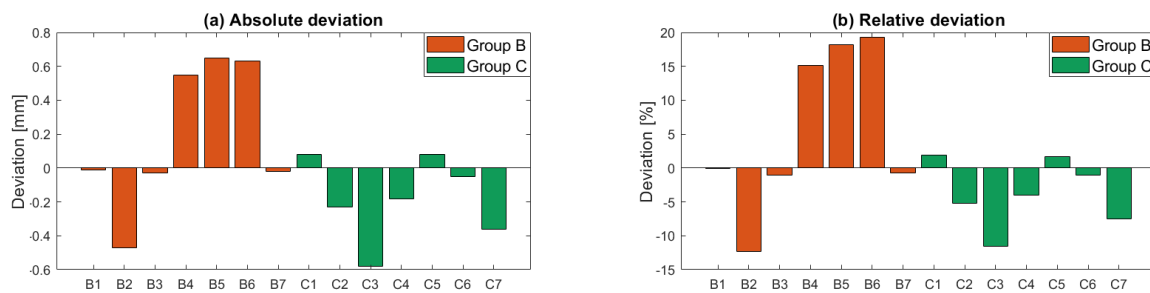


Figure 6.5: Graphs showing the difference between the real and calculated values of the settlement rate

6.2.2. Ratio thickness and depth

The ratio of thickness and depth of the soil layers is introduced to check if the depth of the soil layers is relevant for the amount of settlement rate. Again the results of group A are used to establish a trendline for the clay part, since this group does not contain peat layers. Figure 6.6(a) shows the results of the thickness over depth ratio of the clay layers and the settlement rate, as well as the trendline. The trendline is given by Equation 6.4, where T_c and d_c represent the thickness and depth of the clay layer.

$$S_{clay} = -0.078 * \frac{T_c}{d_c} - 0.35 \quad (6.4)$$

The residual settlement rate is again determined by the total settlement rates minus the settlement rate induced by the clay layer calculated by Equation 6.4. The fitting of the ratio of thickness and depth of the peat layers and the residual settlement rate is given in Figure 6.6(b). The data of Figure 6.6(b) appear to be fitting and therefore also a trendline for the data of this graph is established, given by Equation 6.5. T_p and d_p represent the thickness and depth of the peat layer in the trendline.

$$S_{peat} = -0.66 * \frac{T_p}{d_p} - 2.16 \quad (6.5)$$

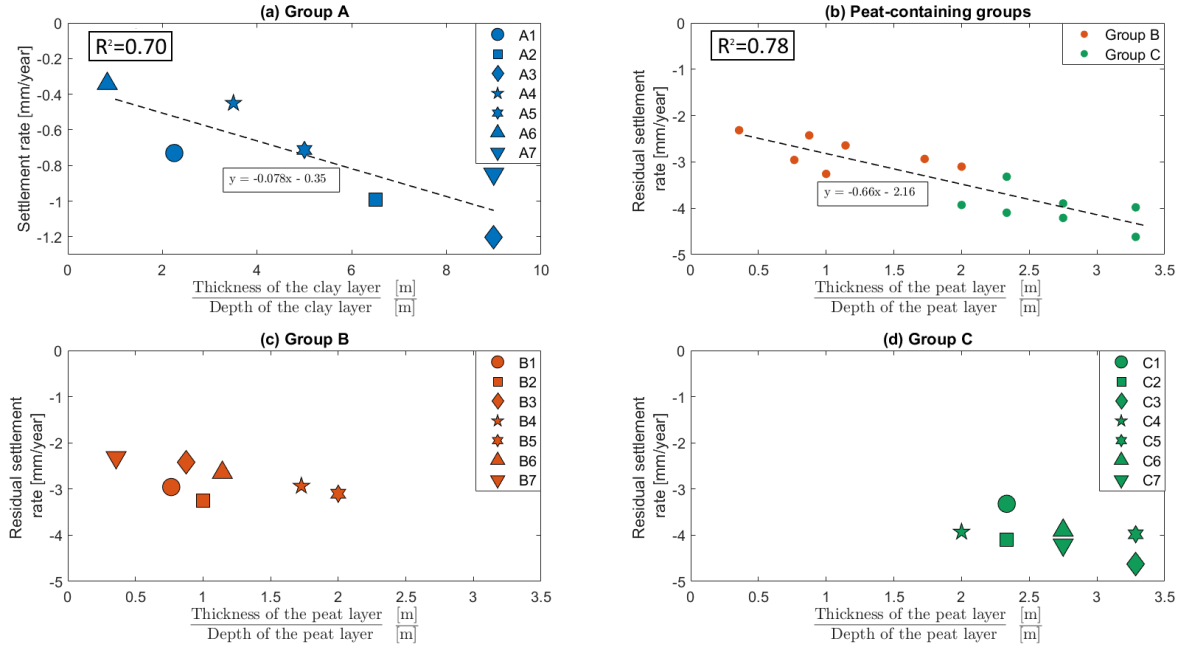


Figure 6.6: Graphs of settlement rate and ratio of thickness and depth

There is an equation for the part of the settlement rate for both the clay and peat component and combining these equations (Equation 6.4 and Equation 6.5) leads to Equation 6.6. This equation estimates the total settlement rate of a location based on the thickness and depth of the soil layers, if only peat and clay layers are present within the soil profile.

$$\begin{aligned}
 S_{total} &= S_{clay} + S_{peat} \\
 &= -0.078 * \frac{T_c}{d_c} - 0.66 * \frac{T_p}{d_p} - 2.51
 \end{aligned} \tag{6.6}$$

The total settlement rate of each location has been calculated with Equation 6.6 and the differences between the obtained and calculated settlement rate have been evaluated in order to check the reliability of the function. The average absolute deviation is given in Figure 6.7(a). The average absolute deviation is 0.29 mm/year for group B and 0.31 mm/year for group C, leading to an average of 0.30 mm/year for all locations. The relative deviation is 8.1% and 6.9% for group B and group C respectively, meaning the average absolute deviation is lower for group B but the relative deviation is higher.

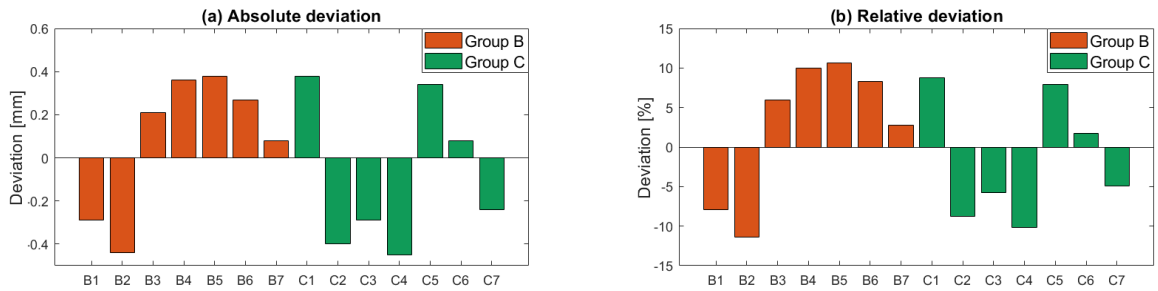


Figure 6.7: Graphs showing the difference between the real and calculated values of the settlement rate

6.3. Amplitude of the seasonal oscillation

The groups have been divided based on the settlement rate and it does not mean the division also holds for the magnitude of the amplitude, which is the magnitude of the seasonal effect shown by the seasonal trendline. However, in this section the initial division of the three groups will remain.

6.3.1. Thickness

First the thickness of the clay layers is taken into consideration. Figure 6.8 displays the graph of the total thickness clay layers and amplitude, valid for a length of 3 metres for the soil profiles. In Figure 6.8(b) however, location A1, A4 and A6 are the three locations where the bottom of the clay layer is identified and looking at the graph these three locations can be roughly linearly related. For the other four locations, it seems that increasing the total amount of clay is only shifting the data on the x-axis. The thickness of the clay layers of these locations is increasing with depth, but these increase of thickness does not enhance the magnitude of the amplitude. In other words, the magnitude of the amplitude is most likely arise from the presence of clay to a limited depth and the presence of the soil layers below that depth does not have any contribution to the magnitude of the amplitude. A depth of 3 metres seems to be too large and therefore, the depth of investigation is reduced to 1.5 metres since.

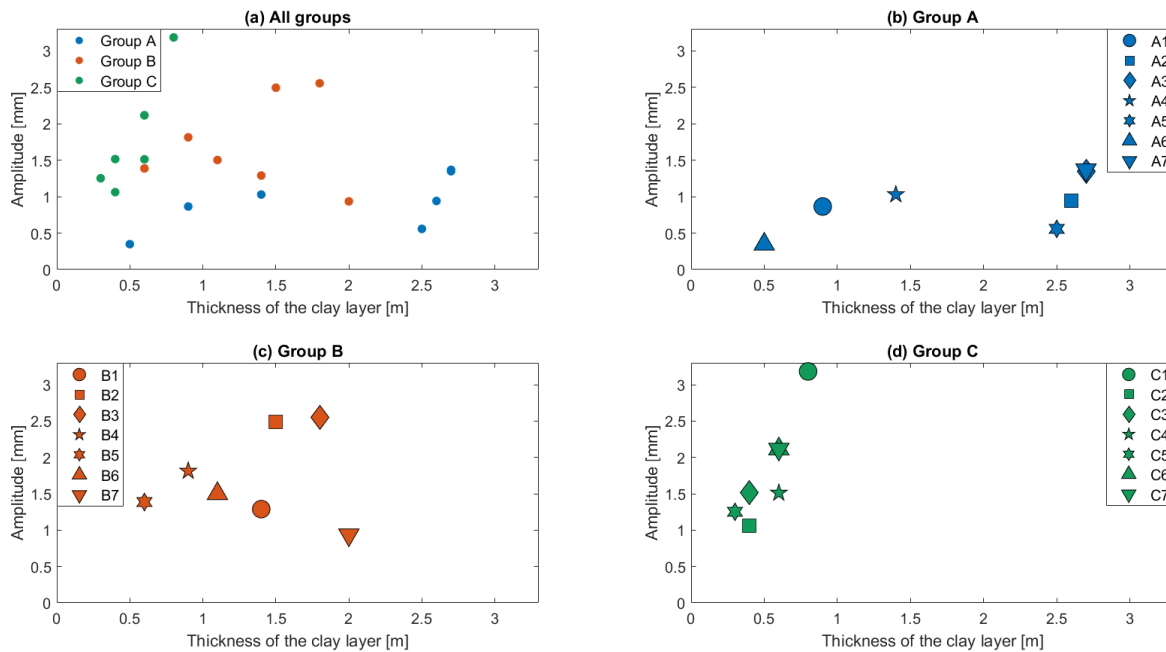


Figure 6.8: Graphs of thickness of the clay layers and amplitude for profile length of 3m

Figure 6.9 shows the graphs are represented for the thickness of the clay when the soil profiles have been cut off at 1.5 metres. The differences between the groups is created by the soil type within the soil profiles of 1.5 metres. Figure 6.9(a) shows the data for all groups, where in the other three graphs the data for the individual groups is represented.

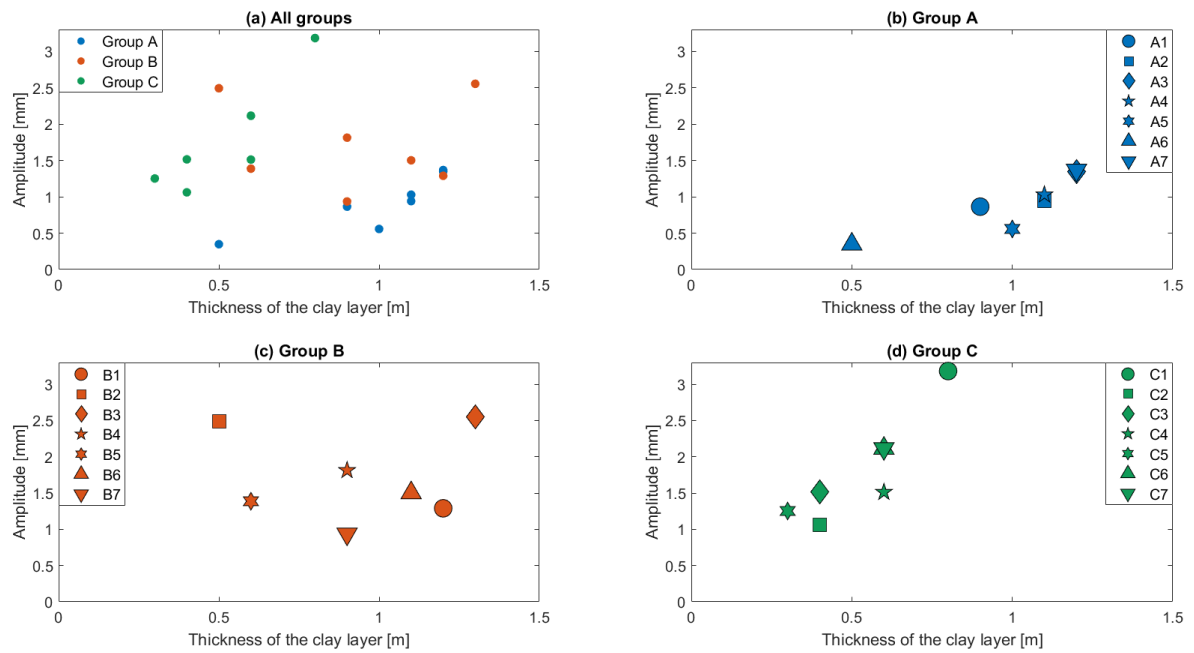


Figure 6.9: Graphs of the thickness of the clay layer and amplitude for the top 1.5m of the profiles

It appears that for group A and group C the amplitude is linearly related to the thickness of the clay layers in the first 1.5 metres of the soil profiles. However, the amplitude is higher for group C than it is for group A. For group B no trend can be seen in Figure 6.9(c).

Because the data for group A and C are linearly related and the amplitude of group C is higher, it seems the presence of peat is affecting the magnitude of the amplitude. The same approach is used it as has been used for the settlement rate. First a trendline is established for the data of group A, since these soil profiles contain mostly clay. The trendline is given by Equation 6.7 and is visualised by Figure 6.10.

$$A_{clay} = 1.33 * T_c - 0.41 \quad (6.7)$$

When only considering the individual data, it can be seen that especially in Figure 6.10(d) the data is not really fitting for just group C. For group B, Figure 6.10(c), there are two locations with zero thickness for the peat layer. These locations do contain peat layer within their soil profile, but not in the top 1.5 metres. For location B1 the residual amplitude is small and therefore Equation 6.7 will hold for this location. This can not be said for location B3, where the residual amplitude is much larger. However, the data considering both groups is fitting much better and a trendline can be drawn fitting the data in Figure 6.10(b). The equation of the trendline is given by Equation 6.8. In Figure 6.10(b) locations B2, B3 and C1 can be indicated as outliers, since their values of amplitude do not match the trendline.

$$A_{peat} = 1.72 * T_p + 0.18 \quad (6.8)$$

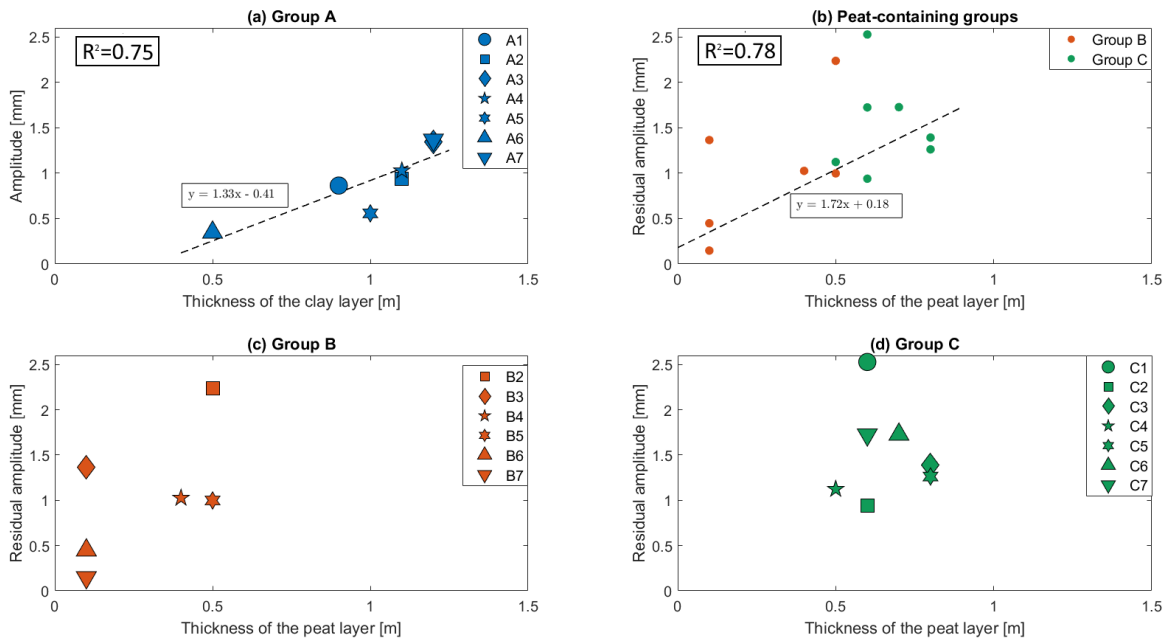


Figure 6.10: Graphs of thickness of the peat layers in group B and group C and amplitude

Combining Equation 6.7 and Equation 6.8 will result in Equation 6.9. The new equation can be used to calculate the amplitude at the locations based on the thickness of the clay and peat layers. The calculated values are compared with the real values of the locations.

$$\begin{aligned}
 A_{total} &= A_{clay} + A_{peat} \\
 &= 1.33 * T_c + 1.72 * T_p - 0.23
 \end{aligned}
 \tag{6.9}$$

Figure 6.11(a) shows the absolute difference between the calculated and real values of the amplitude, given in millimetres. The three outliers, being locations B2, B3 and C1, can be clearly identified. Figure 6.11(b) gives the relative deviation and the figure does not only identify the outliers. The other locations with high relative deviation have a small value for the amplitude and therefore the deviation has a larger impact. The average values for the absolute and relative deviation for all locations, including the outliers, are 0.42 mm and 20.5% respectively. The average absolute deviation per group is 0.45 mm for group B and 0.40 mm for group C, meaning a relative deviation for group B of 21,3% and 19,9% for group C. Whenever the outliers are left out of the calculation of the averages values, the average absolute deviation will reduce to 0.20 mm and the relative deviation reduces to 13.8%.

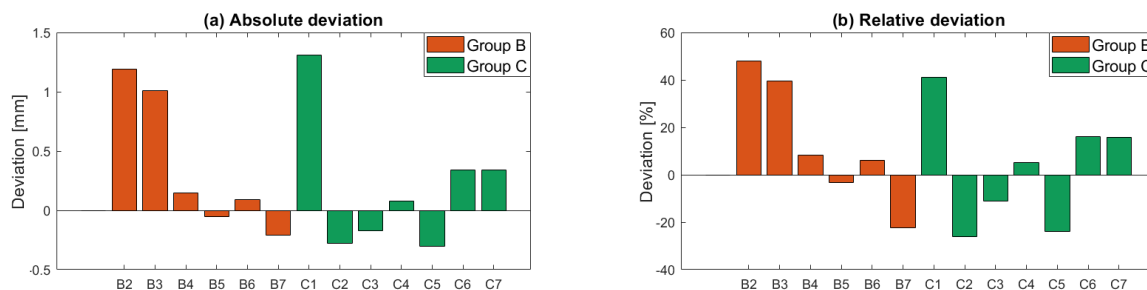


Figure 6.11: Graphs showing the difference between the real and calculated values of the amplitude

6.3.2. Depth

Figure 6.12 shows the fitting of depth of the clay layers and the amplitude of seasonal oscillation. For all three groups a linear relation can be observed. However, the data of group A have in general lower values than the

data of groups B and C and therefore the peat layers should be considered as well.

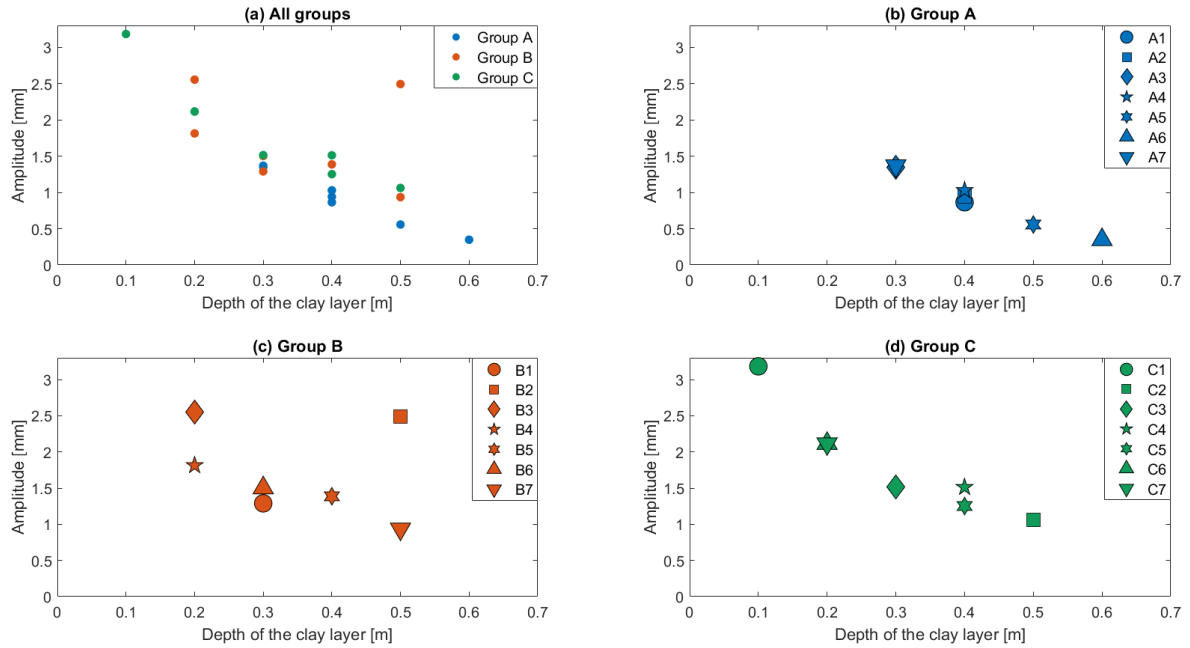


Figure 6.12: Graphs of depth of the clay layers and amplitude of seasonal oscillation

Again a trendline has been established. This trendline is for the data of group A, for depth of the clay layers and the amplitude, given in Figure 6.13(a). This trendline is again used for calculating the amplitude for the depth of the clay layers of groups B and C. The depth of the peat layer and the residual amplitude is given in Figure 6.13(b). There is no fitting trend between only the depth of the peat layers and the amplitude.

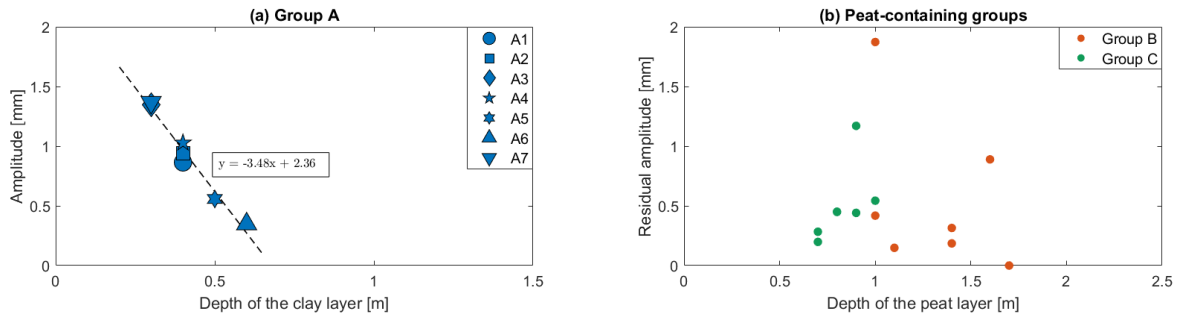


Figure 6.13: Graphs of depth of the soil layers for group A and amplitude of seasonal oscillation (left) and group B and C and the residual amplitude of seasonal oscillation (right)

6.3.3. Ratio thickness and depth

The ratio between the thickness and depth of the clay layer is the last aspect to address. Figure 6.14 shows the graphs of the ratio and the amplitude of seasonal oscillation. It can be seen in Figure 6.14(a) that the results for group A and B appear to be consistent and the results for group C are higher. Figures 6.14(b), 6.14(c) and 6.14(d) show the results for the individual groups and for all three groups a linear connection can be observed. A trendline for group A has been established and visualised in Figure 6.14(a). The equation corresponding to the trendline is given by Equation 6.10.

$$A_{clay} = 0.33 * \frac{T_c}{d_c} + 0.046 \tag{6.10}$$

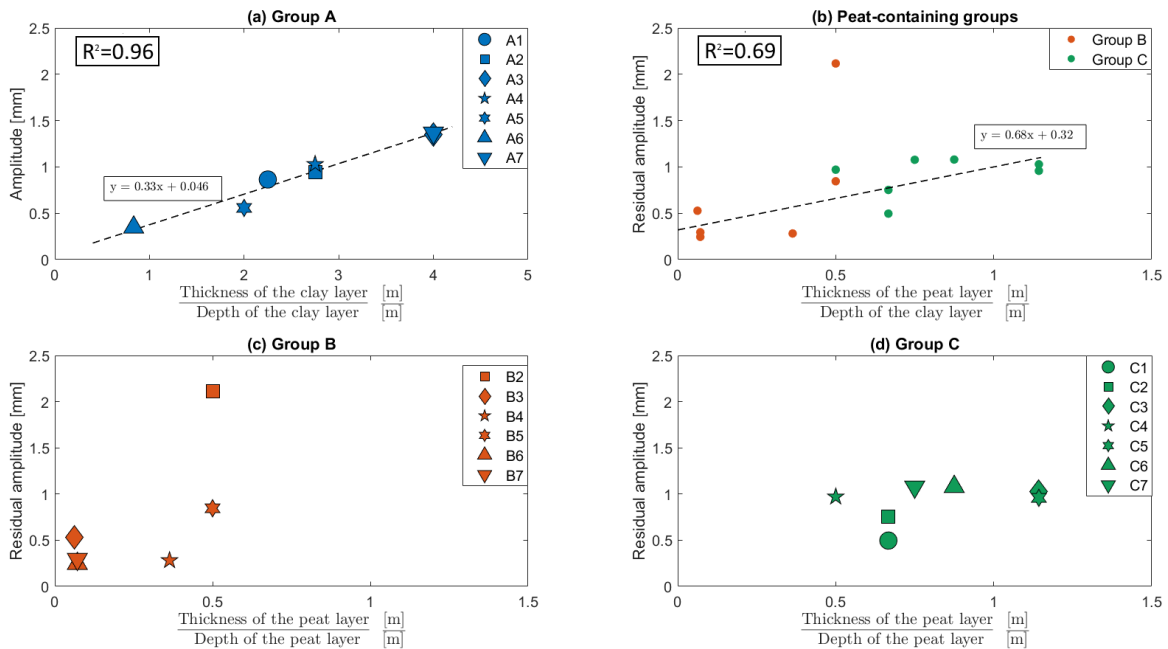


Figure 6.14: Graphs of the ratio between thickness and depth and amplitude for the top 1m of the profiles

Using Equation 6.10 the amplitude for the ratio between thickness and depth of the clay layer of groups B and C are calculated. This value is deducted from the total value of the amplitude and the residual value is given in Figure 6.14(b) alongside with the ratio between thickness and depth of the peat layers. Of the three outliers found when only the thickness of the soil layers was considered only one outlier is left, namely location B2. For the remaining locations a trendline, Equation 6.11, is established.

$$A_{peat} = 0.68 * \frac{T_p}{d_p} + 0.32 \tag{6.11}$$

$$\begin{aligned} A_{total} &= A_{clay} + A_{peat} \\ &= 0.33 * \frac{T_c}{d_c} + 0.68 * \frac{T_p}{d_p} + 0.366 \end{aligned} \tag{6.12}$$

Equation 6.10 and Equation 6.11 can be merged into Equation 6.12, resulting in a formula which can be used when both clay and peat layers are present. The results for the absolute and relative deviation are shown in Figure 6.15 and both Figure 6.15(a) and Figure 6.15(b) both show distinctive values for location B2. The average values for the absolute and relative deviation are 0.26 mm and 13.2% for all locations and when excluding the assigned outlier, these values are reduced to 0.16 mm and 9.5%.

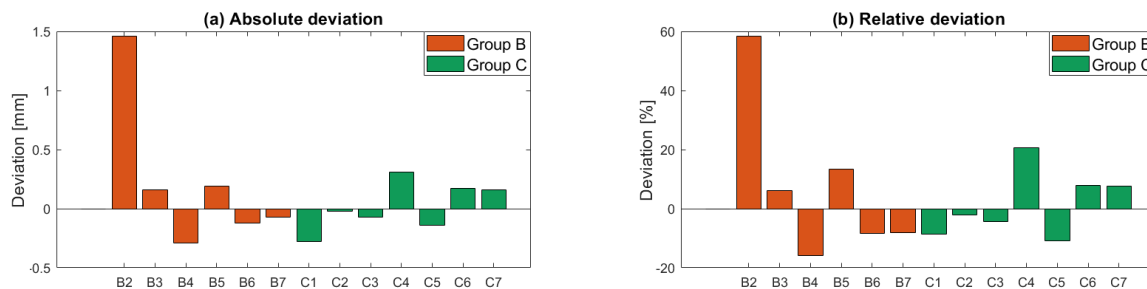


Figure 6.15: Graphs showing the difference between the real and calculated values of the amplitude

6.4. Influence of the water table

In this section it is investigated whether the groundwater level does exert any influence on the obtained values of the amplitude or settlement rate. However, the exact groundwater levels at the locations are not known, therefore the data acquired by the closest monitoring well has been used.

6.4.1. Amplitude of the seasonal oscillation

In Figure 6.16 the trendlines for all locations are represented per group. It can be observed that the amplitudes of the trendlines do not reach its peak values in the same period. Looking at the trendlines for group A, Figure 6.16(a), most of the maximum values of the amplitude are achieved during the winter periods. However, looking at the trendlines of group B and group C, the maximum values for the amplitude are not always found in the winter periods, but are also achieved during summer periods. This means the overall trend in the trendlines is inconsistent. This inconsistency is mainly visible in the trendlines of the locations of group B and group C, located in the *Bedrijventerrein Polanen* district. Also location A7 is located in this district, but the trendline of this location is not inconsistent with the trendlines of the other locations of group A. In

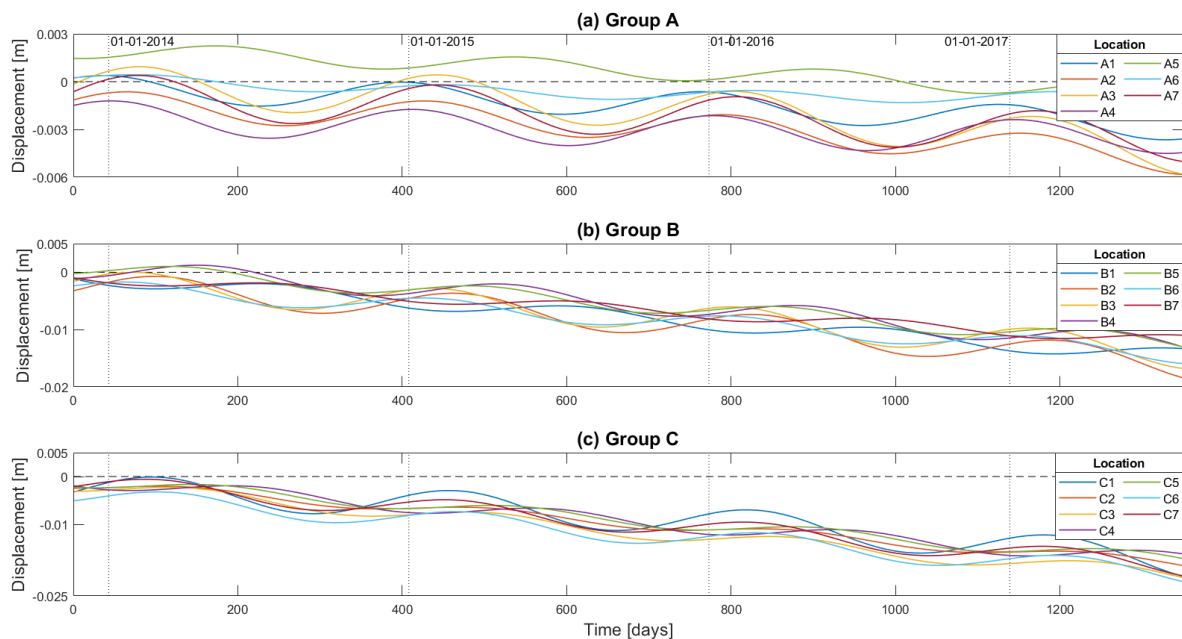


Figure 6.16: Graphs of the seasonal trendlines for all locations of group A (top), group B (middle) and group C (bottom)

Figure 6.17 the data measured by different monitoring wells in the four different districts is shown. The four different graphs seem to have a similar trend, however by looking closely some differences can be observed.

Between approximately days 100 to 200, the top three graphs indicate a decrease in the water table where the bottom graph shows an increase. This difference is also visible in the time range between days 500 to 600 and between days 850 to 950. These time ranges are all corresponding to the months March to July of different years. The data in the bottom graph of Figure 6.17 is measured by a monitoring well located in the *Bedrijventerrein Polanen* district, which is the same district of the locations with contradicting trendlines.

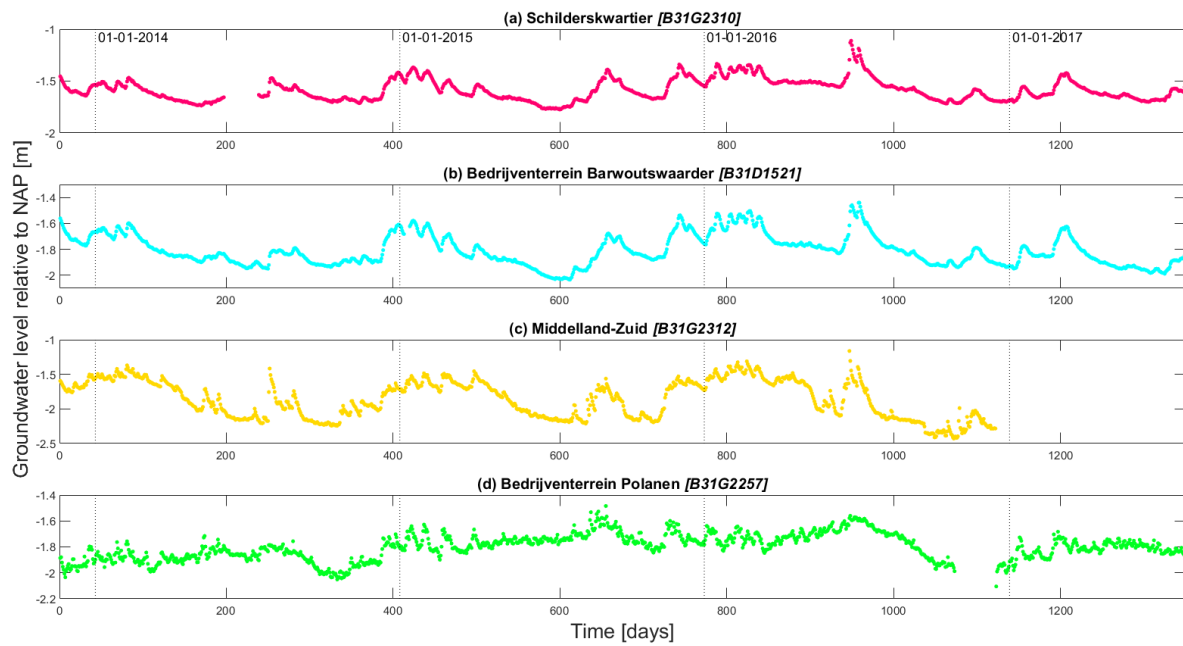


Figure 6.17: Averaged values of the water table per day measured by different monitoring wells located in the four different districts

6.4.2. Settlement rate

For the settlement rate, five different periods have been established. These periods consist of ascending amount of measuring points. The starting date of each period is with the first measuring point and the end the period is the date of the last measuring point within that period. Further specifications of the periods are found in Table 6.4.

Table 6.4: Specification of the different periods

Period	Number of measuring points	End date of the period
Period 1	41	31 - 07 - 2015
Period 2	53	21 - 12 - 2015
Period 3	72	28 - 07 - 2016
Period 4	86	29 - 12 - 2016
Period 5	99	15 - 07 - 2017

The first step is averaging the measuring points of the different points of each location into one series of the measurement values for each location. The series of measurement values of each location is divided into the five different periods. For each period the settlement rate calculated with the *polyfit* function of MATLAB. The results are shown by Figure 6.18.

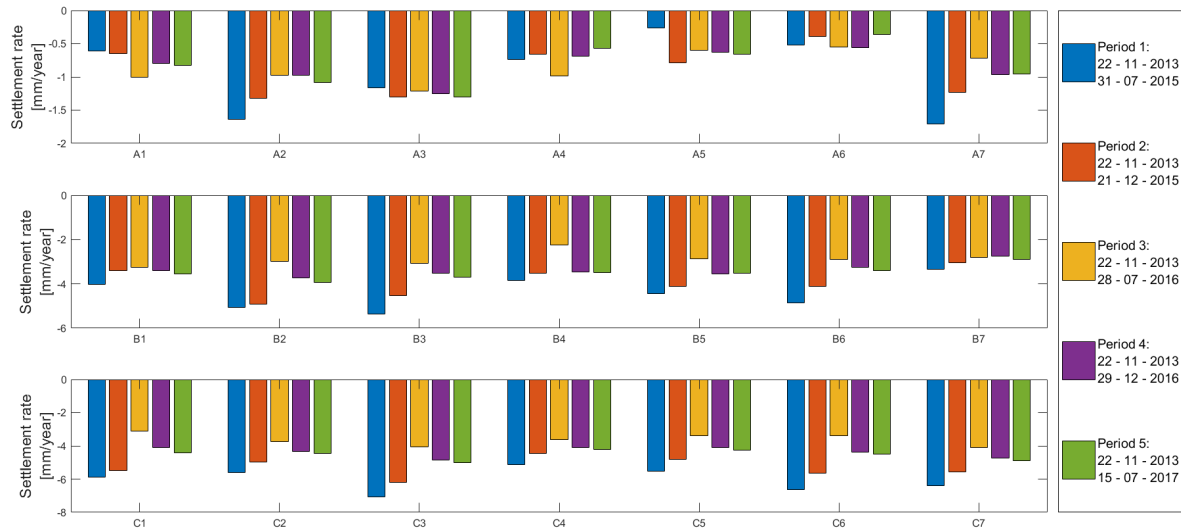


Figure 6.18: Settlement rate calculated per period

It can be noticed the settlement rate is not equal for each period. To corroborate whether the groundwater level has any influence on the variation of the settlement rate, the average values of the groundwater levels are taken for the same time intervals.

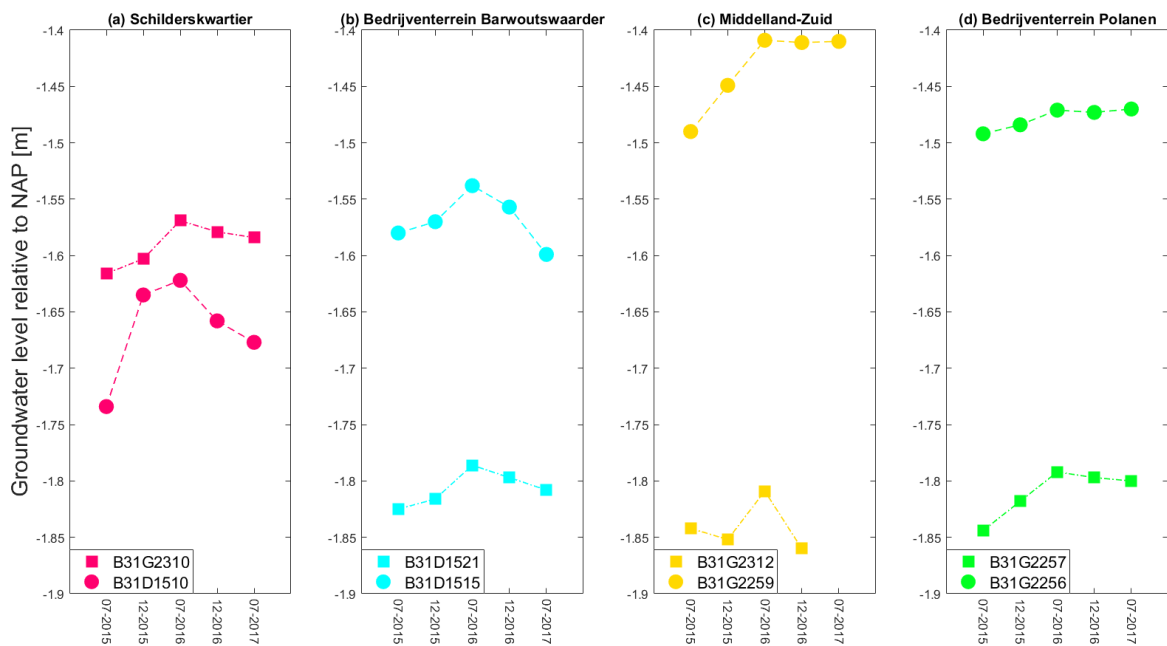


Figure 6.19: Average value for the groundwater levels from starting date

In Figure 6.19 the average values of the groundwater levels of the different monitoring wells are given. The averages are measured from the starting date of the first measurement to the end of the month mentioned on the x-axis. For Figure 6.20 the average groundwater level is calculated between the time intervals used in Figure 6.19. The first value of Figure 6.19 will therefore be equal to the first value of Figure 6.20. For monitoring well *B31G2312*, the fifth value is missing because no data has been collected by this monitoring well in that time period.

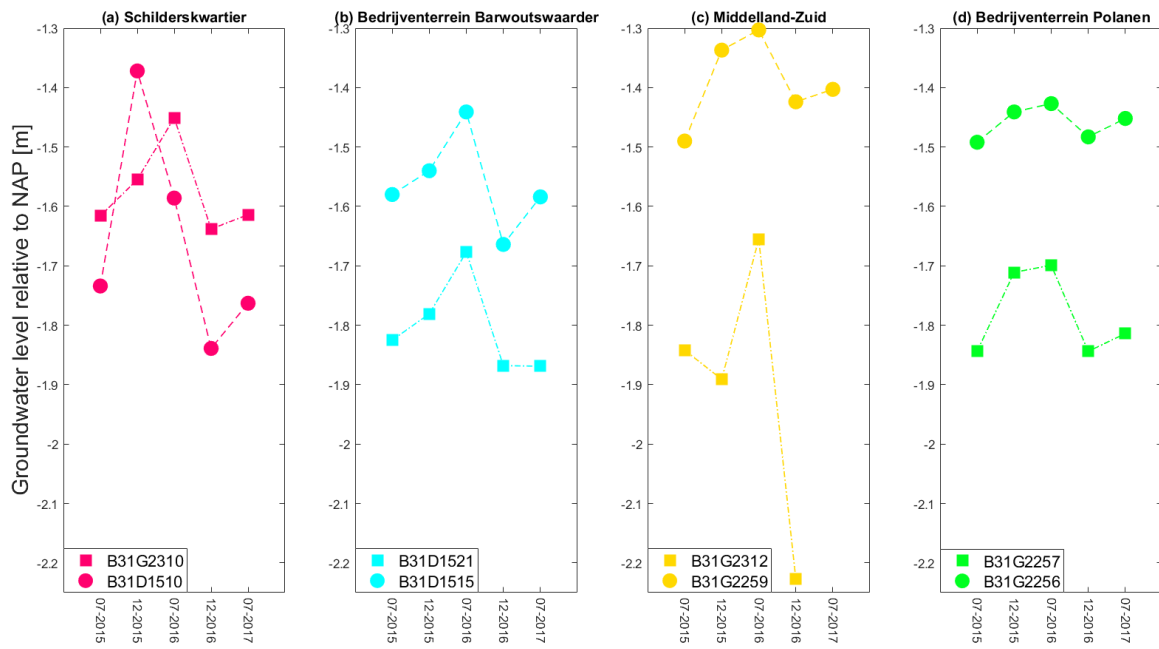


Figure 6.20: Average value for the groundwater levels in time intervals

7

Discussion

In this chapter, the discussion will be performed. In the discussion the three sub-questions are considered as a guideline. In the last section of this chapter the practical eligibility of this research will be discussed.

For the evaluation of the data, some assumptions have been made. First, no distinction has been made for the different types of soils. The soils have been classified as clay, peat and sand. However, different admixture to these soil types can cause of slight difference in characteristics of the soils. Secondly, the presence of (ground)water is not taken into account. The presence of water will reduce the shear strength and stiffness of the clay layers and therefore the height of the water table can be essential to the characteristics of the soils. Thirdly, the soil profiles have been taken alongside the roads and therefore not directly below the position of the data points. Hence, the exact soil profile below the data points can be different than the soil profile that has been assigned to the location. Fourthly, the presence of the road is not implicated in the soil profiles. It is not known whether some soil has been replaced by a ground improvement layer when constructing the roads. This could lead to a different depth and thickness of the clay layers. Lastly, no outliers of the measurements have been excluded. Outliers can have a large impact to the final values of the settlement rate or amplitude of seasonal oscillation.

What coherence exists between the measured settlement rate and the soil types within the soil profile?

The largest values of settlement rate are found at the locations with soil profiles including layers of peat. The soil layers of group A did not include peat and therefore the data of these locations is used to find any connection between the presence of clay and the obtained settlement rate. Two different variables have been tested, namely the thickness of the clay layer, and the ratio of the thickness of the clay layer and the depth of this layer. For both variables a trendline could be drawn. The R-squared values for these trendlines was 0.62 for the thickness of the clay layer and 0.70 for the ratio of thickness and depth. This means the correlation of the ratio of thickness and depth and the measured settlement rate is stronger.

The trendlines are used to calculate the contribution of the clay layers to the settlement rate of the soil profiles containing peat. By subtracting the total (measured) settlement rate by the contribution of the clay layers, the remainder is the contribution to the settlement rate by the peat layers. The two variables are now the thickness of the peat layers, and the ratio of the peat layers and the depth of the peat layer. These variables are plotted against the corresponding residual values of the settlement rate. Again a trendline could be drawn for both variables. The R-squared values for these trendlines was 0.72 for the thickness of the peat layer and 0.78 for the ratio of thickness and depth of the peat layer. Again, the correlation of the ratio of thickness and depth and the measured settlement rate is stronger than for only the thickness of the layers.

The settlement rate is calculated using both the trendline for the clay component and the trendline for the peat component. The absolute and relative deviation of the calculated and measured settlement rate is computed. For the only the thickness of the soil layers, the absolute deviation is 0.28 mm/year, which corresponds to a relative deviation of 7.1%. For the ratio thickness and depth of the soil layers, the absolute deviation is 0.30 mm/year corresponding to a relative deviation of 7.5%. Therefore, the R-squared values for both trendlines regarding the ratio thickness and depth of the soil layers is higher and the deviation to the measured values is higher as well. An explanation could be that the range of the values of deviation is larger for the thickness, hence the difference between the maximum and minimum values for the thickness is 19.2% and

for the ratio thickness and depth 9.6%. However, the range of deviation involving the thickness of the soil layers contain a few values close to zero, and these values have a large impact on the mean value of deviation.

The soil profile of location A7 did show a peat layer within 3 m depth. This peat layer was ignored when evaluating the results but it will now be discussed whether this was justified. The layer of peat is found at a depth of 2.3 m and the thickness of the layer is 0.4 m. If Equation 6.3 and Equation 6.6 are used to calculate the settlement rate of this location, the calculated settlement rates are -2.07 mm/year and -3.24 mm/year respectively. However, the settlement rate obtained by the InSAR data is only -0.78 mm/year. This could indicate the peat layer is not present below the exact location or the depth of investigation is less than the assumed 3.0 m.

In Figure 7.1 the R-squared value for group A is calculated for a depth of investigation ranging from 1.0 tot 3.0 m. It can be observed that from a depth of 1.8 m to 3.0 m the curve of the graph is flattening towards a maximum value of the R-squared value, meaning the highest value will be reached around a depth of 3.0 m. Therefore, a depth of investigation of 3.0 m can be supposed and it is more likely the peat layer is lacking in the soil profile of location A7.

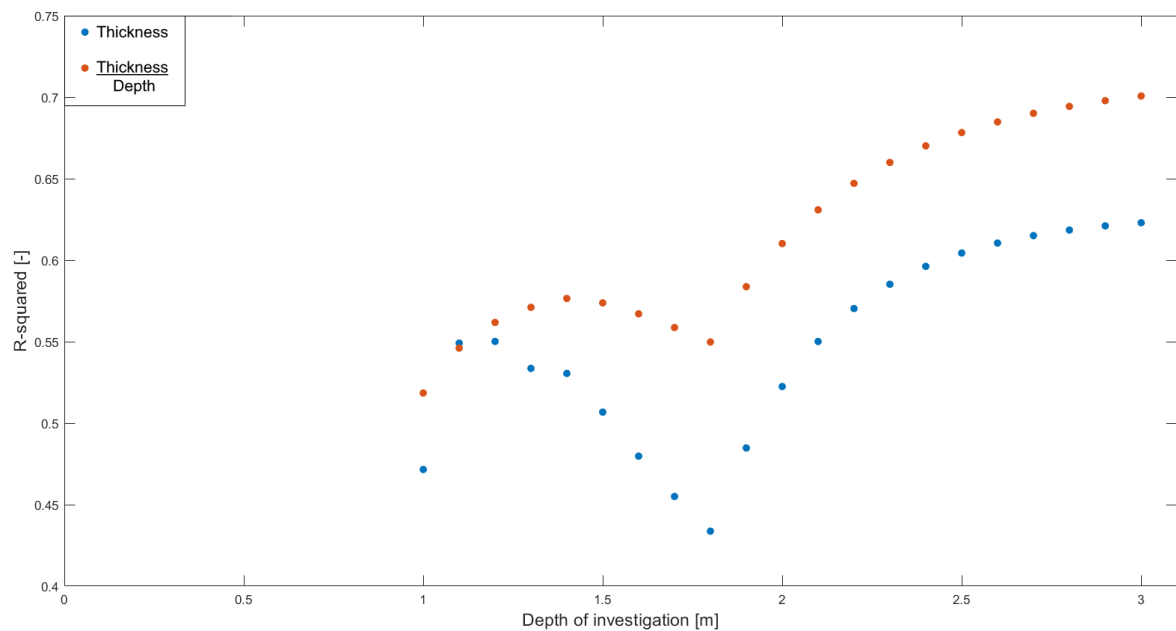


Figure 7.1: Difference value for the depth of investigation with corresponding values of R-squared for group A

There is a coherence established between the settlement rate calculated using the InSAR data and both thickness of the soil layers and the ratio of thickness and depth of the soil layers. The R-squared values for the ratio thickness and depth is higher for the trendline of the only clay containing soil profiles and for the trendline of clay and peat containing soil profiles rather than the trendlines of only thickness of the soil layers. The absolute and consequently relative deviation is lower for only thickness, although the difference with the ratio thickness and depth is very small and the mean values of deviation of the thickness variable are highly influenced by three very low values. To conclude, it can be said that the settlement rate is increasing with increasing presence of peat within the soil profile and that the settlement rate is most likely influenced by the ratio thickness and depth of the soil layers.

What coherence exists between the amplitude of the seasonal oscillation obtained by the InSAR data and the soil types within the soil profile?

For the calculations of the amplitude of seasonal oscillation, the depth of influence has been set to 1.5 m. This has been done since Figure 6.8 indicated that the locations for which the thickness of clay was increasing with depth, the amplitude of seasonal oscillation was not much different than for the locations with limited amount of clay within the soil profile.

First, it can be noticed that the data of the locations of group B and group C show in general higher values for the amplitude of seasonal oscillation than the data of the locations of group A. The main difference is that the soil profiles of group B and group C indicate presence of peat, which is lacking within the soil profiles of group A. The R-squared values for the trendlines of the clay containing group, group A, is 0.75 for only thickness of the clay layers and 0.96 for the ratio of thickness and depth of the clay layers. The equation of these trendlines have been used to calculate the contribution of the clay layers to the amplitude of seasonal oscillation of the other groups. The total amplitude of seasonal oscillation was diminished with this calculated contribution and their residual value should be the contribution of the peat layers of these groups. The trendlines for the peat layers had R-squared of 0.78 for only thickness of the peat layers and 0.69 for the ratio of thickness and depth of the peat layers. However, for the variable thickness three outliers have been removed from the data and only one outlier has been removed for the variable ratio thickness and depth. The outliers can be identified in Figure 6.11(a) and Figure 6.15(a) where the locations which have been designated as outlier have much higher values for the absolute deviation than the other locations. The trendline for the thickness of the soil layers has a mean absolute deviation of 0.20 mm resulting in a relative deviation of 13.8%. For the ratio thickness and depth of the soil layers, the trendline has a mean absolute deviation of 0.16 mm and a relative deviation of 9.5%.

However, by setting the influence depth to 1.5 m location B1 can no longer be ascribed as having a peat containing soil profile and should be included in the only clay containing groups. This means that Equation 6.7 and Equation 6.10 should hold for this location as well. The soil profile of location B1 is characterised by a clay thickness of 1.2 m and a depth of 0.3 m. Using Equation 6.7 and Equation 6.10, the value of the amplitude of seasonal oscillation is calculated as 1.19 mm and 1.37 mm respectively. The amplitude of seasonal oscillation for this location is 1.289 mm and therefore the equations deviate 7.8% and 6.2% and it can be said the equation fulfil the calculation of the amplitude of seasonal oscillation for location B1.

Also the depth of soil layers was investigated as a possible variable of influence. A trendline has been established for the only clay containing groups. However, there was no coherence for the residual values of the amplitude of seasonal oscillation and the depth of the peat layers. This can be explained by the fact that the depth of the clay layers for group A can, for most locations, be written as 1.5 m minus the thickness of the clay layer and the graph of the depth and amplitude of seasonal oscillation is in fact a rewritten graph of thickness of the clay layers.

To answer the question, the amplitude of seasonal oscillation is larger when peat is present within the top 1.5 m of a soil profile. Also, a coherence has been found between the variables thickness and the ratio thickness and depth of soil layers and the magnitude of the amplitude of seasonal oscillation. However, three outliers have been removed for the thickness and only one outlier for the ratio thickness and depth. Therefore, the amplitude of seasonal oscillation is most likely determined by the variable of the ratio thickness and depth of the soil layers.

To which extent can the observed InSAR data be explained by presence of the groundwater level in the soil profile?

To be able to answer this sub-question, a linkage between the observed data and the groundwater level needs to be determined. This section will be divided into two parts. First, any linkage of the amplitude of seasonal oscillation to the groundwater level will be discussed, as well as the possible causes of any established linkage. After, any connection between the settlement rate and the groundwater level will be discussed, followed by any cause of the potential connections.

Amplitude of the seasonal oscillation

Figure 6.16 shows the amplitudes of the seasonal oscillation for the locations of group A are all peaking approximately in the same period, the winter period. The monitoring wells in Figure 6.17 show an elevation in the groundwater levels in the winter periods. This could mean the amplitude of seasonal oscillation is triggered by the fluctuation of the groundwater level. However, the amplitudes for the locations of group B and group C do not all show peaks within the same period. For group B there can be found three sets of similar trendlines. Locations B1 and B7 as a first set, locations B2, B3 and B6 as a second set and locations B4 and B5 as third set. However, locations B2 and B7 are located close to each other. It not likely the groundwater level is

fluctuating opposite on a very short distance. All the locations of group C are located within the same district. Nonetheless, the peaks of amplitudes of seasonal oscillation of these locations do not occur simultaneously.

Although Figure 6.17 shows a contradictory trend in the data of the monitoring well of the *Polanen* district for the period of March to July in each year, this contradiction has not been found in the trendlines of all locations within this district. Based on this data, it cannot be said the groundwater level has a clear effect to the amplitude of seasonal oscillation.

Settlement rate

For the settlement rate, five different periods have been ascribed and the settlement rate for each period is calculated. Figure 6.18 does not show any similarity for group A. However, for group B and C the settlement rates are decreasing from period 1 to period 3 and increasing from period 3 to period 5. The highest values for the settlement rate are all found in period 1 and the lowest values are all found in period 3, except for location B7.

Looking at average groundwater level observed by the monitoring wells, the groundwater level in general is increasing from period 1 to period 3 and after period 3 decreasing. This could indicate that an increase in the groundwater level leads to an decrease of the settlement rate. An explanation could be that by increasing the groundwater level the water pressure is increasing and therefore the grain pressure is decreasing. And the other way around, a decrease in groundwater level leads to an decrease in water pressure and therefore an increase of the grain pressure. Also, a decrease in groundwater level leads to soil desiccation and therefore loss of soil volume. This process can also be called consolidation. The trendlines should have a variable dependent on the change or fluctuation of the groundwater level to adjust the settlement rate to this change or fluctuation.

For location A6, there is a decrease in settlement rate in period 2, an increase in periods 3 and 4 and again a decrease in period 5. Looking at Figure 6.20 the same, inverse, effect is shown in monitoring well *B31D1510*. The groundwater level is increasing in periods 2 and 5 and decreasing in periods 3 and 4. Therefore, location A6 corresponds to the assumed influence of the groundwater level to the settlement rate.

Locations A3 and A5 show a similar trend: an increase in settlement rate is found in period 2 where most other locations show a decrease, although for location A5 the decrease is much larger than for location A3. Monitoring well *B31G2312*, which is located near locations A3 and A5, does show a decrease in period 2 in Figure 6.20. Therefore, locations A3 and A5 are likely to correspond to the assumed influence of the groundwater level to the settlement rate as well.

Nevertheless, for locations A1 and A4 no clear explanation can be found for their deviation in the trend. However, there can be other causes for the deviation which are not related to changes in the groundwater level. For example, any outliers within the obtained InSAR data have not been filtered which could effect the value of the settlement rate, which has been obtained by the *polyfit* function. Also other external aspects could have occurred while obtaining the InSAR data, such as construction to the roads which are not known.

7.1. Practical eligibility

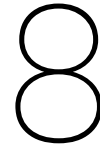
Large amount of ground movement causes damage to roads and infrastructures (cables, sewerage, e.g.) beneath the roads. It is desirable to minimise this damage and in addition the amount of construction needed on the roads to repair the damages. For example, Figure 5.2 shows locations A7 and B3 are located close to each other. The settlement rate of location A7 is -0.85 mm/year, where the settlement rate of location B3 is -3.48 mm/year. Due to the difference in settlement rate, the road is subsiding faster at location B3, leading to differential settlement of the road. Since the houses are founded on piles and therefore do not sustain subsidence, problems with the connections of cables and sewerage between the houses and the main systems be troublesome. Also pavements and gardens need to be levelled up to prevent too much height difference with the houses.

If the settlement rates or seasonal oscillation can be properly approximated based on the soil profile of the location, prevention or limiting of damage to roads can be achieved. The research shows the settlement rate and amplitude of the seasonal oscillation can be approximated with linear trendlines in which the thickness of the soil layer and the ratio of thickness and depth of the soil layers are used. Both the thickness or depth can be reduced by removing the top layer of the soil. However, removing several metres of soil is not econom-

ical or achievable in urban areas.

Furthermore, the depth and fluctuation of the groundwater level might be an influencing factor. The groundwater level is hard to maintain at a certain level. Very dry summers or wet rainy winters cause a fluctuation in the groundwater level. To lower the groundwater level, drainage systems can be installed. However, clayey soils do not drain well. Conversely, it is hard to increase the groundwater level during dry summers as well. Additionally, in Section 6.4.2. a connection between the fluctuation of the groundwater level and variation in the settlement rate was shown. It was found that a lower groundwater level would increase the settlement rate. This means a higher groundwater level would be favourable for the amount of ground settlement. However, a high groundwater level can be troublesome for other purposes, such as construction works in which dry soil conditions is desirable.

InSAR data of the Netherlands is available for free with the introduction of the *Bodemdalingskaart*. However, the locations of the measuring points of the *Bodemdalingskaart* are in general located within ~10 to 15 m of their actual location [11]. Consequently, a lot of measuring points generated by buildings are shown on the roads instead of their actual location. This might lead to underestimation of the settlement rate of the roads. The *Bodemdalingskaart* is not suitable for local subsidence problems on roads [43]. Therefore, the (free) *Bodemdalingskaart* cannot be used for settlement rate estimation on roads and commercial data processing techniques are necessary.



Conclusions and recommendations

The purpose of this research is to investigate how satellite data can be applied in the prediction of land movement in the shallow subsurface. The satellite data used in this research has been obtained by Interferometric Synthetic Aperture Radar (InSAR). Displacement values can be obtained by every passing of the satellite. By combining the different displacement values, a series of displacement measurements in time can be produced for a single measurement point. These series of displacement measurements are used to distract the settlement rate and amplitude of the seasonal oscillation for each measurement point. The settlement rate and amplitude of the seasonal oscillation for each location is analysed and correlated to the soil profile of that location. The locations are all located on roads. It has been assumed these roads did not have any road construction for at least 10 years. It was not possible to obtain the soil profiles beneath the roads and therefore boreholes have been made beside the roads. The exact soil profiles of the locations can therefore be slightly different. In addition, the foundation of the roads have not been considered, which might lead to a deviant soil profile as well.

In this report, the results are presented and discussed. The results are divided into the analysis of the settlement rate and analysis of the amplitude of the seasonal oscillation. Three different groups, group A to C, of locations are constructed based on the settlement rate of the locations. In group A the soil profiles do contain only sand and clay, where the soil profiles of group B and group C contain sand, clay and peat. The settlement rate was found to be the highest for the locations of group C, where the largest amounts of peat is present within the soil profiles. The amplitude of the seasonal oscillation was found lower for group A than for group B or C. The thickness of the soil layers and the ratio of thickness and depth of the soil layers have been analysed to find whether the satellite data is reflecting the soil profiles. For the amplitude of seasonal oscillation, the overall trendline for the thickness of the soil layers deviates 0.20 mm on average from the satellite data. For the ratio of thickness and depth of the soil layers, the overall trendline deviates 0.16 mm on average from the satellite data. This leads to a divergence of 13.8% and 9.5% respectively. The overall trendlines for the settlement rate deviate 0.28 mm/year and 0.30 mm/year from the satellite data for the thickness and ratio of the thickness and depth of the soil layers respectively. The divergence 7.1% for the overall trendline of the thickness of the soil layers and 7.5% for the overall trendline comprising the ratio thickness and depth of the soil layers.

In addition, the influence of the groundwater level to the settlement rate or amplitude of the seasonal oscillation has been analysed. For the settlement rate, five different time periods have been analysed. The periods with a high groundwater level show a decrease in the settlement rate. The effect of the groundwater level to the amplitude of the seasonal oscillation is not as clear. Although the seasonal trendlines show a seasonal effect, the peaks and troughs of the graphs are not occurring simultaneously.

So to give an answer to the research question:

To what extent can InSAR be used to monitor land movement mechanisms in the shallow subsurface on urban roads?

The satellite data obtained by InSAR has been used to establish equations that predict the settlement rate and amplitude of the seasonal oscillation based on the thickness of the soil layers or ratio thickness and depth of the soil layers within the soil profile. The equations for calculating the amplitude of the seasonal oscillation can be used to calculate the expected amplitude based on the soil profile of the top 1.5 metres below ground

level. The equations for the settlement rate are based on a soil profile of 3 metres below ground level. Based on the R-squared values, for the settlement rate the coherence with the thickness of the soil layers is lower than the coherence with the ratio thickness and depth of the soil layers. For the amplitude the coherence with the thickness of the soil layers is higher than the coherence with the ratio thickness and depth of the soil layers.

Further, the satellite data can give an estimate of the expected soil profile at a certain location. By an obtained value of the amplitude of seasonal oscillation of less than 1 mm, it is unlikely to have peat layers within the top 1.5 metres. With a settlement rate of more than 4.0 mm/year, it can be expected to have peat layers of at least 2 metres within the top 3 metres below the subsurface. This works the other way around as well. Depending on the amount of peat present at a certain location, settlement rates of more than 3 mm/year can be expected.

8.1. Recommendations

Now that the results have been presented and the conclusions have been drawn, it can be reviewed how these results can be improved (Section 8.1.1) and what research can be performed as a result of this research (Section 8.1.2). In the first section some improvements on the current research are suggested. In the second section additional research to expand the current research is proposed.

8.1.1. Improvements

Increase of locations in area of interest

In total 21 locations have been analysed in this research. Since the locations are divided into three different groups, each group contains 7 locations and therefore the total number of locations per group is limited. This could be improved by increasing the total number of locations per group or add other groups to the total data set.

Length of soil profiles

The soil profiles have been cut off at three metres due to the fact that some of the used soil profiles were limited in length. For the amplitude of the seasonal oscillation the length of three metres is sufficient. However, for the settlement rate it might be that a larger length of the soil profiles is necessary. Due to the presence of groundwater it was not possible to drill the boreholes deeper by hand. Deeper boreholes can be made by drilling machines.

Soil classification

In this research the soil types have been classified to peat, clay and sand. However, in practice these soil types are mixed, giving soils consisting of one main soil type and one or more admixture of other soil types. In general it can be said that a peaty clay or sandy clay both behave as clay, but in small-scale the soil types will have different characteristics and therefore conduct differently. By implementing different soil characteristics, the trendlines can be optimised and will be more accurately applicable to specified soil types.

Soil characteristics

No distinction has been made between soil layers above the groundwater level and below the groundwater level. The soil characteristics change by the presence of groundwater. For a fully saturated soil the shear strength and stiffness will be reduced compared to a non-saturated state of the soil. The soil layers above the groundwater level are also subjected to dehydration, which might change the soil characteristics as well. However, to be able to implement these soil characteristics, the groundwater levels should be known accurately. This is not known in the current research and therefore distinguishing the soil into above and below the groundwater level might be part of additional research.

8.1.2. Additional research

Increase the area of interest

The current area of interest is limited to the city of Woerden. The area of interest might be expanded to cities in the neighbouring surroundings, where the soil profile will be corresponding to the soil profile in the current area of interest. Figure 2.1a and Figure 2.1b show a large region where both the Echteld Formation and Nieuwkoop formation is present. Another way of expanding the area of interest is to consider rural roads in addition to urban roads. The rural roads must comply with the condition of no road constructions for at least 10 years as well.

Groundwater implementation

By evaluating the results, it was suggested to implement a variable of the groundwater level to the trendlines of the settlement rate. However, the groundwater level is only measured at fixed locations, but these locations do not coincide with the research locations. Therefore, accurate data of the depth and fluctuation of the groundwater level at the current locations is not available in the time span of the satellite data acquisition. At areas with new construction work, multiple monitoring wells can be installed to use InSAR monitoring at a later stage.

Bibliography

- [1] 06-GPS. GNSS. <https://www.06-gps.nl/gnss/>. [Online; accessed <09-2020>].
- [2] A. Belhadj-Aissa A. Bouaraba and D. Closson. Drastic improvement of change detection results with multilook complex sar images approach. *Progress In Electromagnetics Research C*, 82:55 – 66, 2018.
- [3] C. Prati A. Ferretti, A. Monti-Guarnieri and F. Rocca. *InSAR Principles: Guidelines for SAR Interferometry Processing and Interpretation*. ESA Publications, Noordwijk, 2007. ISBN 92-9092-233-8.
- [4] P.A. Fokker A.G. Muntendam-Bos, I.C. Kroon and G. de Lange. Bodemdaling in Nederland. Technical Report TNO-Rapport 2007-U-R0566B, TNO, 2006.
- [5] European Space Agency. RADAR and SAR Glossary. <https://earth.esa.int/handbooks/asar/CNTR5-2.html#eph.asar.gloss.radsar:RADAR>. [Online; accessed <09-2020>].
- [6] M. Allaby. *A dictionary of Geology and Earth Sciences*. Oxford University Press, Oxford, 2013. ISBN 978-0-19-965306-5.
- [7] Reyhan Azeriansyah, Yudo Prasetyo, and Bambang Yuwono. Land subsidence monitoring in semarang and demak coastal areas 2016-2017 using persistent scatterer interferometric synthetic aperture radar. *IOP Conference Series: Earth and Environmental Science*, 313:012040, 2019.
- [8] H.J.A Berendsen. *De vorming van het land*. Fysische geografie van nederland. Van Gorcum and Comp, Assen, 2004. ISBN 9023240758.
- [9] H.J.A Berendsen. *Fysisch-geografisch onderzoek*. Fysische geografie van nederland. Van Gorcum and Comp, Assen, 2005. ISBN 902324138x.
- [10] H.J.A Berendsen. *Landschap in delen*. Fysische geografie van nederland. Van Gorcum and Comp, Assen, 2005. ISBN 9023241495.
- [11] Bodemdalingskaart. Veel gestelde vragen. <https://bodemdalingskaart.nl/nl/veel-gestelde-vragen>. [Online; accessed <06-2021>].
- [12] Bodemdalingskaart.nl. De Bodemdalingskaart van Nederland. <https://bodemdalingskaart.nl/nl/>, . [Online; accessed <09-2020>].
- [13] Bodemdalingskaart.nl. Geodetische analyse. <https://bodemdalingskaart.nl/nl/kennis-datacentrum/>, . [Online; accessed <09-2020>].
- [14] Bodemdalingskaart.nl. Zwaartekrachtmetingen. <https://bodemdalingskaart.nl/nl/kennis-datacentrum/zwaartekrachtsdata/>, . [Online; accessed <09-2020>].
- [15] G. de Lange C. Bremmer, R. van Eijs and A. van der Spek. Geologische en antropogene factoren in relatie tot relatieve bodemdaling. In *FB.J. Barends et al. (eds) Bodemdaling langs de Nederlandse kust*, pages 29 – 33. Delft University Press, Amsterdam, 2008. ISBN 978-90-5199-521-3.
- [16] J. de Jong. Use of InSAR data for building deformation monitoring. <http://resolver.tudelft.nl/uuid:fac1829b-6d5e-42b6-b77c-986d967f73f4>. [Online; accessed <09-2020>].
- [17] Sebastiaan N. Jonkman E. Ozer, F.J. van Leijen and R.F. Hanssen. Applicability of satellite radar imaging to monitor the conditions of levees. *Flood Risk Management*, e12509, 2018.
- [18] K.M. Cohen E. Stouthamer and W.Z. Hoek. *De vorming van het land*. Fysische Geografie van Nederland. Perspectief Uitgevers, Utrecht, 2015. ISBN 9789491269110.

- [19] Kennis en exploitatiecentrum Officiële Overheidspublicaties. Waterschappen. <https://www.overheid.nl/wie-vormen-de-overheid/waterschappen>. [Online; accessed <07-2020>].
- [20] F. B. Enders. Coefficient of determination. <https://www.britannica.com/science/coefficient-of-determination>. [Online; accessed <09-2020>].
- [21] A.G. Jongmans et al. *Landschappen van Nederland: geologie, bodem en landgebruik*. Wageningen Academic Publishers, Wageningen, 2013. ISBN 978-90-8686-213-9.
- [22] R.F. Hanssen F.B.J. Barends, D. Dillingh and K.I. van Onselen. *Bodemdaling langs de Nederlandse kust*. Delft University Press, Amsterdam, 2008. ISBN 978-90-5199-521-3.
- [23] et al. G.J. van den Born. Dalende bodems, stijgende kosten. Technical Report 1064, Planbureau voor de Leefomgeving, Nov. 2016.
- [24] K. Lambeck H. Kooi, P. Johnston and C. Smither. Geological causes of recent (~ 100 yr) vertical land movement in the Netherlands. *Tectonophysics*, 299: 297 – 316, 1998.
- [25] R.F. Hanssen. *Radar Interferometry; Data Interpretation and Error Analysis*. Vol. 2. Kluwer Academic Publishers, Dordrecht, 2001. ISBN 0-7923-6945-9.
- [26] M.P. Hijma and H. Kooi. Bodemdaling in het kustfundament en de getijdenbekkens. Technical Report report 11200538-008-ZKS-0001, Deltares, 2018.
- [27] J. P. Mehl Jr. K. K. E. Neuendorf and J. A. Jackson. *Glossary of geology, 5th ed.* Virginia : American Geological Institute, Virginia, 2011. ISBN 978-1-68015-178-7.
- [28] H. Kooi. Land subsidence due to compaction in the coastal area of The Netherlands: the role of lateral fluid flow and constraints from well-log data. *Global and Planetary Change*, 27: 207 – 222, 2000.
- [29] H. Kooi. Compactiebijdragen aan bodemdaling langs de kust. In *F.B.J. Barends et al. (eds) Bodemdaling langs de Nederlandse kust*, pages 19 – 28. Delft University Press, Amsterdam, 2008. ISBN 978-90-5199-521-3.
- [30] H. Kooi and J.J. de Vries. Land subsidence and hydrodynamic compaction of sedimentary basins. *Hydrology and Earth System Sciences*, 2: 159 – 171, 1998.
- [31] MathWorks. Interactive Fitting. https://nl.mathworks.com/help/matlab/data_analysis/interactive-fitting.html#f1-15488, . [Online; accessed <09-2020>].
- [32] MathWorks. What is MATLAB? <https://nl.mathworks.com/discovery/what-is-matlab.html>, . [Online; accessed <09-2020>].
- [33] NAM. Bodemdaling door Aardgaswinning - NAM-gasvelden in Groningen, Friesland en het noorden van Drenthe. Technical Report Statusrapport 2015 en Prognose tot het jaar 2080, NAM, 2015.
- [34] Nedmag. Alles over zoutwinning en bodemdaling. <https://www.nedmag.nl/omgeving/alles-over-zoutwinning-en-bodemdaling>. [Online; accessed <08-2020>].
- [35] Nedmag. Winningsplan 2018. Technical report, Nedmag, 2018.
- [36] G. Nichols. *Sedimentology and stratigraphy*. Wiley-Blackwell, Chichester, 2009. ISBN 978-1-4051-3592-4.
- [37] L.J. Pons and I.S. Zonneveld. *Soil ripening and soil classification : initial soil formation of alluvial deposits with a classification of the resulting soils*. H. Veenman and Zonen, Wageningen, 1965.
- [38] Hoogheemraadschap De Stichtse Rijnlanden. Peilbesluiten. <https://www.hdsr.nl/beleid-plannen/peilbesluiten-0/>. [Online; accessed <07-2020>].
- [39] R.F. Houtgast R.T. van Balen and S.A.P.L. Cloetingh. Neotectonics of the Netherlands. *Quaternary Science Reviews*, 24: 439 – 454, 2005.
- [40] A. Singh. R-Squared and Adjusted R-Squared. <https://nl.mathworks.com/discovery/what-is-matlab.html>. [Online; accessed <09-2020>].

- [41] B.J. Skinner and S.C. Porter. *Physical Geology*. John Wiley and Sons, New York, 1987. ISBN 978-04-7105-668-3.
- [42] SkyGeo. Customer case studies with InSAR applications in various industries. <https://skygeo.com/case-studies/>, . [Online; accessed <09-2020>].
- [43] SkyGeo. Hoe zet je InSAR optimaal in om gemeentelijk wegonderhoud te plannen? <https://https://skygeo.com/nl/wegonderhoud-in-kockengen/>, . [Online; accessed <06-2021>].
- [44] SkyGeo. InSAR Technical Background. <https://skygeo.com/insar-technical-background/>, . [Online; accessed <09-2020>].
- [45] K. Stüwe. *Geodynamics of the lithosphere*. Springer, Berlin, New York, 2007. ISBN 978-3-540-71236-7.
- [46] TNO. Oil and gas fields overview. <https://www.nlog.nl/en/oil-and-gas-fields-overview>. [Online; accessed <08-2020>].
- [47] E.J. van Leijen. *Persistent Scatterer Interferometry based on geodetic estimation theory*. Ph.D. Thesis, Delft University of Technology, 2014.
- [48] Technische Adviescommissie voor de Waterkeringen. Geotechnische classificatie van veen. Technical report, Rijkswaterstaat, Juni 1996.
- [49] H.J.T. Weerts and F.S. Busschers. Formatie van Echteld. In: *Lithostratigrafische Nomenclator van de Ondiepe Ondergrond*. <https://www.dinoloket.nl/formatie-van-echteld>, 2003. [Online; accessed <03-2020>].
- [50] H.J.T. Weerts and F.S. Busschers. Formatie van Nieuwkoop. In: *Lithostratigrafische Nomenclator van de Ondiepe Ondergrond*. <https://www.dinoloket.nl/formatie-van-nieuwkoop>, 2003. [Online; accessed <03-2020>].

A

Points per location

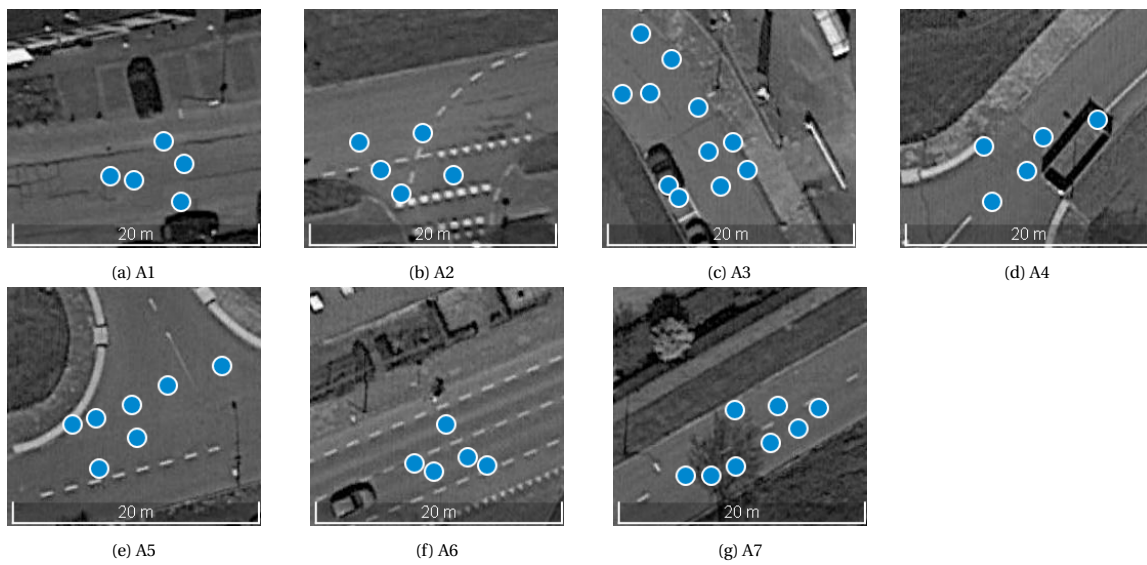


Figure A.1: Point positions of the locations attributed to group A

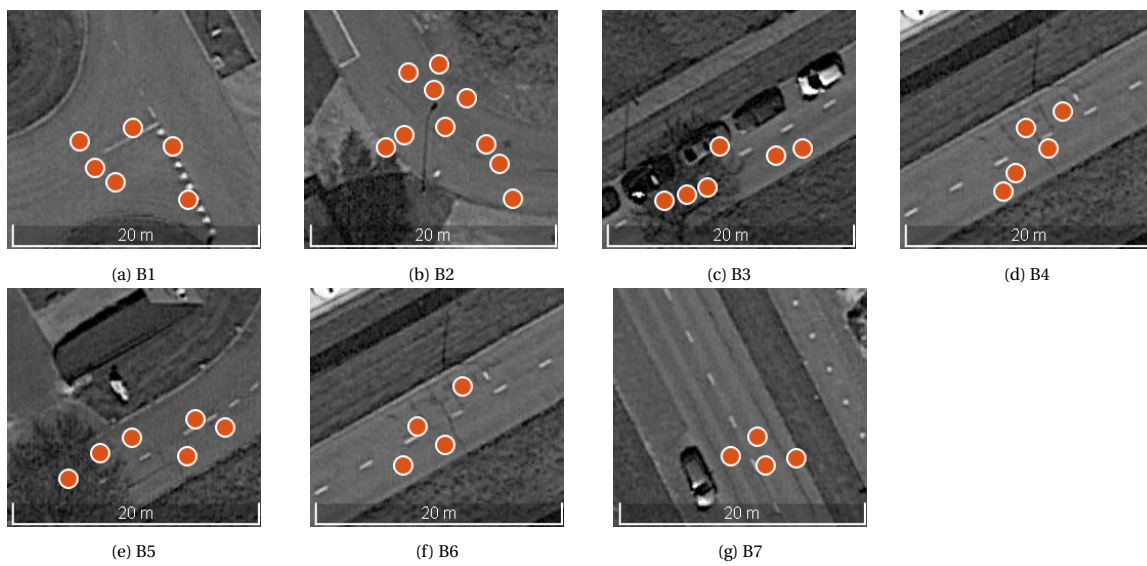


Figure A.2: Point positions of the locations attributed to group B

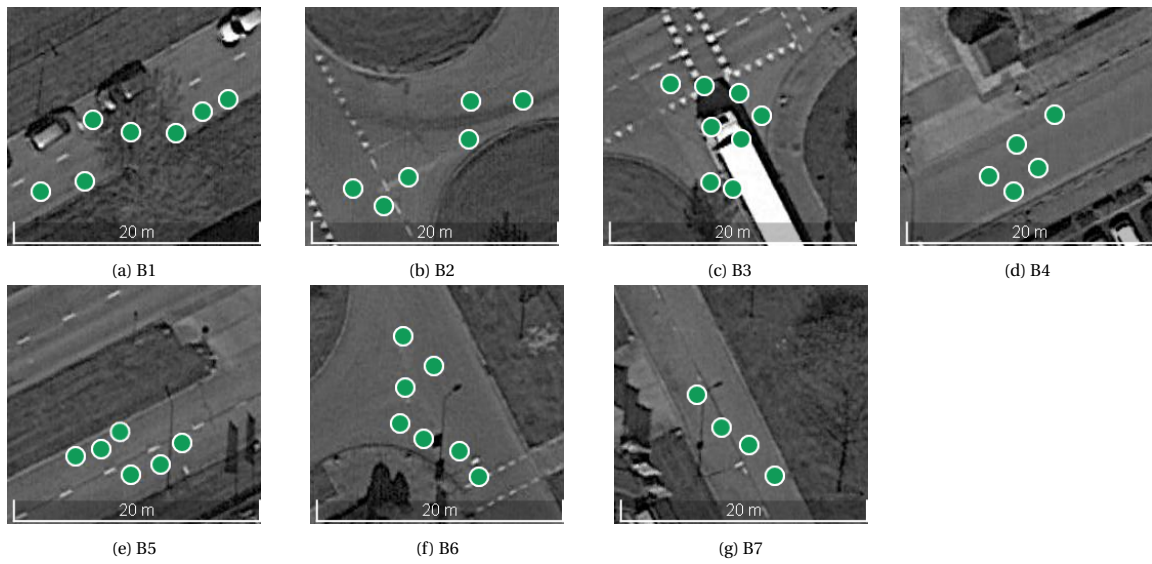


Figure A.3: Point positions of the locations attributed to group C

B

Data of the locations of group A

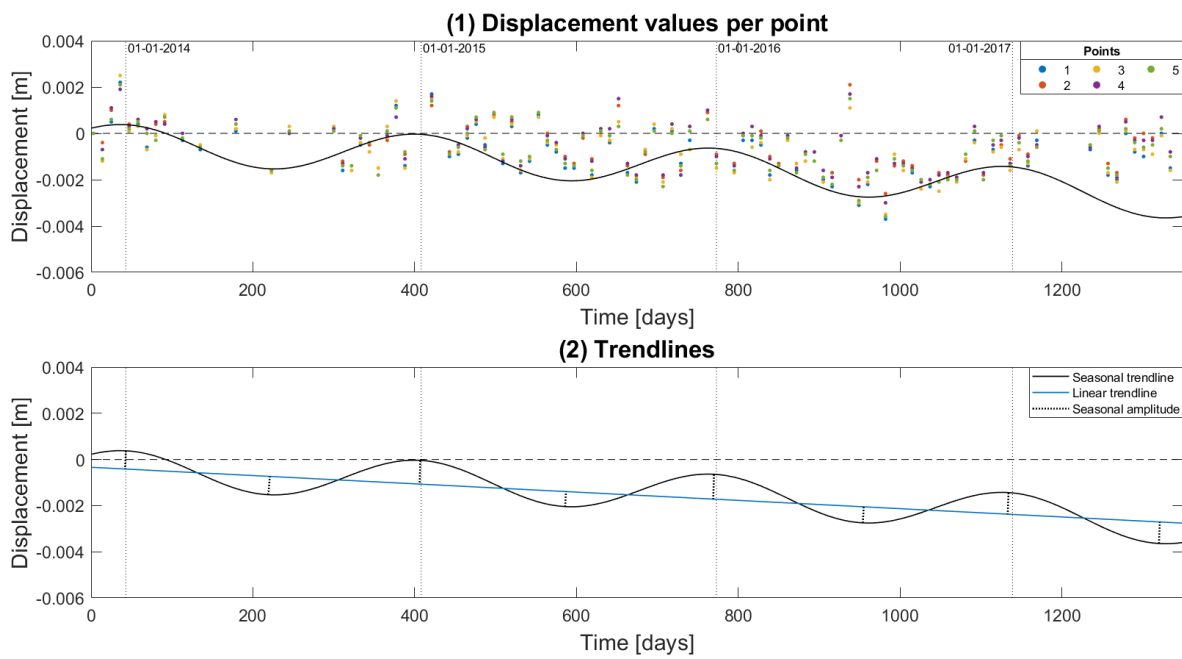


Figure B.1: Individual measurement series (top) and trendlines (bottom) for location A1

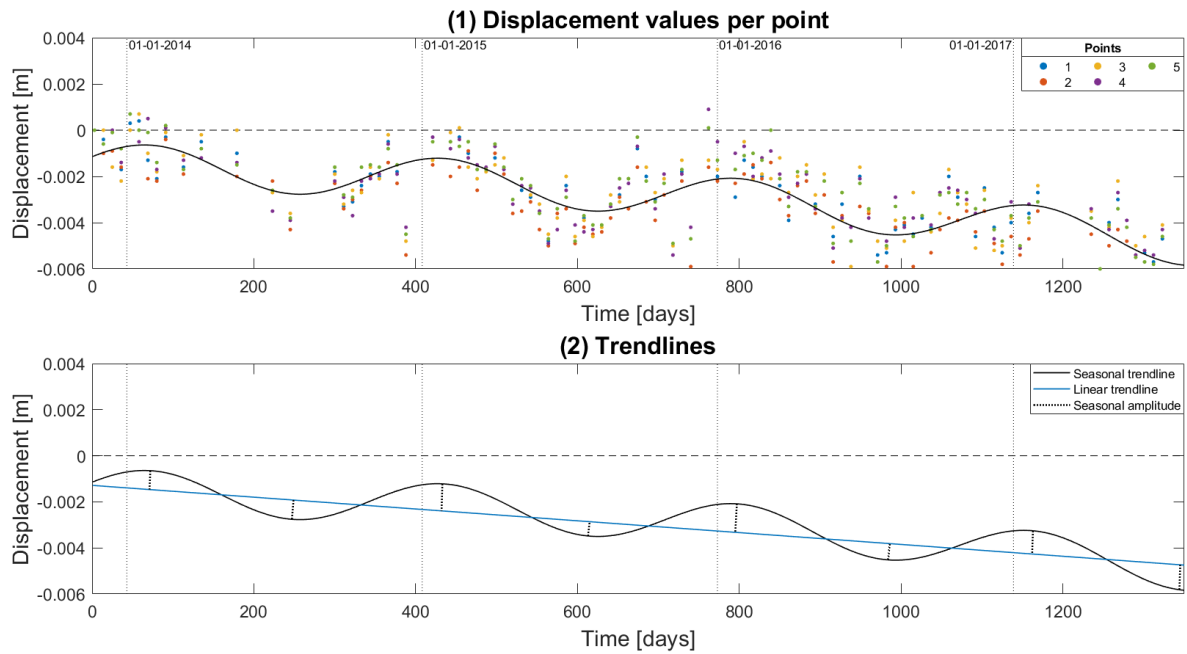


Figure B.2: Individual measurement series (top) and trendlines (bottom) for location A2

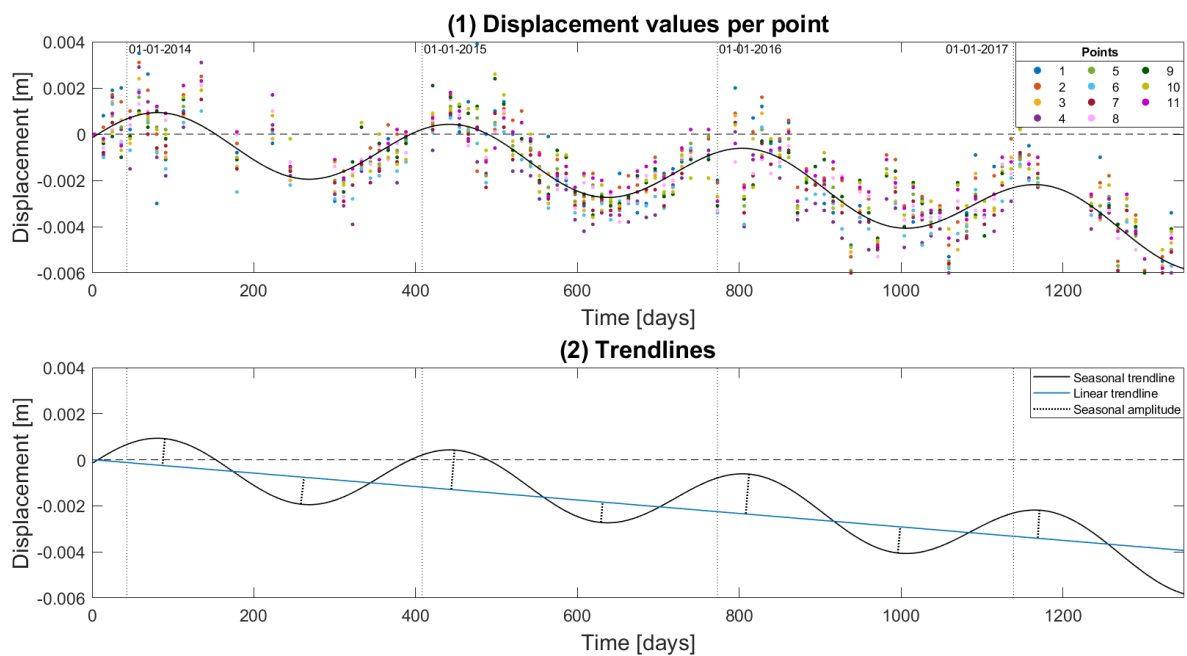


Figure B.3: Individual measurement series (top) and trendlines (bottom) for location A3

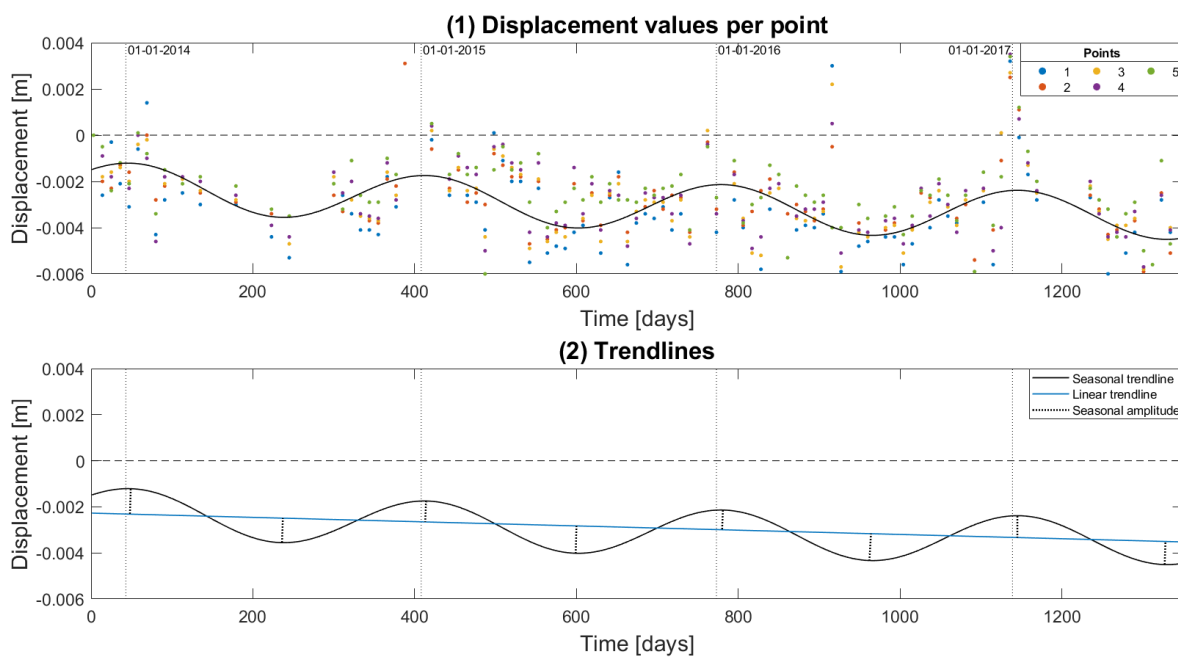


Figure B.4: Individual measurement series (top) and trendlines (bottom) for location A4

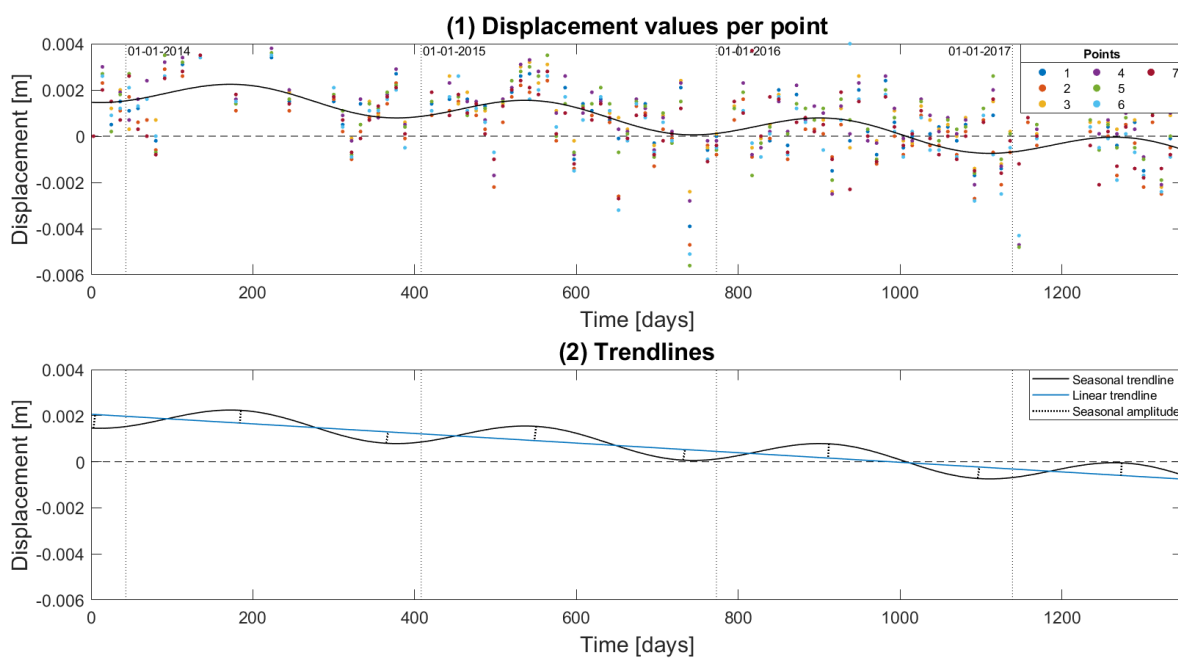


Figure B.5: Individual measurement series (top) and trendlines (bottom) for location A5

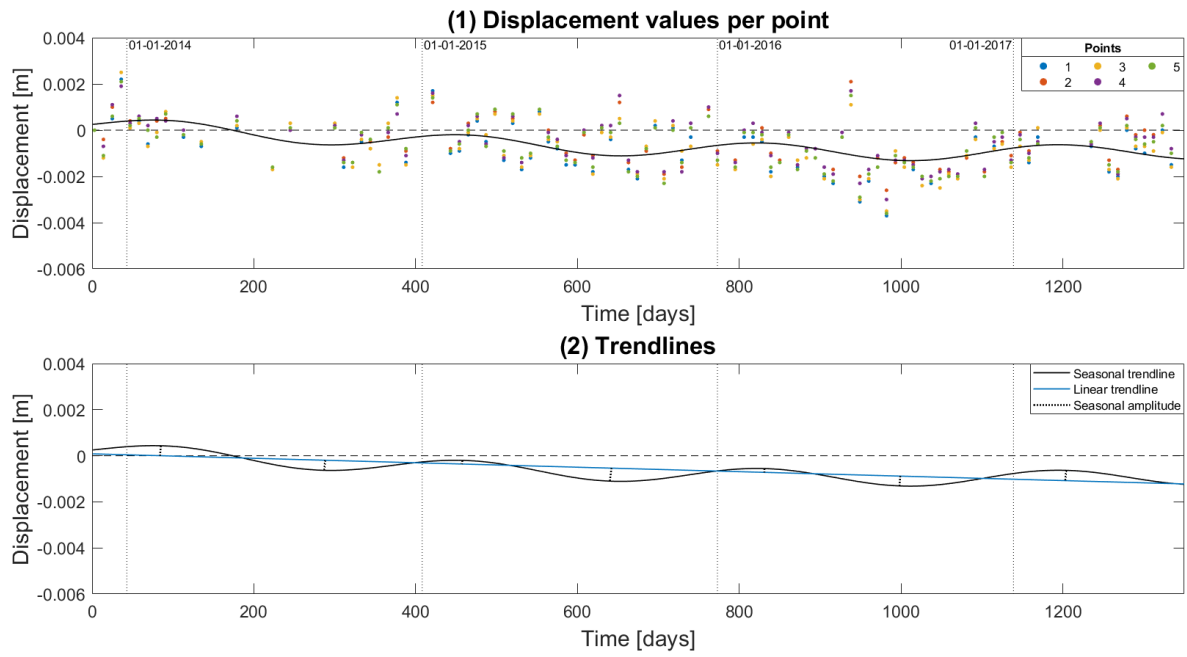


Figure B.6: Individual measurement series (top) and trendlines (bottom) for location A6

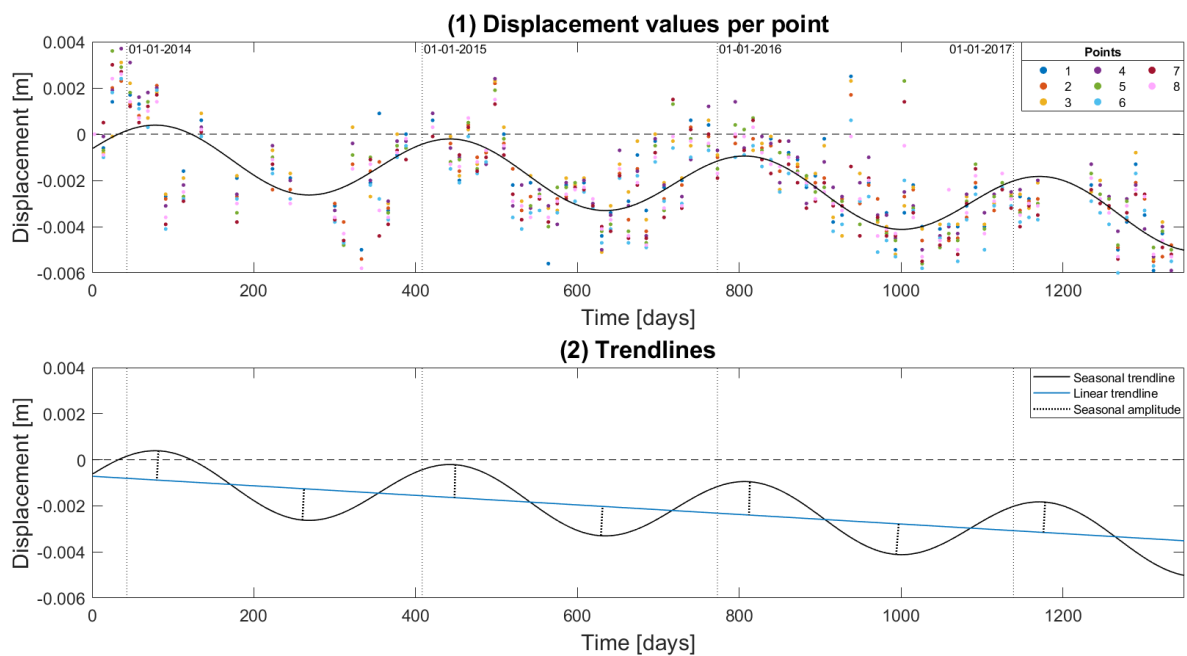


Figure B.7: Individual measurement series (top) and trendlines (bottom) for location A7

C

Data of the locations of group B

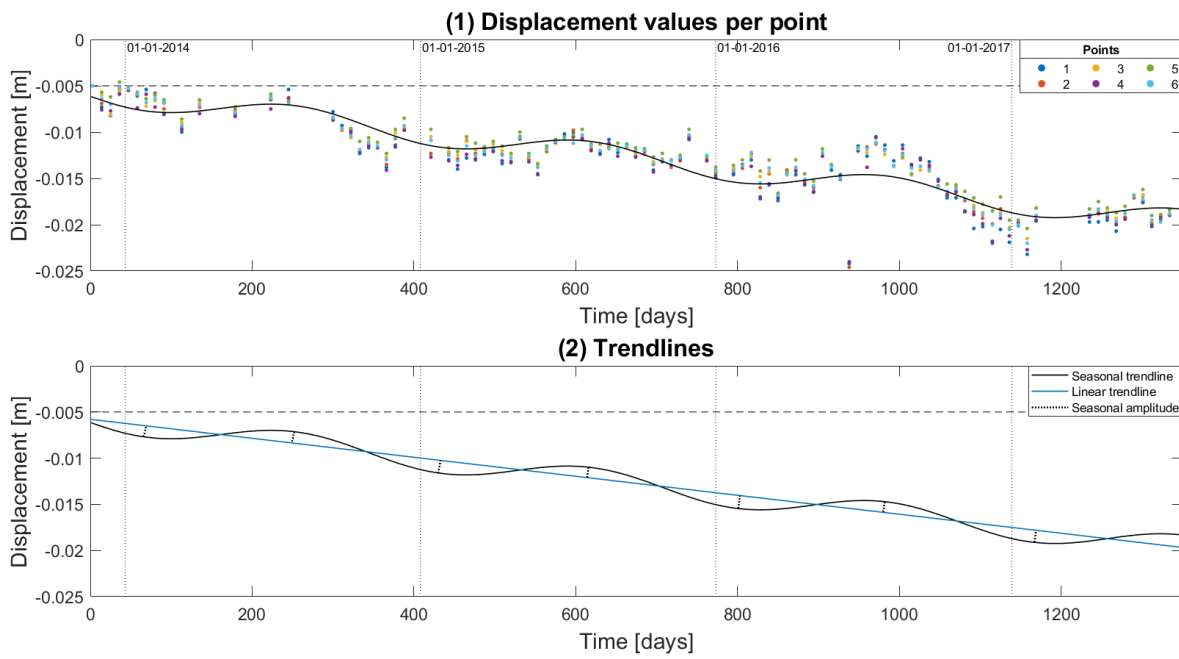


Figure C.1: Individual measurement series (top) and trendlines (bottom) for location B1

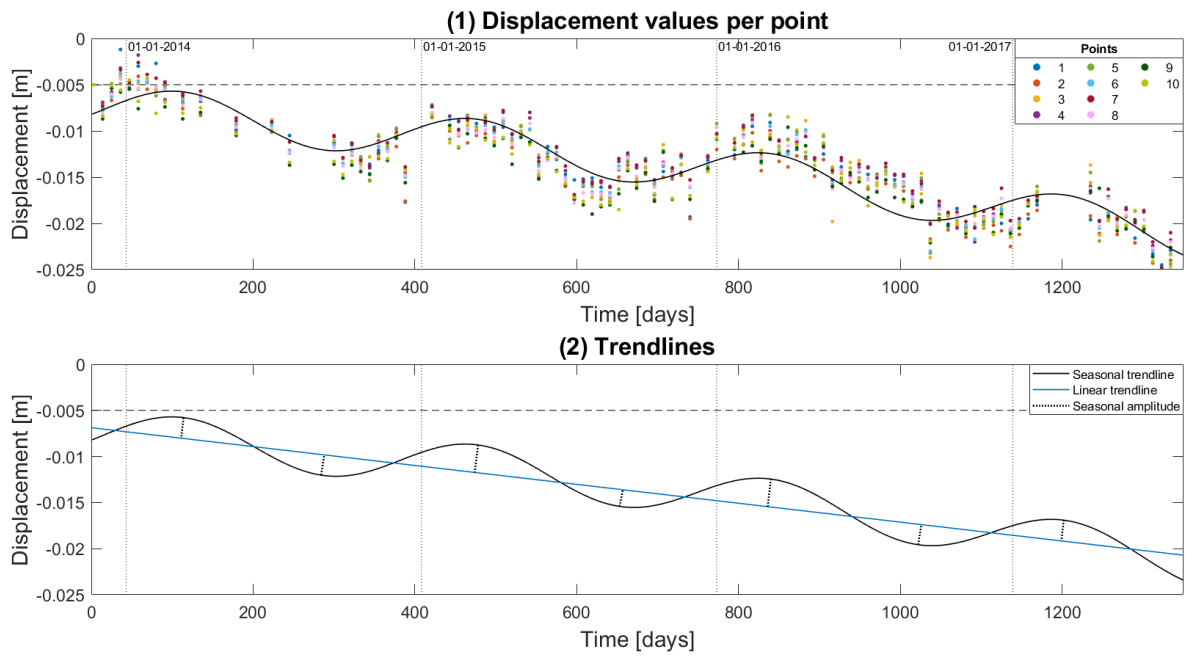


Figure C.2: Individual measurement series (top) and trendlines (bottom) for location B2

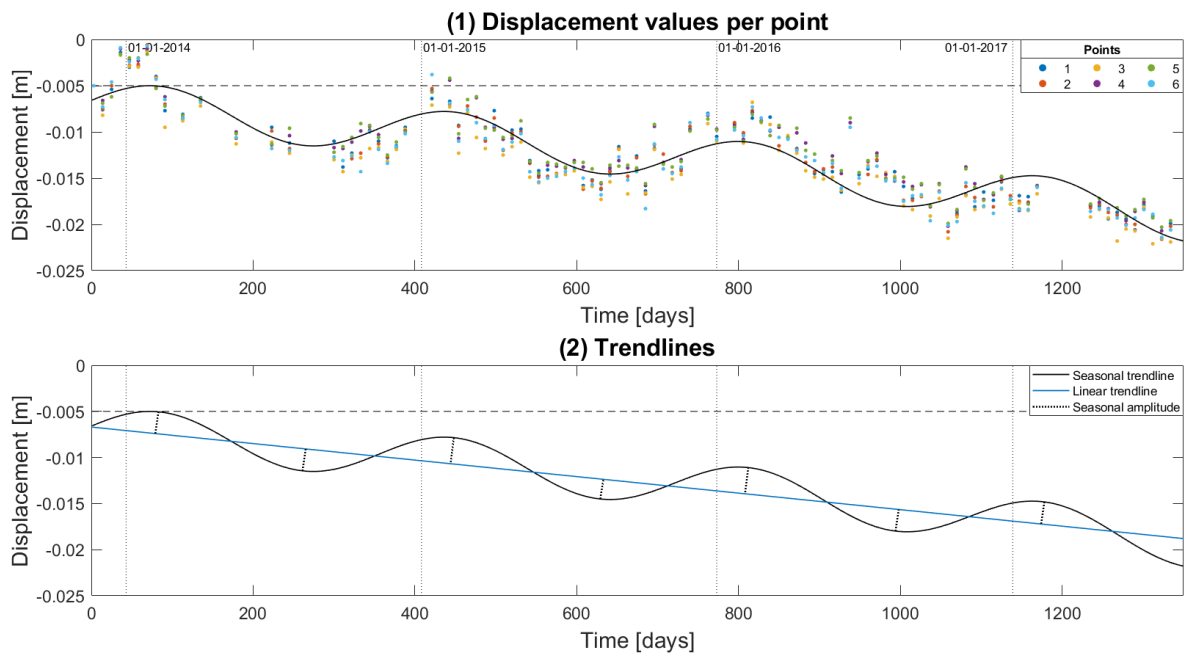


Figure C.3: Individual measurement series (top) and trendlines (bottom) for location B3

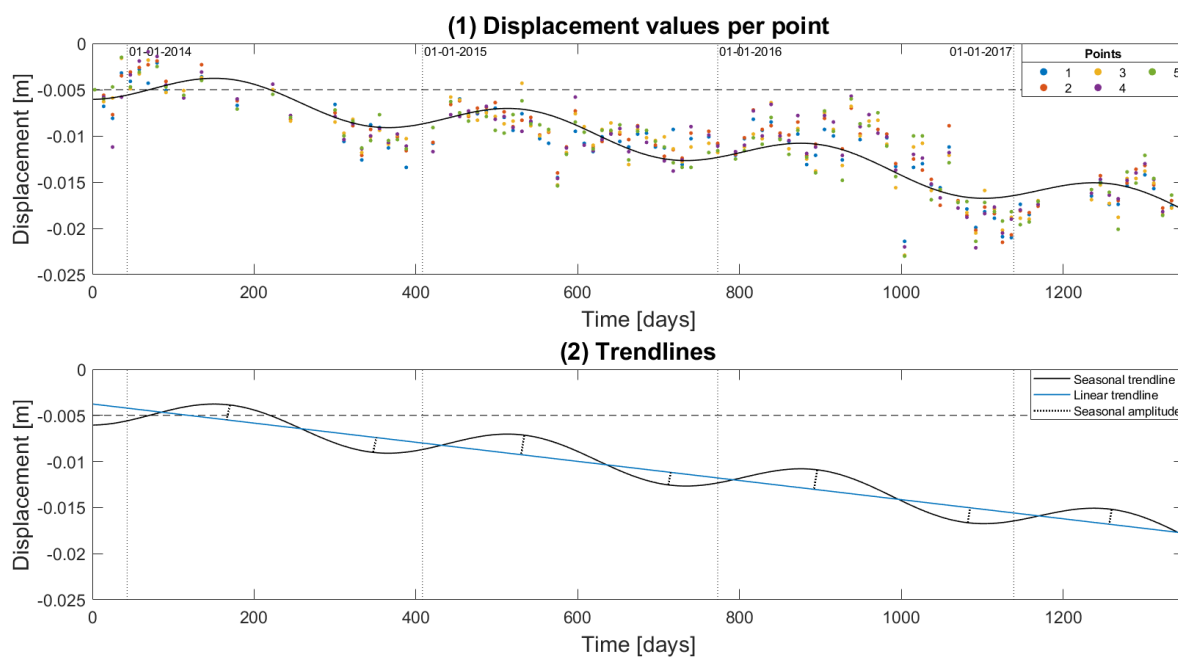


Figure C.4: Individual measurement series (top) and trendlines (bottom) for location B4

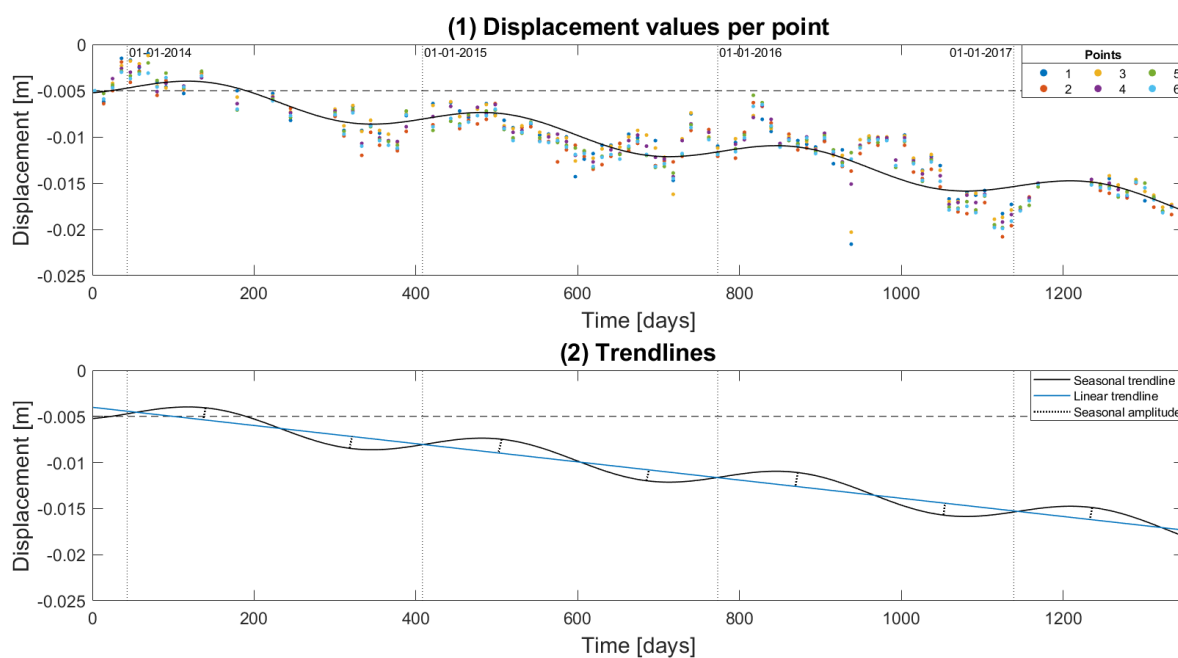


Figure C.5: Individual measurement series (top) and trendlines (bottom) for location B5

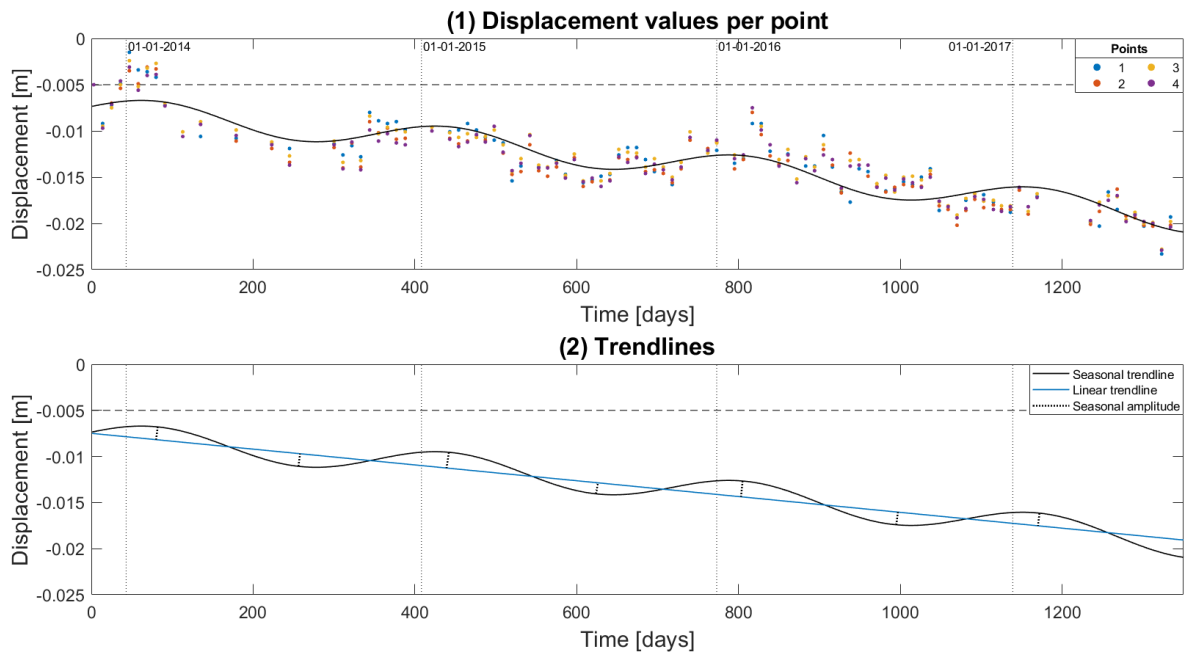


Figure C.6: Individual measurement series (top) and trendlines (bottom) for location B6

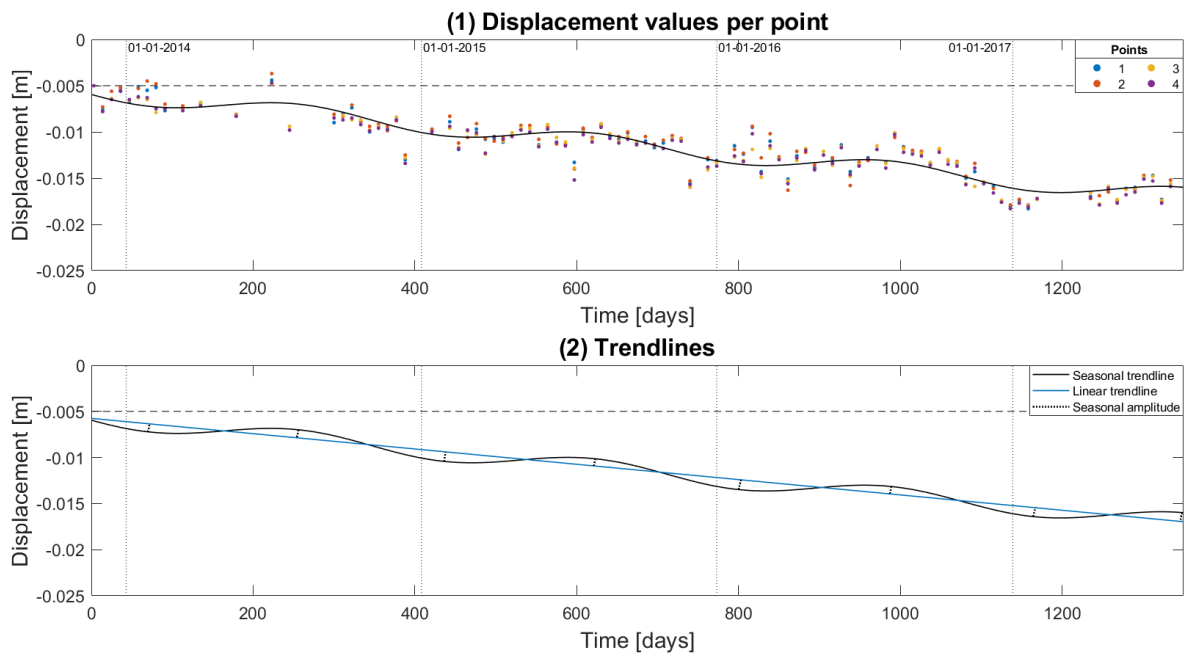


Figure C.7: Individual measurement series (top) and trendlines (bottom) for location B7

D

Data of the locations of group C

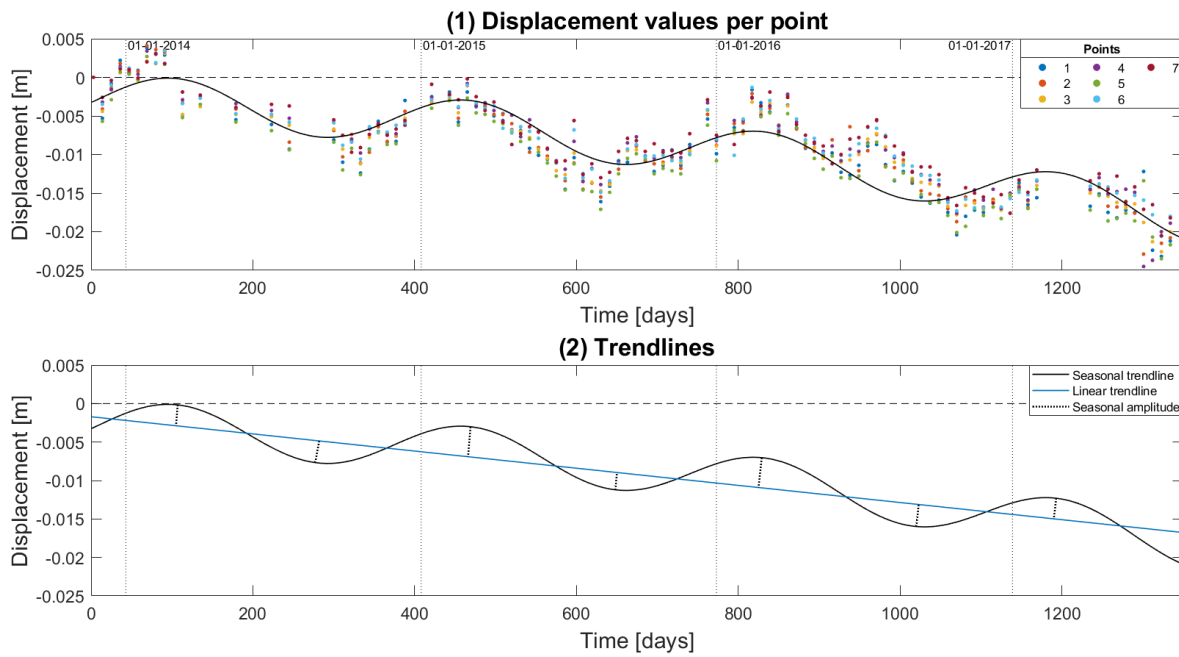


Figure D.1: Individual measurement series (top) and trendlines (bottom) for location C1

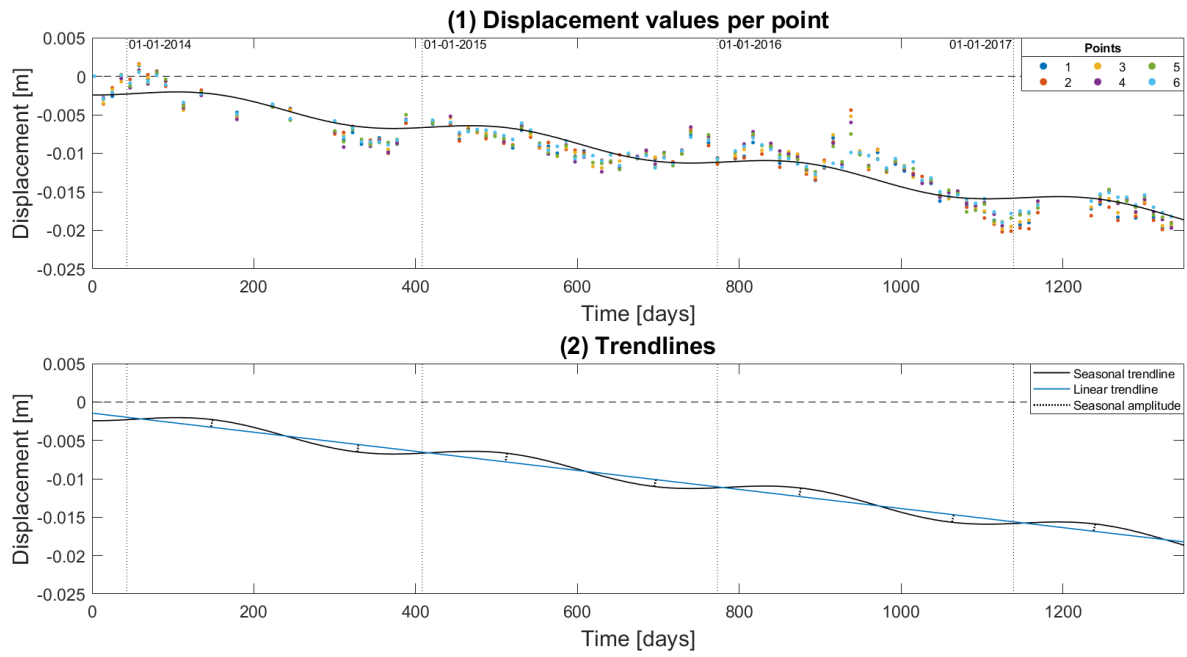


Figure D.2: Individual measurement series (top) and trendlines (bottom) for location C2

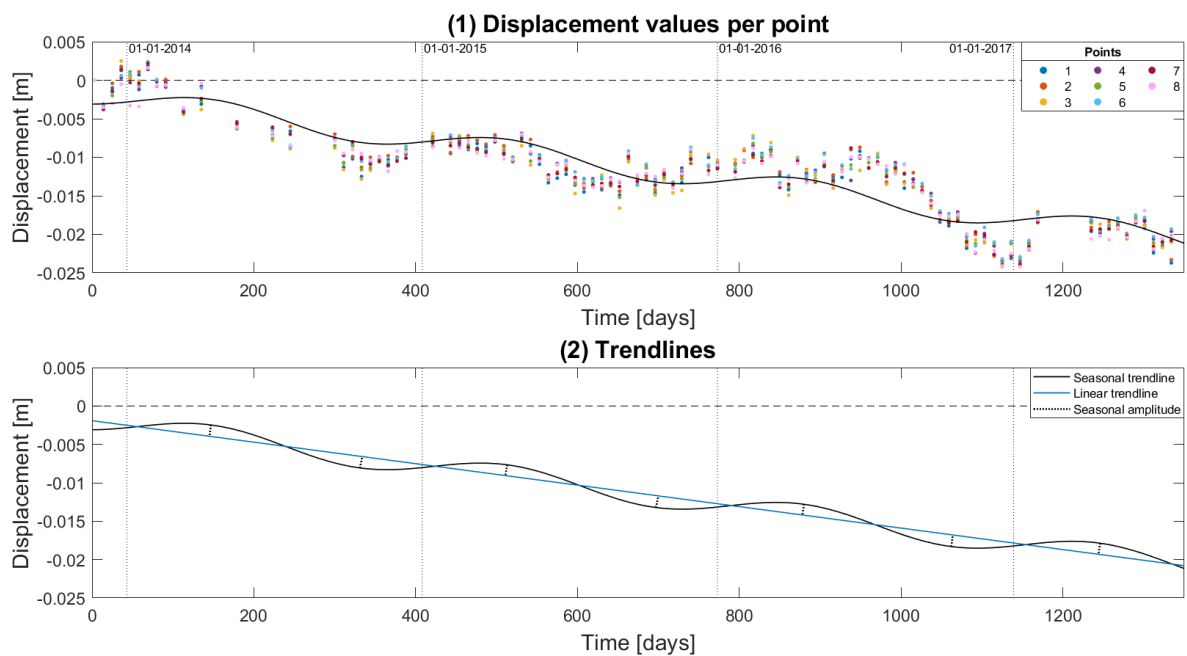


Figure D.3: Individual measurement series (top) and trendlines (bottom) for location C3

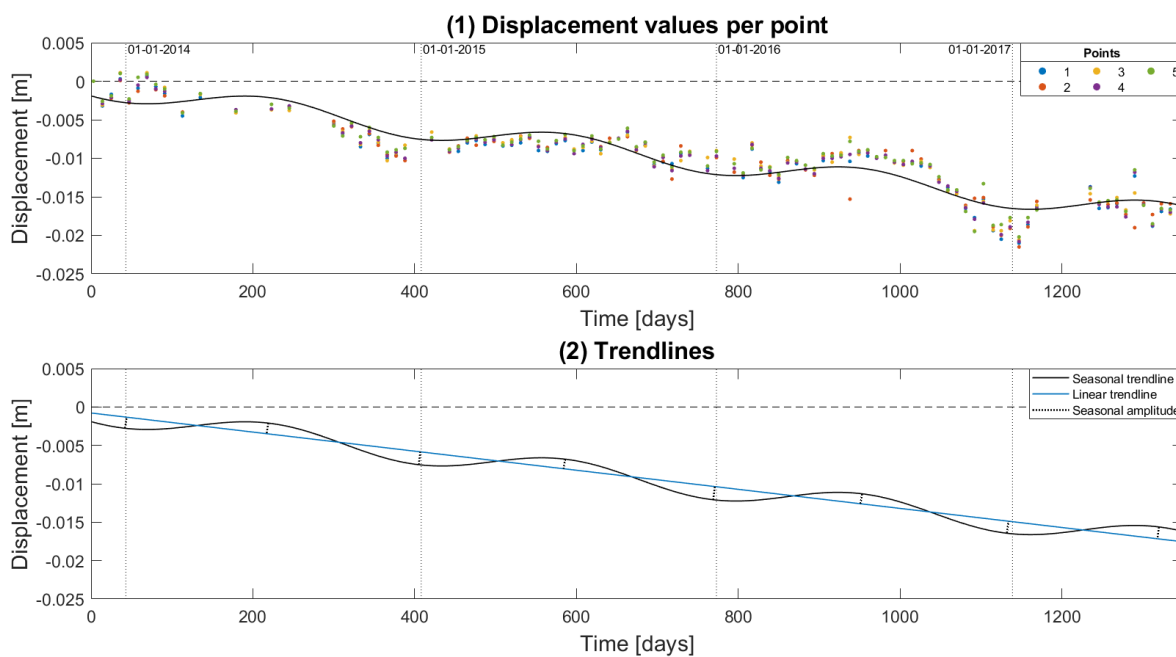


Figure D.4: Individual measurement series (top) and trendlines (bottom) for location C4

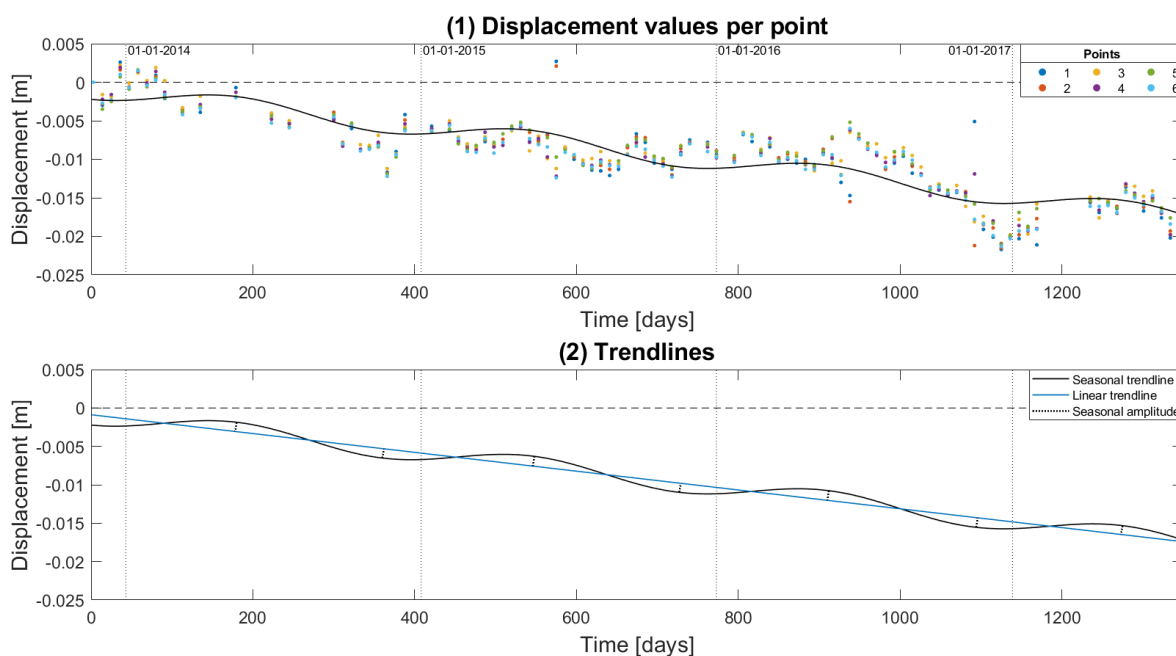


Figure D.5: Individual measurement series (top) and trendlines (bottom) for location C5

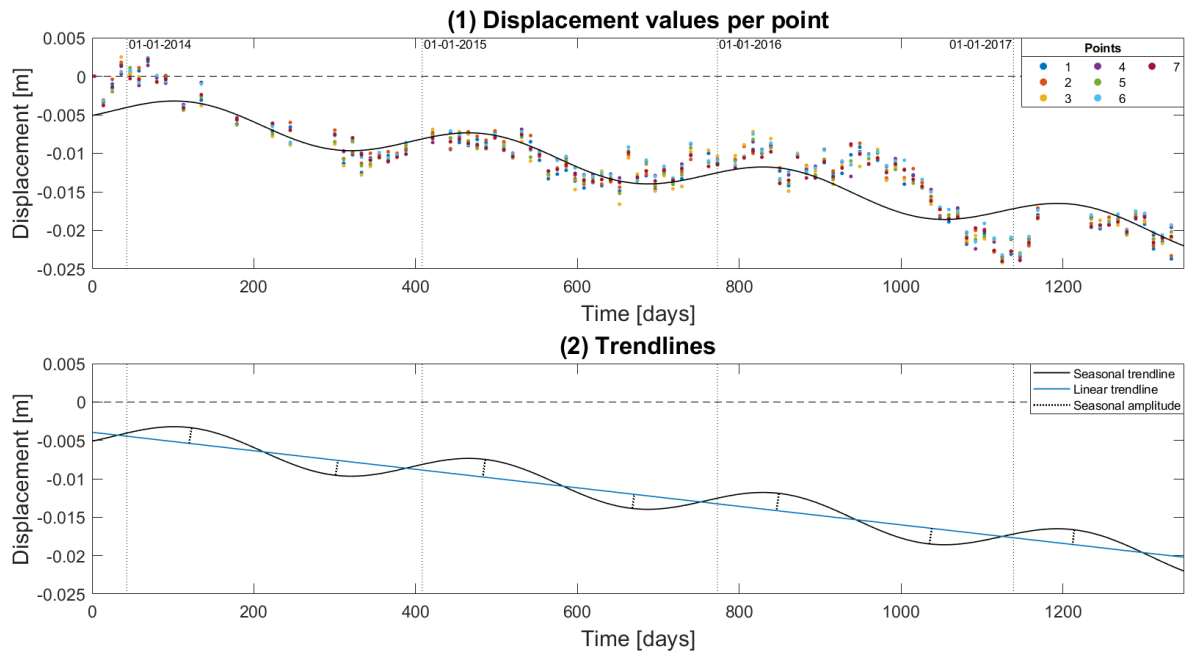


Figure D.6: Individual measurement series (top) and trendlines (bottom) for location C6

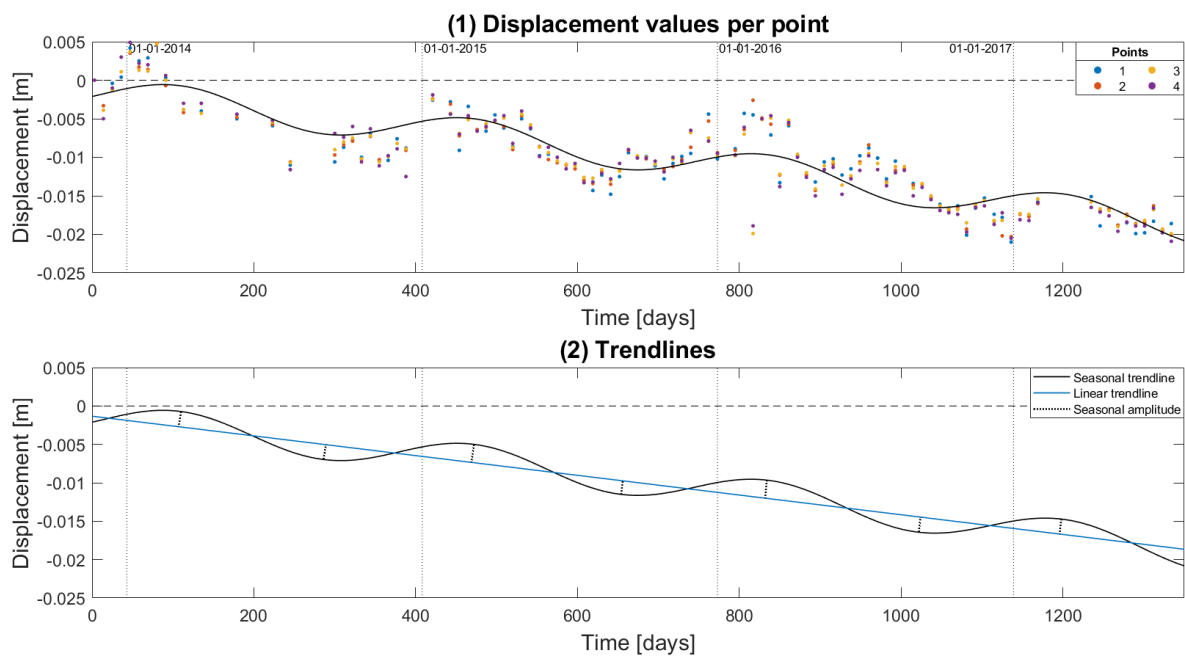
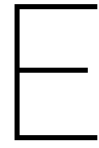


Figure D.7: Individual measurement series (top) and trendlines (bottom) for location C7



Soil profiles

Legend

<i>Soil type</i>	
	Clay
	Silt
	Sand
	Gravel
	Peat

<i>Admixture</i>	
	Weak
	Moderately
	Strong

Figure E.1: Declaration of the different soil types shown in the soil profiles

E.1. Soil profiles - Group A

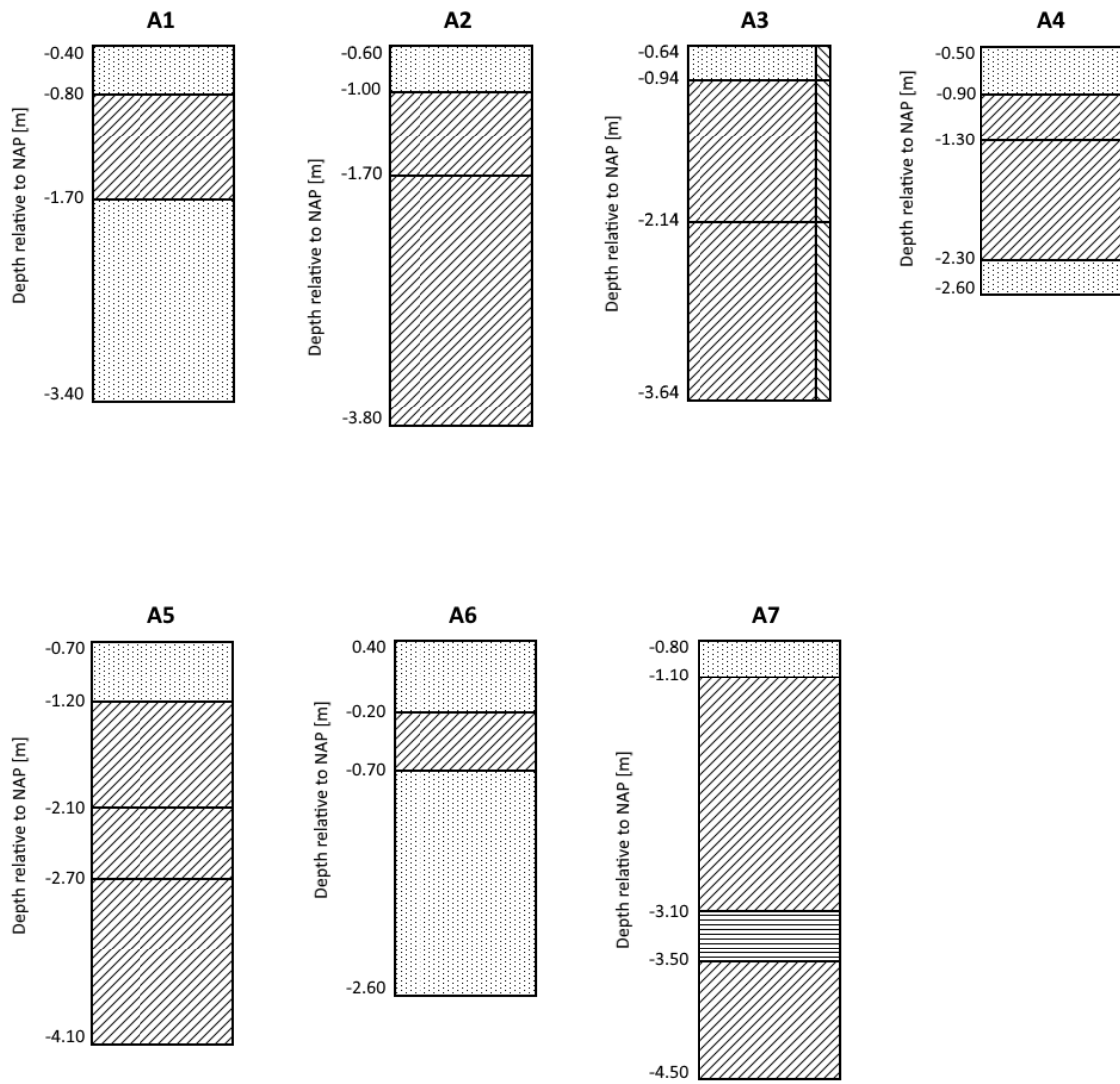


Figure E.2: Soil profiles belonging to the locations of group A

E.2. Soil profiles - Group B

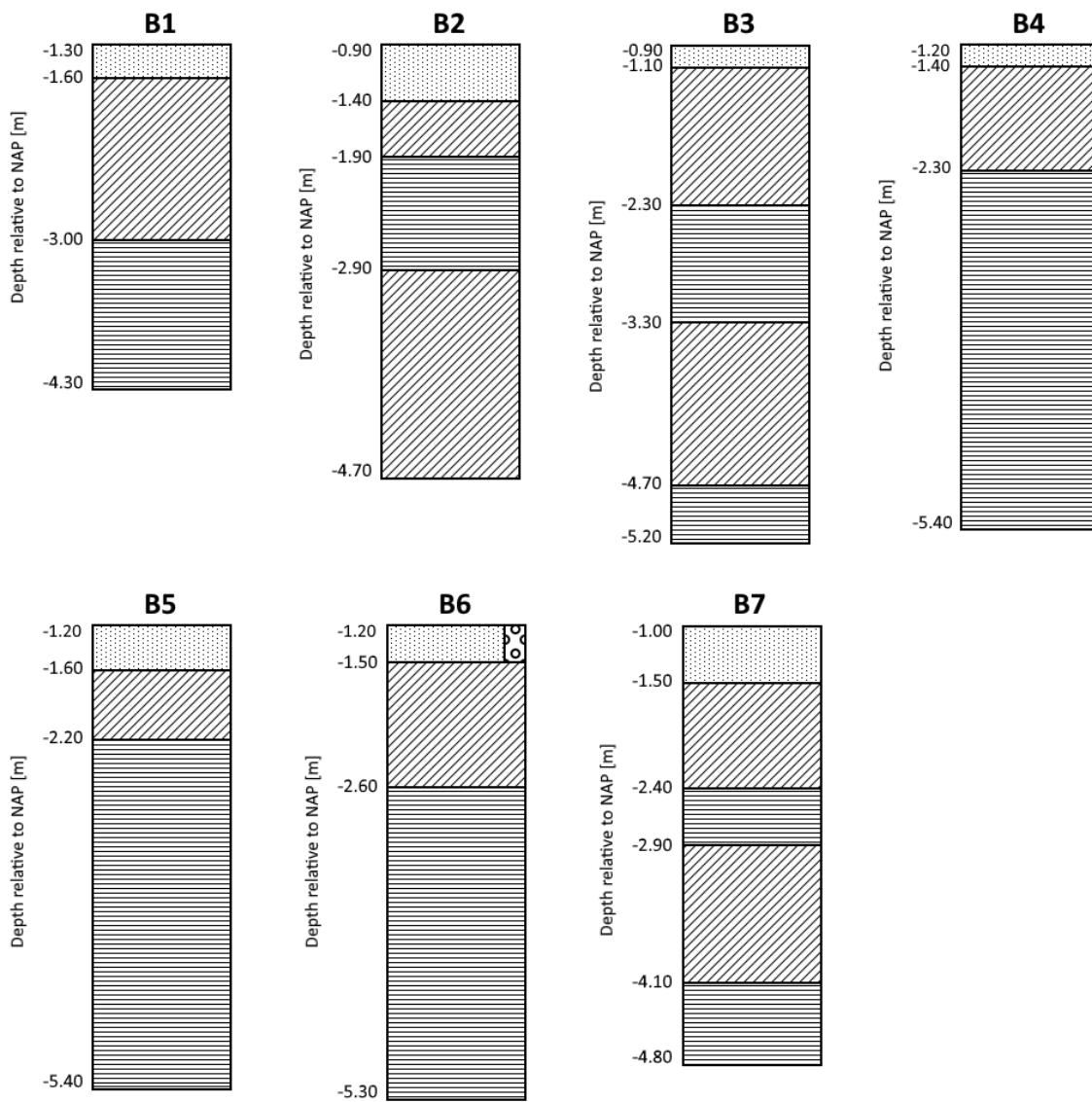


Figure E.3: Soil profiles belonging to the locations of group B

E.3. Soil profiles - Group C

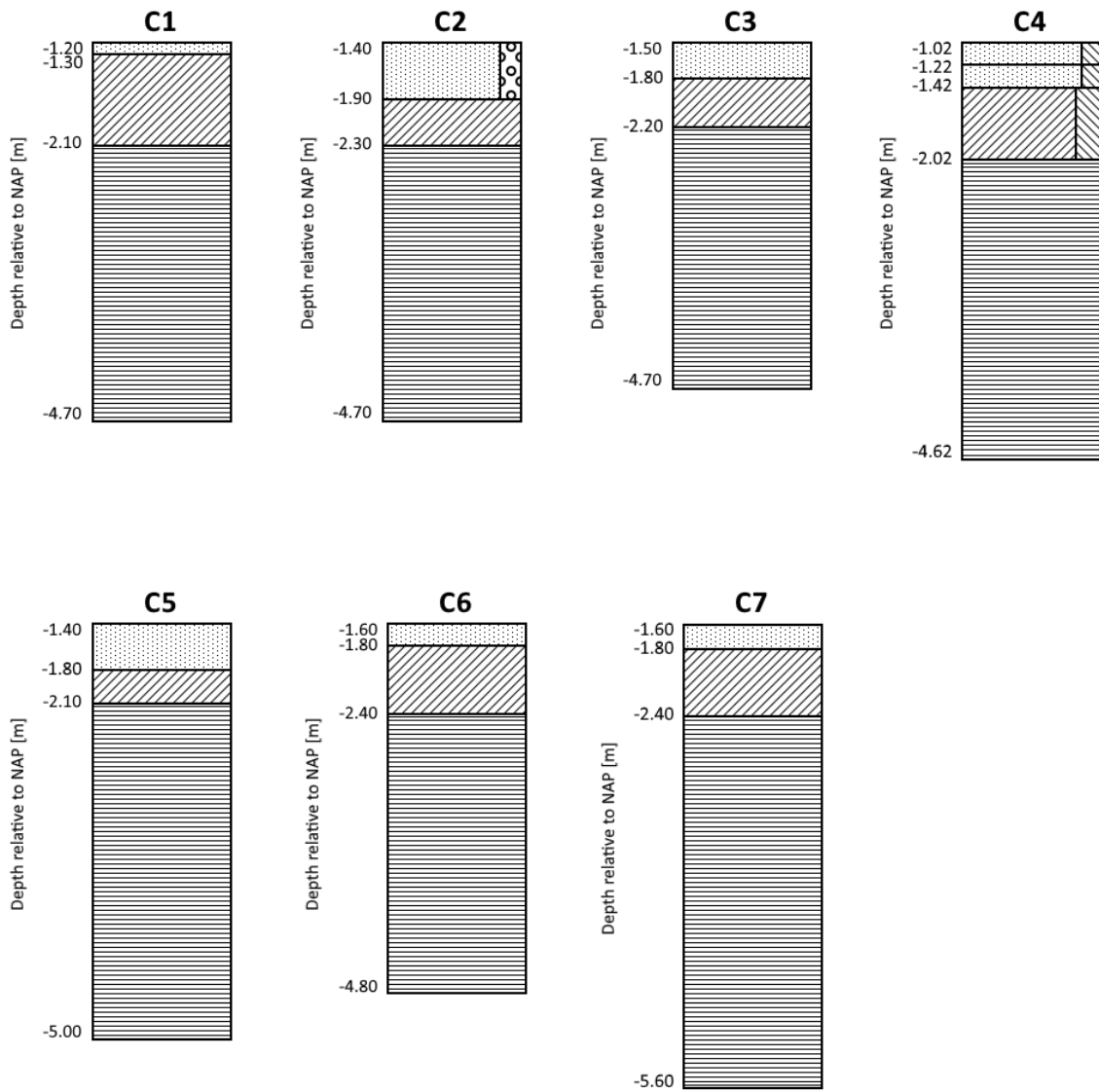


Figure E.4: Soil profiles belonging to the locations of group C